STRUCTURAL, FUNCTIONAL AND COMPUTATIONAL CHARACTERIZATION OF *PSEUDOMONAS AERUGINOSA* SIDEROPHORE BIOSYNTHETIC PATHWAY ACCESSORY PROTEINS PCHB AND PVDA

BY

Jose Olucha

Submitted to the graduate degree program in the Department of Molecular Biosciences and the Graduate Faculty of the University of Kansas in partial fulfillment of the requirements for the degree of Doctor of Philosophy.

_____

Chairperson Audrey Lamb

_____

Mark Richter

_____

Roberto De Guzman

_____

Yoshiaki Azuma

_____

Scott Hefty

_____

Thomas Prisinzano

Date Defended: 3/30/2012

The Dissertation Committee for Jose Olucha
certifies that this is the approved version of the following dissertation:

STRUCTURAL, FUNCTIONAL AND COMPUTATIONAL CHARACTERIZATION OF *PSEUDOMONAS AERUGINOSA* SIDEROPHORE BIOSYNTHETIC PATHWAY ACCESSORY PROTEINS PCHB AND PVDA

_____

Chairperson Audrey Lamb

Date approved: 3/30/2012

Abstract

To survive and establish infections in host tissues, pathogens must compete with the host organism for iron. One strategy for iron acquisition is to excrete iron-chelators, called siderophores, with very high affinity to ferric iron. Studies have shown siderophores to be associated with growth and virulence of some pathogens. Inhibition of siderophore production is therefore considered an attractive target for the development of novel antimicrobial agents. This dissertation describes biochemical investigations of two enzymes involved in siderophore production in Pseudomonas aeruginosa, an opportunistic pathogen.

PchB catalyzes two pericyclic reactions in a single active site: **1.)** an isochorismate-pyruvate lyase reaction (breakdown of isochorismate to salicylate and pyruvate) and **2.)** a chorismate mutase reaction (rearrangement of chorismate to prephanate). There is an ongoing debate in the field over the relative contributions of Near Attack Conformations (NAC) and Transition State Stabilization (TSS) to the molecular mechanism of pericyclic reactions. Steady-state kinetics of a K42H-PchB mutant with a pH-dependent charge on position 42 on the active site loop, previously shown to be important for catalysis reveals that lyase and mutase activities require the positive charge at that position for efficient catalysis. Covalent and non-covalent chemical-rescue experiments on mutants deficient of the positive charge at position 42 suggest that the positive charge at the 42 position must be organized within the active site for efficient catalysis. Finally, quantum mechanical/molecular mechanical experiments on wild type and K42H PchB models look at the mechanism of catalysis of the lyase activity in more detail.

PvdA is an accessory enzyme to the siderophore pyoverdin biosynthetic pathway of *Pseudomonas aeruginosa*. PvdA is an N-hydroxylating ornithine hydroxylase: it catalyzes the FAD dependent addition of oxygen to the N^5-amine of the ornithine using NADPH as electron donor and molecular oxygen. Here we present two structures of PvdA with FAD in oxidized (1.9 Å resolution) and reduced (3.03 Å resolution) flavin forms. These are the first two structures of an N-hydroxylating Class B flavoprotein monooxygenase *and* the first structures of a Class B flavoprotein monooxygenase to

contain redox center, electron donor and product/substrate in the active site bound simultaneously

Acknowledgements

I would like to thank everyone who helped me in my graduate education and research. I would like to acknowledge Dr. Richard L. Schowen for his enzymology lectures and his scientific advice. Thank you to Dr. Christopher Gamblin, and the members Gamblin lab, for their support and for the use of their equipment. Thank you to Dr. Adrian Mulholland and Dr. Kara Ranaghan for their invaluable computational enzymology knowledge and advice, and for hosting me for two summers as a visiting student. Thank you to Dr. Thomas Prisinzano and the Prisinzano lab, who I worked with in the synthesis of hydroxyornithine.

I would like to acknowledge the Stanford Synchrotron Radiation Laboratory, for the use of their facilities, where I collected the data for the PvdA structures.

A special thank you to the NIH Dynamic Aspects of Chemical Biology Fellowship for funding.

I would like to thank all the undergraduate members of the lab who helped with my projects: Katie Waugh, Allison Ho, Stephen Davidson, Surya Lakhanpal, Bernadette Goudreau, Maddie Schuman, Sarah Bergkamb, Anita Moudgal and Alec Hermanson. Thank you to of the previous and current graduate members of the Lamb lab: Dr. Qianyi Luo, Andrew Ouellette, Anindita Basu and Blake Balcomb. I would also like to thank Dr. Kathy Meneely and Annemarie Chilton for their help, support and friendship.

I would like to thank my committee members: Dr. Mark Richter, Dr. Roberto De Guzman, Dr. Yoshiaki Azuma, Dr. Scott Hefty and Dr. Thomas Prisinzano for providing suggestions and reading this dissertation.

Finally, a very special thank you goes to my advisor, Dr. Audrey Lamb for her scientific expertise, guidance, continuous support, friendship and encouragement throughout my graduate career.

Table of Contents

Page

List of Figures

List of Tables

Chapter 1: Introduction

1.1 *Pseudomonas aeruginosa*

Pseudomonas aeruginosa is an aerobic rod shaped bacterium belonging to the bacterial family of Pseudomonadaceae, which includes all twelve members of the genus *Pseudomonas.* Like other Pseudomonads, *Pseudomonas aeruginosa* is a free-living bacterium, omnipresent in soil and water environments, and occasionally on the surfaces of plants and animals [1].

Pseudomonas aeruginosa is a pathogen of clinical importance. According to the Centers for Disease Control, the overall incidence of *P. aeruginosa* infections in U.S. hospitals is about 4 per 1000 discharges [2]. *P. aeruginosa* is the fourth most commonly-isolated nosocomial (hospital-acquired) pathogen and accounts for 10.1 percent of all nosocomial infections [2, 3]. *Pseudomonas aeruginosa* is an opportunistic pathogen; it is very successful at initiating infection in immunocompromised human hosts such as burn victims, AIDS patients, cystic fibrosis patients, or cancer patients undergoing chemo or radiotherapy [4-7]. *Pseudomonas aeruginosa* rarely infects uncompromised tissues. However, once tissue defenses are somehow compromised, there is hardly any tissue that it cannot infect. *Pseudomonas* infections range from simple joint, bone, ear, eye or gastro-intestinal infections [8] to more severe cardio-respiratory infections and meningitis [9].

1.1.1 Characteristics

Pseudomonas aeruginosa is a diderm (Gram-stain negative) rod, with a single polar flagellum [10-12]. It is ubiquitous in a wide variety of soil and water environments. Pseudomonas is a facultative anaerobe: it is able to grow in the absence of O_2 if NO_3 is available as an electron acceptor [13]. Typically, *Pseudomonas* is able to grow as a biofilm, attached to some surface, or as a unicellular organism swimming by means of its flagellum [14, 15].

Pseudomonas aeruginosa has very simple nutritional requirements[15]. It has the ability to grow *in vitro* using acetate as a source of carbon and ammonium sulfate as a source of nitrogen[12]. Like most pseudomonads, *P. aeruginosa* has evolved a wide metabolic versatility; organic growth factors are not required, and it can use a wide variety of hydrocarbons for growth [16-18]. Although optimal growth temperature is 37° C, it is able to grow at temperatures as high as 42° C and is resistant to high concentrations of salts, dyes and weak antiseptics [19]. Unfortunately, *Pseudomonas aeruginosa* strains have been found to be resistant to one or more commercially available antibiotics [20-23].

1.2 Current antimicrobials/antibiotics

Current antibiotics can be classified into four major categories, according to their target **(Table 1-1)**: cell wall synthesis, protein synthesis, membrane function and nucleic acid synthesis [24].

Table 1-1: Current Available Antibiotics[1]

Class	Representative Compounds	Mode of Action
1. Cell Wall Synthesis Inhibitors	*B-lactams (e.g. penicillins)*	Irreversibly bind to transpeptidase.
	Vancomycin	Inihibit peptidoglycan synthesis by binding to NAM/NAG peptides
	bacitracin	Interferes with dephosphorylation of C55-isoprenyl pyrophosphate.
2. Protein Synthesis Inhibitors	*Rifamycins (e.g. rifampicin)*	Inhibit mRNA synthesis by binding to β subunit of RNA polymerase
	Linezolid	Blocks translation initiation complex binding to the 50S subunit of the ribosome
	Tetracyclines	Bind A site on ribosome, preventing aminoacyl-tRNA entry.
	Aminoglycosides	Bind to the 30S subunit of the ribosome, blocking translocation and proofreading process
	Chloramphenicols	Bind 50S subunit of the ribosome and prevent peptidyl transfer step during elongation
	Macrolides	Bind to P site on 50S subunit of the ribosome, blocking elongation
	Fusidic acids	Block turnover of EF-G
	Puromycins	Bind to ribosome A site, participate in peptidyl formation, inducing early termination.
3. Cell Membrane Disruptors	*Polymixins*	Binds LPS on diderm bacteria, disrupts cell membrane phospholipid organization (like a detergent)
4. Nucleic Acid Synthesis Inhibitors	*Quinolones*	Binds and interferes with DNA gyrase and topoisomerases
	Sulphonamides Trimethoprim Metronizadole	Inhibit synthesis of folate nucleic acid precursors.

Table adapted from Walsh, 2003 [25]

1.2.1 Cell wall synthesis inhibitors.

Cell wall synthesis inhibitors can be classified into two groups: beta-lactam antibiotics and cell wall synthesis inhibitors **(Table 1-1, 1)**. This class of antibiotics includes penicillins, cephalosporins, monobactams and carbapenems. Beta lactam antibiotics act by irreversibly binding to the catalytic serine residue in the active site of transpeptidase blocking the final transpeptidation step in the synthesis of the peptidoglycan layer in bacterial cell walls[26]. Bacteria have evolved several mechanisms of resistance against beta-lactam antibiotics, including production of beta-lactamases, decreased cell wall permeability, and mutations to transpeptidases [27]. Cell wall synthesis inhibitors, such as vancomycin and bacitracin, inhibit production of phospholipids and peptidoglycan, either via binding to the D-alanyl-D-ala moieties of the NAM/NAG peptides in Gram-positive bacteria (vancomycin) [28], or by interfering with the dephosphorylation of the C_{55}-isoprenyl pyrophosphate thus blocking transport of peptidoglycan building blocks to the periplasm (bacitracin) [29].

1.2.2 Protein synthesis inhibitors

This class of antibiotics includes a wide variety of compounds that target most stages of protein synthesis in prokaryotes **(Table 1-1, 2)**. Rifamycins (rifampicin) act on mRNA synthesis; they inhibit the DNA-dependent RNA polymerase by binding its beta subunit, preventing transcription [30, 31]. Linezolid, an oxazolidinone, blocks the formation of the translation initiation complex by binding to the 50S subunit of the ribosome [32, 33]. Tetracyclines block the A site of the ribosome, also preventing translation, in this case by preventing aminoacyl-tRNA entry [34]. Aminoglycosides bind to the 30S subunit of the ribosome, and have several mechanisms of action, including inhibition of ribosomal

translocation and have also been suggested to disrupt the integrity of the cell membrane [35]. Chloramphenicols block elongation by binding to the 30S subunit of the ribosome and preventing the peptidyl transfer step during elongation[36, 37]. Marcrolides and fusidic acid inhibit ribosomal translocation. Macrolides do so by binding to the P site on the 50S subunit of the ribosome. Fusidic acids also block ribosomal translocation by blocking turnover of elongation factor G from the ribosome [38-40]. Puromycins bind to the ribosome's A site, and participates in peptide formation, producing a peptidyl-puromicin that induces early termination [41-43].

1.2.3 Cell membrane disruptors.

The integrity of outer and cytoplasmic membranes is vital to survival of bacteria. Compounds that can disrupt and disorganize the cell membranes rapidly kill the cells. Unfortunately, due to the similarities in phospholipid composition of bacterial and eukaryotic membranes, cell membrane disruptors are rarely specific enough to be used systemically. This class of antibiotics functions by disrupting the structure of the cell membrane or by inhibits its function **(Table 1-1, 3)**. Polymyxin, a cell membrane disruptor, is effective mainly against diderms, binding to lipopolysaccharides on the cell surface and disrupting cell membrane phospholipids like a detergent[44].

1.2.4 Nucleic acid synthesis antibiotics

Nucleic Acid Synthesis inhibitors comprise a wide variety of molecules that interfere with DNA replication. They include quinolones, trimethoprim and metronizadole **(Table 1-1, 4)**. Quinolones are a group of antibiotics that block DNA synthetic apparatus in bacteria by interfering with DNA gyrase and topoisomerases [45, 46]. Most other antibiotics that

interfere with nucleic acid synthesis, like sulphonamides, trimethoprim, and metronizadole, block or inhibit precursor metabolites to nucleic acid biosynthesis, such as folates[25, 47].

Unfortunately, pathogenic bacteria such as *Pseudomonas aeruginosa* have evolved resistance to antibiotics from one or more of these categories and there is an increased prevalence of multidrug resistant strains (MDR), extensive drug-resistant strains (XDR) and in some cases pandrug-resistant strains (PDR)[48, 49]. Mechanisms of resistance can include hypermutability, efflux pump over-expression, over-expression of metallo-betalactamases, and point mutations in topoisomerases[49, 50]. Multi-drug resistance results in many first-line antimicrobials/antibacterials being completely ineffective in combating *Pseudomonas* infections. In such cases, antimicrobial cocktails and less conventional drugs with higher human toxicity might need to be used. It is therefore imperative to find new antimicrobial targets. One such possible target is nutrient (in particular iron) acquisition.

1.3 Iron usage in bacteria

Most known living organisms, including pathogenic bacteria, require iron for survival. However, because of its toxicity at high concentrations in its ferrous form (Fe^{2+}) and low solubility in its ferric form (Fe^{3+}), iron bioavailability is very low in host tissues[51-53]. The concentration of unbound iron in humans can be as low as 10^{-18} – 10^{-24} molar in an average individual [54]. Due to hypoferremia during an infection, where ferritin and lactoferrin production is increased, soluble iron concentrations can dip even lower[55, 56]. Most iron in mammals is bound in heme containing proteins (e.g. hemoglobin, myoglobin) and iron transport proteins (e.g. lactoferrin, transferrin, ferritin). Because of

such low iron availability in host environments, pathogenic bacteria have evolved multiple methods of iron uptake, the most prevalent being the production and secretion of siderophores [56-60].

1.3.1 Transferrin binding

Some pathogenic bacteria, notably members of the *Neisseraceae* and *Pasteurellaceae* genera, are able to acquire iron directly from the host by producing soluble transferrin binding proteins targeting host transferrins **(Figure 1-1, A)**. Transferrin binding proteins are able to extract the iron from the transferrin. The iron is transported across the outer membrane and subsequently periplasmic-protein-dependent transport systems transfer the iron from the periplasm into the cytoplasm [58].

1.3.2 Heme binding

Other pathogenic bacteria, including most diderms and *Pseudmonas aeruginosa*, are able to obtain required iron from hemes. These organisms are able to acquire hemes from the environment, either via heme binding directly to outer membrane receptors, or through the secretion of hemophores, heme carrier proteins, that are able to sequester heme from their host counterparts, and internalize it through TonB-dependent outer membrane receptors **(Figure 1-1, B)** [61-64].

1.3.3 Environment modification

Some facultative anaerobes, such as some *Listeria* species, are able to obtain iron by generating an acidic and anaerobic microenvironment around themselves that results in

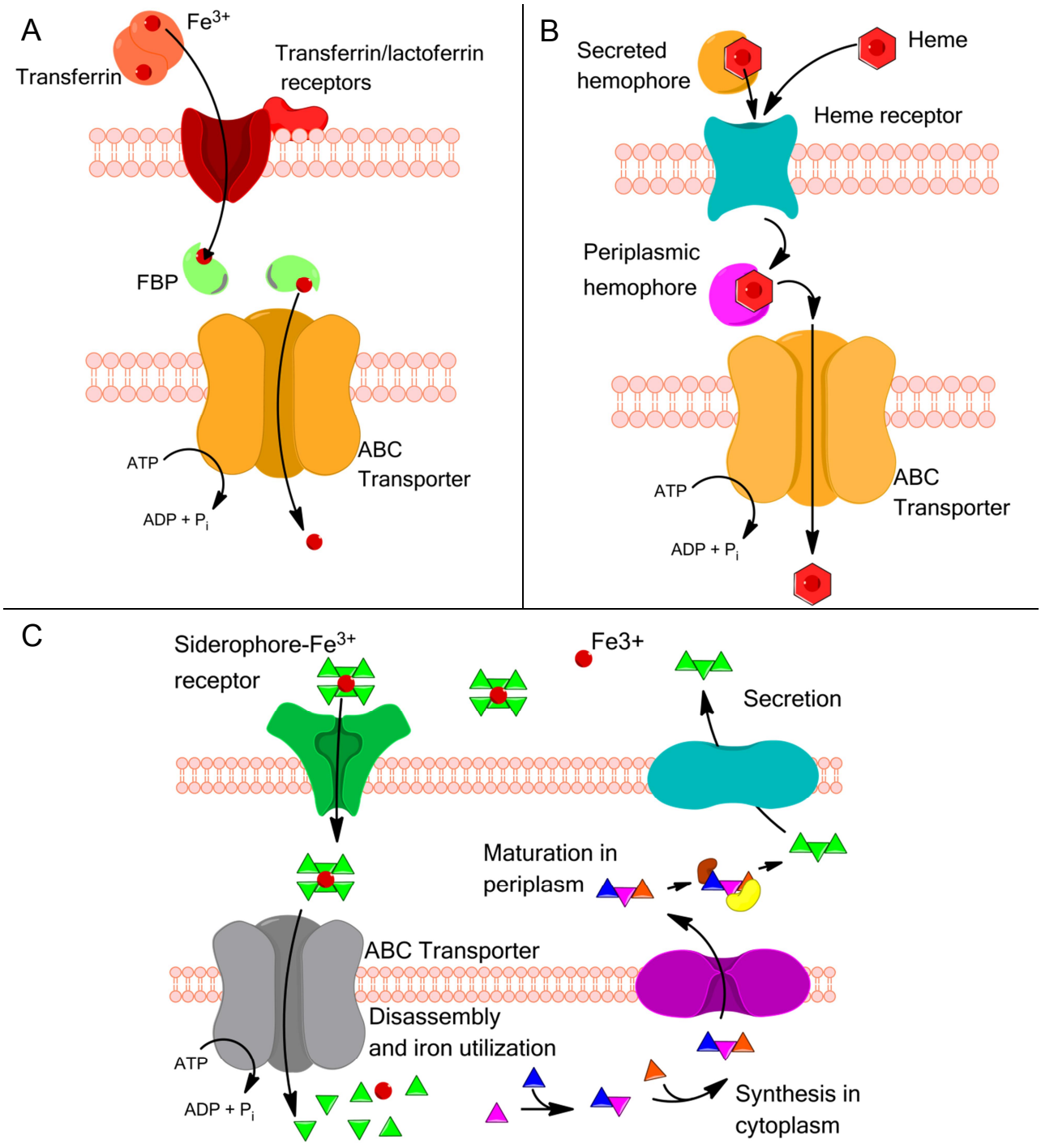

Figure 1-1: Iron uptake pathways in diderm bacteria. (A) Transferrin receptors recognize iron-bound transferrin, sequester and internalize the iron. (B) Heme intake occurs either through secreted hemophores or receptors recognizing free hemes. (C) Siderophore mediated iron uptake. Siderophores are synthesized in the cytoplasm, matured in the periplasm and secreted via specialized secretory channels. Iron-bound siderophores are recognized and internalized via siderophore receptors in the outer membrane. ABC transporters transport the iron-siderophore and the iron can be utilized.

the reduction of Fe^{3+} to Fe^{2+} in transferrins and lactoferrins, inducing iron release. The now soluble Fe^{2+} is actively transported into the cell [65, 66].

1.3.4 Siderophore mediated iron acquisition

Siderophore mediated iron acquisition is similar to the hemophore system in that it is based on a shuttle mechanism. However, the siderophore mediated iron acquisition system makes use of small compounds called siderophores with a high affinity for ferric iron (with Ka of 10^{20} – 10^{50} M) [67-70] **(Figure 1-1 C)**. In contrast to the hemophore system, siderophores are able to sequester ferric iron from a wide variety of host sources, including transferrins and lactoferrins (but interestingly, not hemes)[71]. Siderophore-dependent iron acquisition pathways can be found both in bacteria and yeast, and some plants are able to utilize siderophores secreted by other organism for their own iron acquisition[67, 71]. However, mammals do not have siderophore mediated iron acquisition pathways. Siderophore production mostly occurs during periods of iron starvation, when the intracellular iron concentration drops below the 10^{-6} M critical for microbial growth [72]. Secreted siderophores complex with Fe^{3+} and either the iron-bound siderophore is taken up by specific transporters, or siderophore-bound Fe^{3+} is reduced to Fe^{2+} by extracellular or membrane ferric-chelate reductases. Some bacteria (as well as some yeast and plants) possess the ability to uptake and use xenosiderophores: they possess ferric-chelate reductases or uptake systems for siderophores not synthesized by themselves [57, 62, 65, 73]. Iron that is not released outside of the cell or in the periplasm, is released by intracellular ferric-siderophore reductases or by ferric-siderophore hydrolases that disassemble the siderophore-iron complex[74]. However these mechanisms are not very well understood. It is uncertain

whether the iron can be used immediately by the bacterium once the siderophore-iron complex is disassembled, or if an intermediate storage step is required prior to usage [75].

1.3.4.1 Classes of siderophores

Siderophores are highly varied in structure. There are over 500 known siderophores that can be divided into three main classes depending on the nature of the moieties donating the oxygen ligands for Fe(III) coordination: **1.)** catecholates and phenolates that contain an aryl cap with carbonyl oxygens, **2.)** hydroxamates that contain a hydroxamic acid cap, **3.)** and (α-hydroxy-)carboxylates. A fourth "mixed-type" siderophore class groups all those siderophores with more than one type of iron binding moiety **(Figure 1-2)** [76].

1.3.4.2 Siderophore chemistry

Siderophores form tight and stable complexes with ferric iron. Fe^{3+} is a hard Lewis acid, and is thus strongly solvated in aqueous solution (forming an octahedral $Fe(H_2O)_6^{3+}$ complex). The siderophore donor oxygen groups replace the water molecule interactions, surrounding the Fe^{3+} in a hexacoordinated state with an octahedral geometry mimicking the geometry of the aqueous ion. A 1:1 complex or a 1:2 complex with Fe^{3+} is generally formed, depending on the number of coordinating oxygens in the siderophore iron binding pocket. Vacancies may be occupied by alternative oxygen donors such as water molecules. Or even the formation of mixed complexes[67-70].

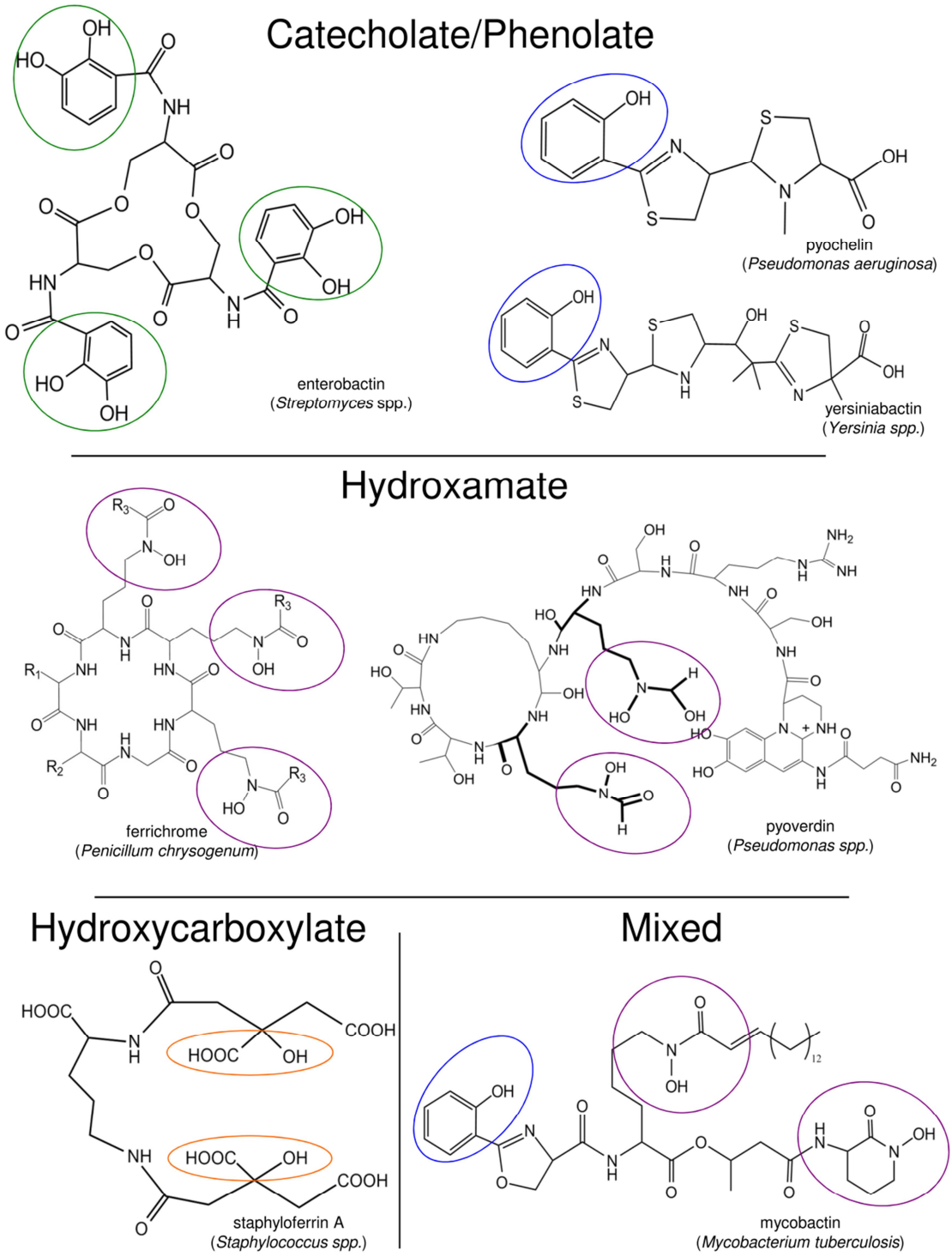

Figure 1-2: Types of siderophores: Siderophores can be classified into 4 categories: Catecholate/phenolate siderophores (siderophores with salicylate or catechol moieties), Hydroxamate siderophores (siderophores with hydroxamic acid iron binding moieties), hydroxycarboxylate siderophores (with (α-hydroxy-)carboxylates as iron binding moieties), and finally mixed siderophores containing more than one type of iron binding moiety in the structure.

1.3.4.3 Siderophore regulation

In bacteria, iron homeostasis, including siderophore gene regulation, is mediated by ferric uptake repressor Fur and various activators, including alternative sigma factors, two-component sensory transduction systems, and AraC-type regulators, which sense extra or intracellular Fe-siderophores [15].

1.3.4.4 Siderophore biosynthesis

Siderophores are generally comprised of a peptide backbone with a prevalence of non-proteogenic amino acids, with iron chelating moieties generated by accessory proteins forming the oxygen rich iron-binding core of the siderophore [72]. Although I will give a brief overview of siderophore biosynthesis and non-ribosomal peptide synthetases in the following paragraphs, more detailed comprehensive reviews of siderophore biosynthesis can be found in references [67, 71, 76, 77]. The peptide backbones of siderophores are nonribosomal peptides; nonribosomal peptide synthetases (NRPS) are responsible for the synthesis of these peptide backbones instead of ribosomes [76]. These enzymes enable peptide bond formation between amino acids that cannot be incorporated through ribosomal synthesis. NRPS's, originally identified as catalyzing the synthesis of antibiotics, are multi-modular enzymes that produce peptide products of a particular sequence without the need for an RNA template [78, 79]. Instead, the order of NRPS domains dictates the order of the amino acids in the peptide, essentially like an assembly line [78, 80]. The elongating chains are tethered via thiol groups, incorporated as phosphopantetheinyl arms bound to the NRPS via peptidyl carrier protein domains (PCPs). The NRPS assembly line runs via a multiple-thiol templating process, with the

phosphopantetheinyl-tethered peptide translocating down to the next carrier protein domain[78, 81].

The NRPS assembly complex is composed of autonomous domains, each of which carries out steps of monomer selection and activation, chain elongation, and chain termination. Each NRPS complex needs to carry out four kinds of catalytic operations. Typically, an elongation module of an NRPS assembly line has the three domains; peptidyl carrier protein (PCP), adenylation domain, and a catalytic condensation domain[78, 80]. First, the enzyme phosphopantetheinyl transferase (PPTase) catalyzes the post-translational modification of a serine through the addition of a phosphopantathenate (P-pant) moiety to a PCP domain side chain. Once the PCP domain is activated, an adenylation domain selects and activates the amino acids or other metabolites to be incorporated into the siderophore chain. The adenylation domains behave similarly to aminoacyl tRNA synthetases: the amino acid selected by the adenylation domain active site is converted to an activated aminoacyl-AMP using ATP as cosubstrate. The activated aminoacyl-AMP monomer is then tethered to the thio-pant-PCP domain to form an activated aminoacyl thioester (aminoacyl-S-PCP). The elongation step is carried out by the condensation domains of the NRPS. The peptide bond-forming step involves the peptidyl-S-PCP as the donor cosubstrate and the proximal downstream aminoacyl-S-PCP as the attacking acceptor substrate. The translocated chain grows by one peptide bond but is still tethered as a thermodynamically activated acyl-S-PCP, and is ready for another elongation cycle by the condensation domain of the next downstream module. Chain termination and

release of the full-length peptide requires chemical cleavage from the enzyme assembly line via a thioesterase found in the C-terminus of the NRPS[78-81].

1.4 Siderophores of *Pseudomonas aeruginosa*

Pseudomonas aeruginosa produces two siderophores, pyochelin and pyoverdin, produced via two distinct biosynthetic pathways.

1.4.1 Biosynthesis of pyochelin

Two biosynthetic operons, pchDCBA and pchEF, have been identified, clustered together in the chromosome with the pyochelin receptor gene *fptA* [82]. The products of these genes produce not only pyochelin, and precursor building blocks, dihidroaerugionate and salicylate. Both operons are repressed by the Fur protein in the presence of iron, and autoregulated by a positive-feedback loop requiring transcriptional regulator PchR. The *pchR* gene is located between the two biosynthetic operons[83].

In the initial steps of pyochelin biosynthesis, salicylate is made from chorismate (derived from the shiikimate pathway) via isochorismate **(Figure 1-3, A) [83]**. Production of salicylate from chorismate is catalyzed by two accessory enzymes. PchA, an isochorismate synthase, catalyzes the chorismate to isochorismate reaction. Isochorismate-pyruvate lyase PchB subsequently breaks down the isochorismate to produce salicylate and pyruvate[83-85]. L-cysteine the other precursor building block, is adenylated by the adenylation domain of PchE (an NRPS), and tethered to PchE via a

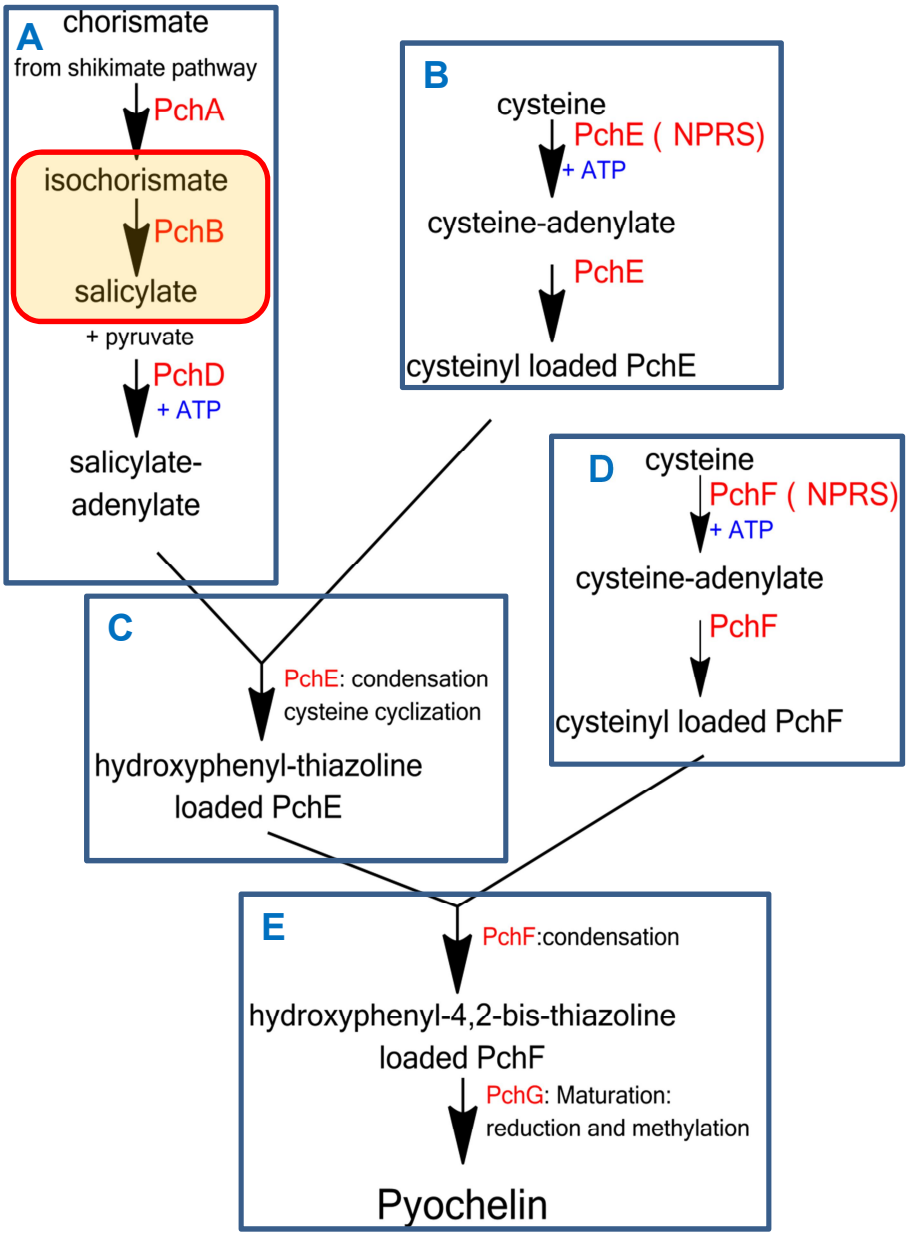

Figure 1-3: Pyochelin Biosynthesis in *P. aeruginosa*: **(A)** Enzymes PchA and PchB generate salicylate from chorismate, which is subsequently adenylated by PchD. **(B)** PchE, an NRPS, loaded with activated cysteine, catalyzes the condensation of the salicylate-adenylate with the cysteine, and the cyclization of the cysteine **(C)** to form hydroxyphenyl-thiazoline. **(D and E)** A second NRPS, PvdF, incorporates and cyclizes a second cysteine to the hydroxyphenyl-thiazoline to form pyochelin precursor hydroxyphenyl-4,2-bis-thiazoline, which upon release from PchF is reduced and methylated by maturation enzymes including PchG[83]. Red box identifies the focus chapters 2-5 of this dissertation. PchC (not shown) is a thioesterase hypothesized to play a role in proofreading and NRPS recycle [83]

PPT prosthetic group **(Figure 1-3, B)**. Salicylate is also adenylated by PchD and subsequently tethered to PchE **(Figure 1-3, C)** [83]. Subsequent cysteine cyclization and condensation reactions form a hydroxyphenyl-thiazoline intermediate, released by thioesterase PchC to form hydroxyphenyl-thiazolinyl-carboxylate. PchF, another NRPS, adenylates a second molecule of L-cysteine and catalyzes the condensation of the hydroxyphenyl-thiazolinyl-carboxylate intermediate with cysteinyl-*S*-PchF and generates the second thiazoline ring **(Figure 1-3, D)** [83]. The hydroxyphenyl-4,2-bis-thiazoline backbone undergoes reduction and methylation before biosynthesis is terminated and pyochelin is released from PchF via cleavage of the remaining thioester bond **(Figure 1-3, E)** releasing pyochelin **(Figure 1-4)** [83].

1.4.2 Biosynthesis of Pyoverdin

Pyoverdin synthesis has been studied in most detail in the *P. aeruginosa* strain PAO1 [86]. Synthesis of pyoverdin requires four NRPSs: PvdL, PvdI, PvdJ and PvdD[86]. Based on the order of amino acids in pyoverdin, the transfer of intermediates occurs sequentially from PvdL through PvdI and PvdJ to PvdD. Pyoverdin synthesis starts with PvdL, which incorporates L-Glu, D-Tyr and L-Dab (generated by accessory enzyme PvdH, **Figure 1-5, A**) into a precursor peptide. L-Dab and D-Tyr are condensed to a tetrahydropyrimidine ring and then modified to form the dihydroxyquinoline chromophore. PvdI and PvdJ elongate the peptide backbone, via the sequential addition of D-Ser, L-Arg, D-Ser, and N^5-formy, N^5-hydroxyornithine (fOHOrn) by PvdI, and L-Lys and fOHOrn by PvdJ **(Figure1-5, C)** [86, 87]. N^5-formyl,N^5-hydroxyornithine is generated through the hydroxylation of ornithine to N^5-hydroxyornithine by FAD-dependent ornithine hydroxylase (PvdA) and formylation by

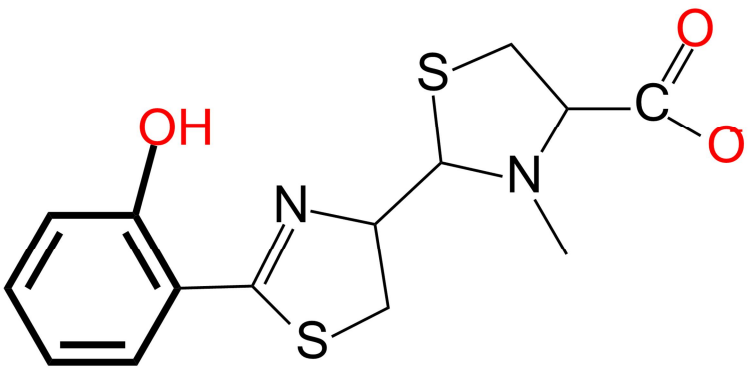

Figure 1-4: Structure of Pyochelin from *Pseudomonas aeruginosa* strain PAO1. Pyochelin is composed of two cyclized cysteines and a salicylate moiety (in bold). It has two iron binding moieties (in red), and therefore hexacoordinated Fe^{3+} has to coordinate with two pyochelin molecules in order to form a stable complex.

hydroxyornithine transformylase PvdF **(Figure 1-5 B)**[86, 87]. L-Serine is epimerized to D-Serine via the epimerase domain found in PvdI prior to incorporation onto the backbone. Finally, PvdD adds two threonines to the backbone, completing the immature peptide **(Figure 1-5, C and D)**. Although synthesis of the immature peptide occurs in the cytoplasm, there is evidence to suggest that the immature peptide is transported to the periplasm with the help of PvdE and PvdM, via ABC transporters, and it is in the periplasm, with the help of accessory enzymes PvdG, PvdO, PvdP, PvdQ and PvdN, that the mature Pyoverdin is formed **(Figure 1-6)** [86, 87].

1.5 Siderophore Biosynthesis: Implications for Drug Discovery

Targeting siderophore biosynthesis for antimicrobial drug discovery offers multiple advantages. First and foremost, siderophore biosynthetic pathways are very specific to bacteria and fungi, but not mammals. Inhibitors developed to target siderophore biosynthetic pathways have a lower chance of inhibiting human pathways as secondary targets. Although over 500 siderophores have been identified, these can be classified into 4 discrete groups each of which share common biosynthetic pathways. Inhibitors developed to target a specific biosynthetic pathway are likely to inhibit homologous pathways in other organisms. While reducing virulence and reducing growth rate, inhibition of siderophore biosynthesis does not kill the bacteria, reducing pressure on the bacterial population to evolve mechanisms against the inhibitors, preventing development of resistance. Likewise, these inhibitors would offer new targets for which the bacteria have yet to develop resistance.

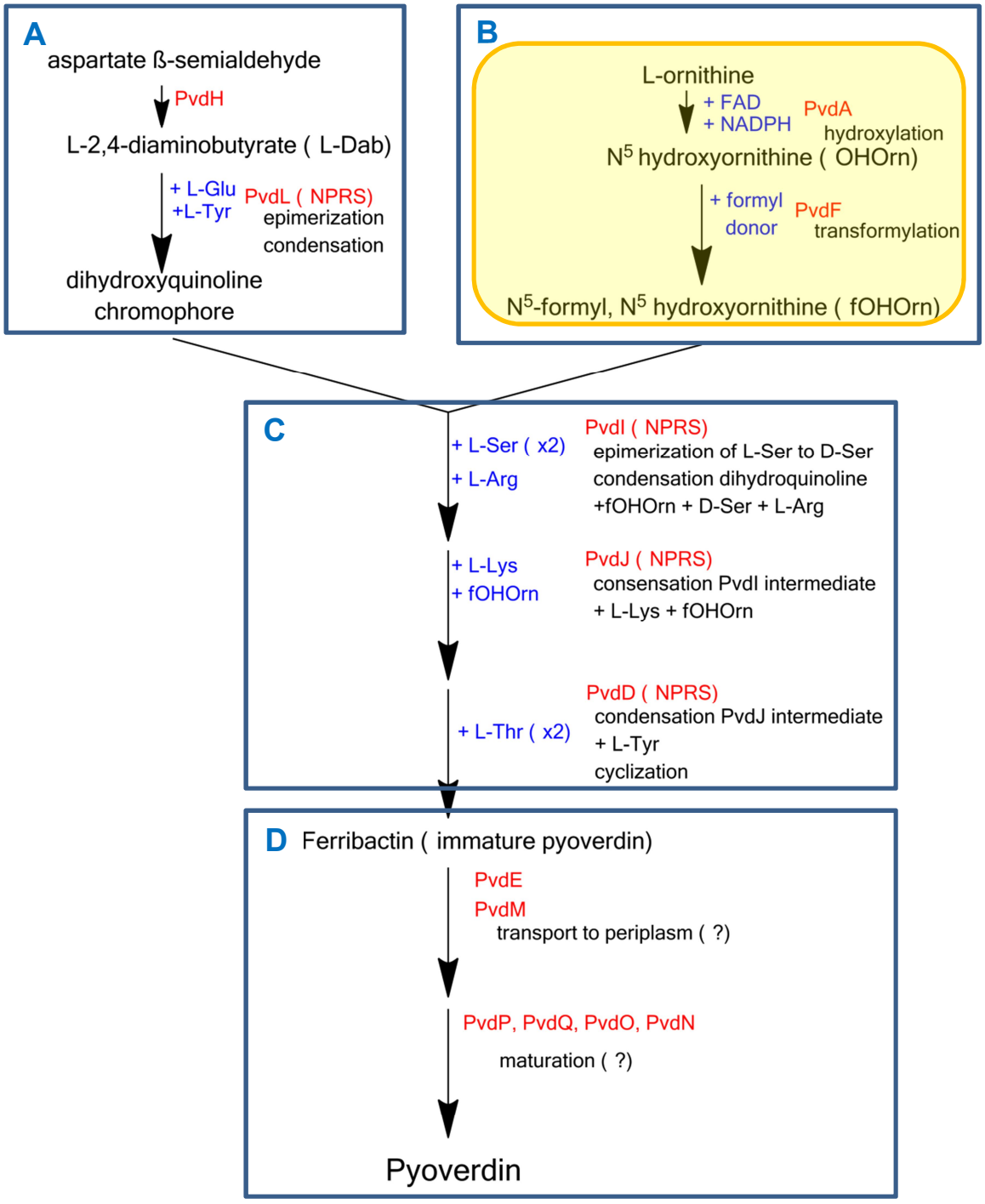

Figure 1-5: Pyoverdin Biosynthesis: (A) L-Dab generated by PvdH, L-Glu and L-Tyr are condensed by NRPS PvdL to form the dyhydroxyquinolone chromophore intermediate. **(B)** PvdA hydroxylates ornithine, and PvdF transformylates the PvdA product to form N^5-formyl-N^5-hydroxyornithine (fOHOrn) with the iron binding hydroxamate moiety. **(C)** Precursors are assembled by NRPSs PvdI, PvdJ and PvdD to form the backbone of the Pyoverdin (Ferribactin). **(D)** Ferribactin is exported to the periplasm, where maturation enzymes reduce and methylate the ferribactin to form the mature pyoverdin. Yellow box indicates enzymes PvdA and PvdF, which are the focus of chapters 6-8 and Appendix.

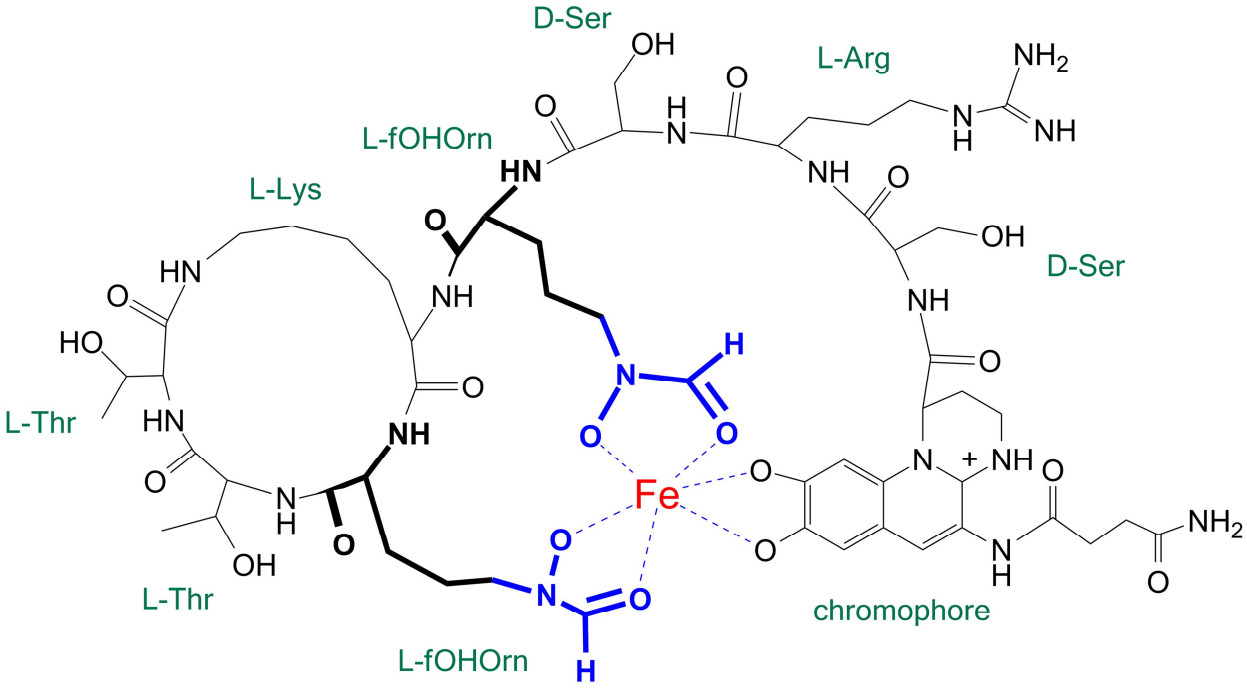

Figure 1-6. Structure of Pyoverdin from *Pseudomonas aeruginosa* strain PAO1. The pyoverdin backbone is assembled from amino acid building blocks assembled together by non-ribosomal peptide synthetases: the chromophore is assembled from L-Glu, D-Tyr and L-Dab. D-Ser, LArg, L-Lys, and L-Thr serve as the peptide backbone of the molecule, while the hydroxamates of L-fOHOrn serve as iron binding moieties.

1.6 References

1. Green, S.K., et al., *Agricultural Plants and Soil as a Reservoir for Pseudomonas aeruginosa.* Applied Microbiology, 1974. **28**(6): p. 987-991.

2. 2011; Available from: www.cdc.gov.

3. Fine, M.J., et al., *Prognosis and outcomes of patients with community-acquired pneumonia - A meta-analysis.* Jama-Journal of the American Medical Association, 1996. **275**(2): p. 134-141.

4. Grisaru-Soen, G., et al., *Pseudomonas aeruginosa bacteremia in children: analysis of trends in prevalence, antibiotic resistance and prognostic factors.* Pediatr Infect Dis J, 2000. **19**(10): p. 959-63.

5. Caselli, D., et al., *Multidrug resistant Pseudomonas aeruginosa infection in children undergoing chemotherapy and hematopoietic stem cell transplantation.* Haematologica, 2010. **95**(9): p. 1612-5.

6. Rodriguez-Rojas, A., A. Oliver, and J. Blazquez, *Intrinsic and environmental mutagenesis drive diversification and persistence of Pseudomonas aeruginosa in chronic lung infections.* J Infect Dis, 2012. **205**(1): p. 121-7.

7. Hoiby, N., *Microbiology of lung infections in cystic fibrosis patients.* Acta Paediatrica Scandinavica, 1982: p. 33-54.

8. Snydman, D.R., *Empiric antibiotic selection strategies for healthcare-associated pneumonia, intra-abdominal infections, and catheter-associated bacteremia.* Journal of Hospital Medicine, 2012. **7**: p. S2-S12.

9. Michalopoulos, A.S. and D.C. Karatza, *Multidrug-resistant Gram-negative infections: the use of colistin.* Expert Review of Anti-Infective Therapy, 2010. **8**(9): p. 1009-1017.

10. Knirel, Y.A., *Polysaccharide antigens of Pseudomonas aeruginosa.* Critical Reviews in Microbiology, 1990. **17**(4): p. 273-304.

11. Michelbriand, Y., B. Alkhalafhaddad, and M. Bonnin, *Pseudomonas aeruginosa and Antibiotics.* Bulletin De L Institut Pasteur, 1989. **87**(2): p. 125-170.

12. Salyers, A.A.W.D.D., *Bacterial pathogenesis : a molecular approach*. 1994, Washington, D.C.: ASM Press. xxvii, 418 p.

13. Palmer, K.L., S.A. Brown, and M. Whiteley, *Membrane-bound nitrate reductase is required for anaerobic growth in cystic fibrosis sputum.* Journal of Bacteriology, 2007. **189**(12): p. 4449-4455.
14. Klausen, M., et al., *Dynamics of development and dispersal in sessile microbial communities: examples from Pseudomonas aeruginosa and Pseudomonas putida model biofilms.* Fems Microbiology Letters, 2006. **261**(1): p. 1-11.

15. Poole, K. and G.A. McKay, *Iron acquisition and its control in Pseudomonas aeruginosa: Many roads lead to Rome.* Frontiers in Bioscience, 2003. **8**: p. D661-D686.

16. O'Toole, G.A. and R. Kolter, *Flagellar and twitching motility are necessary for Pseudomonas aeruginosa biofilm development.* Molecular Microbiology, 1998. **30**(2): p. 295-304.

17. Vanderwauven, C., et al., *Pseudomonas aeruginosa mutants affected in anaerobic growth of arginine - Evidence for a 4-gene cluster encoding the arginine deaminase pathway.* Journal of Bacteriology, 1984. **160**(3): p. 928-934.

18. Leahy, J.G. and R.R. Colwell, *Microbial Degradation of Hydrocarbons in the Environment* Microbiological Reviews, 1990. **54**(3): p. 305-315.

19. Ikonne, E. and O. Odozor, *Comparative Efficacy Of Topical Ciprofloxacin On Staphylococcus aureus and Pseudomonas aureginosa in vitro.* Journal of the Nigerian Optometric Association 2009. **15**.

20. Miyasaki, Y., et al., *In vitro activity of antibiotic combinations against multidrug-resistant strains of Acinetobacter baumannii and the effects of their antibiotic resistance determinants.* Fems Microbiology Letters, 2012. **328**(1): p. 26-31.

21. Nikaido, H. and J.M. Pages, *Broad-specificity efflux pumps and their role in multidrug resistance of Gram-negative bacteria.* Fems Microbiology Reviews, 2012. **36**(2): p. 340-363.

22. Piyakul, C., R. Tiyawisutsri, and K. Boonbumrung, *Emergence of metallo-beta-lactamase IMP-14 and VIM-2 in Pseudomonas aeruginosa clinical isolates from a tertiary-level hospital in Thailand.* Epidemiology and Infection, 2012. **140**(3): p. 539-541.

23. Zhong, L., et al., *Multidrug-resistant gram-negative bacterial infections after liver transplantation - Spectrum and risk factors.* Journal of Infection, 2012. **64**(3): p. 299-310.

24. Schwalbe, R.S.-M.L.G.A.C., *Antimicrobial susceptibility testing protocols*, 2007, CRC Press.
25. Walsh, C., *Antibiotics : actions, origins, resistance*, 2003, ASM Press.

26. Hou, J.P. and J.W. Poole, *Betal-Lactam Antibiotics - Their Physicochemical Properties and Biological Activities in Relation to Structure.* Journal of Pharmaceutical Sciences, 1971. **60**(4): p. 503-&.

27. Drawz, S.M. and R.A. Bonomo, *Three Decades of beta-Lactamase Inhibitors.* Clinical Microbiology Reviews, 2010. **23**(1): p. 160-+.

28. Barna, J.C.J. and D.H. Williams, *The Structure and Mode of Action of Glycopeptide Antibiotics of the Vancomycin Group.* Annual Review of Microbiology, 1984. **38**: p. 339-357.

29. Dickerhof, N., et al., *Bacitracin inhibits the reductive activity of protein disulfide isomerase by disulfide bond formation with free cysteines in the substrate-binding domain.* Febs Journal, 2011. **278**(12): p. 2034-2043.

30. Calvori, C., et al., *Effects of Rifamycin on Protein Synthesis.* Nature, 1965. **207**(4995): p. 417-&.

31. Floss, H.G. and T.W. Yu, *Rifamycin-mode of action, resistance, and biosynthesis.* Chemical Reviews, 2005. **105**(2): p. 621-632.

32. Skripkin, E., et al., *R chi-01, a new family of oxazolidinones that overcome ribosome-based linezolid resistance.* Antimicrobial Agents and Chemotherapy, 2008. **52**(10): p. 3550-3557.

33. Ament, P.W., N. Jamshed, and J.P. Horne, *Linezolid: Its role in the treatment of gram-positive, drug-resistant bacterial infections.* American Family Physician, 2002. **65**(4): p. 663-670.

34. Connell, S.R., et al., *Ribosomal protection proteins and their mechanism of tetracycline resistance.* Antimicrobial Agents and Chemotherapy, 2003. **47**(12): p. 3675-3681.

35. Shakil, S., et al., *Aminoglycosides versus bacteria - a description of the action, resistance mechanism, and nosocomial battleground.* Journal of Biomedical Science, 2008. **15**(1): p. 5-14.

36. Grunberger, D., J. Skoda, and F. Sorm, *The Mechanism of Antibiotic Action 5. Effect of Chloramphenicol, Chlorotetracycline and Oxytetracycline on the Synthesis of Glutamic Acid Decarboxyalse in Escherichia coli and of Tyrosine Decarboxylase in Streptococcus jaecalis* Collection of Czechoslovak Chemical Communications, 1955. **20**(2): p. 507-510.

37. Wisseman, C.L., *Mechanisms of Antimicrobial Action by Chloramphenicol.* Journal of Clinical Investigation, 1956. **35**(6): p. 745-745.

38. Tenson, T., M. Lovmar, and M. Ehrenberg, *The mechanism of action of macrolides, lincosamides and streptogramin B reveals the nascent peptide exit path in the ribosome.* Journal of Molecular Biology, 2003. **330**(5): p. 1005-1014.

39. Falagas, M.E., A.P. Grammatikos, and A. Michalopoulos, *Potential of old-generation antibiotics to address current need for new antibiotics.* Expert Review of Anti-Infective Therapy, 2008. **6**(5): p. 593-600.

40. Leclercq, R., et al., *In vitro activity of fusidic acid against streptococci isolated from skin and soft tissue infections.* Journal of Antimicrobial Chemotherapy, 2000. **45**(1): p. 27-29.

41. Azzam, M.E. and Algranat.Id, *Mechanism of Puromycin Action - Fate of Ribosomes After Release of Nascent Protein Chains From Polysomes.* Proceedings of the National Academy of Sciences of the United States of America, 1973. **70**(12): p. 3866-3869.

42. Farnham, A.E. and D.T. Dubin, *Studies On Mechanism of Action of Puromycin Aminonucleoside In L Cells.* Biochimica Et Biophysica Acta, 1967. **138**(1): p. 35-&.

43. Pestka, S., *Studies On Formation of Transfer Ribonucleic Acid - Ribosome Complexes .8. Survey of Effects of Antibiotics on N-Acetyl-Phenylalanyl-Puromycin Formation. Possible Mechanism of Chloramphenicol Action.* Archives of Biochemistry and Biophysics, 1970. **136**(1): p. 80-&.

44. Martin, N.I., et al., *Isolation, structural characterization, and properties of mattacin (Polymyxin M), a cyclic peptide antibiotic produced by Paenibacillus kobensis* Journal of Biological Chemistry, 2003. **278**(15): p. 13124-13132.

45. Heeb, S., et al., *Quinolones: from antibiotics to autoinducers.* Fems Microbiology Reviews, 2011. **35**(2): p. 247-274.

46. Wong, A. and R. Kassen, *Parallel evolution and local differentiation in quinolone resistance in Pseudomonas aeruginosa.* Microbiology-Sgm, 2011. **157**: p. 937-944.

47. Gale, E.F., *The Molecular basis of antibiotic action*. 1972, London: New York, Wiley. xviii, 456 p. illus. 24 cm.

48. Falagas, M.E. and D.E. Karageorgopoulos, *Pandrug resistance (PDR), extensive drug resistance (XDR), and multidrug resistance (MDR) among gram-negative bacilli: Need for international harmonization in terminology.* Clinical Infectious Diseases, 2008. **46**(7): p. 1121-1122.

49. Poole, K., *Efflux-mediated multiresistance in Gram-negative bacteria.* Clinical Microbiology and Infection, 2004. **10**(1): p. 12-26.

50. Cornelis, P., *Pseudomonas : genomics and molecular biology*. 2008, Norfolk, UK: Caister Academic Press. vii, 244 p.

51. Weinberg, E.D., *Role of Iron in Host-Parasite Interactions.* Journal of Infectious Diseases, 1971. **124**(4): p. 401-&.

52. Payne, S.M. and R.A. Finkelstein, *Critical Role of Iron In Host-Bacterial Interactions* Journal of Clinical Investigation, 1978. **61**(6): p. 1428-1440.

53. Finkelstein, R.A., C.V. Sciortino, and M.A. McIntosh, *Role of Iron in Microbe-Host Interactions.* Reviews of Infectious Diseases, 1983. **5**: p. S759-S777.

54. Cartwright, G.E. and M.M. Wintrobe, *The Anemia of Infection 8: Chemical, Clinical, and Immunological Studies on the Products of Human Plasma Fractionation .39. The Anemia of Infection - Studies on the Iron Binding Capacity of Serum.* Journal of Clinical Investigation, 1949. **28**(1): p. 86-98.

55. Wintergerst, E.S., S. Maggini, and D.H. Hornig, *Contribution of selected vitamins and trace elements to immune function.* Annals of Nutrition and Metabolism, 2007. **51**(4): p. 301-323.

56. Letendre, E.D., *Iron-Metabolism During Infection and Neoplasia.* Cancer and Metastasis Reviews, 1987. **6**(1): p. 41-53.

57. Brown, J.S. and D.W. Holden, *Iron acquisition by Gram-positive bacterial pathogens.* Microbes and Infection, 2002. **4**(11): p. 1149-1156.

58. Cornelissen, C.N., *Transferrin-iron uptake by gram-negative bacteria.* Frontiers in Bioscience, 2003. **8**: p. D836-D847.

59. Ekins, A., et al., *Lactoferrin receptors in Gram-negative bacteria: Insights into the iron acquisition process.* Biometals, 2004. **17**(3): p. 235-243.

60. Stojiljkovic, I. and K. Hantke, *Hemin Uptake System of Yesrsinia enterocolitica - Similarities With Other TonB-Dependent Systems in Gram-negative Bacteria.* Embo Journal, 1992. **11**(12): p. 4359-4367.

61. Otto, B.R., A. Verweijvanvught, and D.M. Maclaren, *Transferrins and Heme-Compounds as Iron Sources For Pathogenic Bacteria.* Critical Reviews in Microbiology, 1992. **18**(3): p. 217-233.

62. Ratledge, C. and L.G. Dover, *Iron metabolism in pathogenic bacteria.* Annual Review of Microbiology, 2000. **54**: p. 881-941.

63. Wandersman, C. and I. Stojiljkovic, *Bacterial heme sources: the role of heme, hemoprotein receptors and hemophores.* Current Opinion in Microbiology, 2000. **3**(2): p. 215-220.

64. Zhu, W.M., A. Wilks, and I. Stojiljkovic, *Degradation of heme in gram-negative bacteria: the product of the hemO gene of Neisseriae is a heme oxygenase.* Journal of Bacteriology, 2000. **182**(23): p. 6783-6790.

65. Bullen, J.J., *The Significance of Iron in Infection.* Reviews of Infectious Diseases, 1981. **3**(6): p. 1127-1138.

66. Deneer, H.G. and I. Boychuk, *Reduction of Ferric Iron By Listeria monocytogenes and Other Species of Listeria.* Canadian Journal of Microbiology, 1993. **39**(5): p. 480-485.

67. Boukhalfa, H. and A.L. Crumbliss, *Chemical aspects of siderophore mediated iron transport.* Biometals, 2002. **15**(4): p. 325-339.

68. Dhungana, S., et al., *Fe(III) coordination properties of two new enterobactin synthetic analogs based on a saccharide platform.* Abstracts of Papers of the American Chemical Society, 2001. **221**: p. U744-U744.

69. Dhungana, S., et al., *Fe(III) coordination properties of two new saccharide-based enterobactin analogues: Methyl 2,3,4-tris-O-{N- 2,3-di(hydroxy)benzoyl-glycyl -aminopropyl}-alpha-D-glu copyranoside and methyl 2,3,4-tris-O-{N- 2,3-di-(hydroxy)-benzoyl -aminopropyl}-alpha-D-glucopyr anoside.* Inorganic Chemistry, 2001. **40**(27): p. 7079-7086.

70. Dhungana, S., P.S. White, and A.L. Crumbliss, *Crystal structure of ferrioxamine B: a comparative analysis and implications for molecular recognition.* Journal of Biological Inorganic Chemistry, 2001. **6**(8): p. 810-818.

71. Neilands, J.B., *Siderophores - Structure and Function of Microbial Iron Transport Compounds.* Journal of Biological Chemistry, 1995. **270**(45): p. 26723-26726.

72. Wandersman, C. and P. Delepelaire, *Bacterial iron sources: From siderophores to hemophores.* Annual Review of Microbiology, 2004. **58**: p. 611-647.

73. Braun, V. and H. Killmann, *Bacterial solutions to the iron supply problem.* Trends in Biochemical Sciences, 1999. **24**(3): p. 104-109.

74. Robinson, N.J., et al., *A ferric-chelate reductase for iron uptake from soils.* Nature, 1999. **397**(6721): p. 694-697.

75. Andrews, S.C., *Iron storage in bacteria.* Advances in Microbial Physiology, Vol 40, 1998. **40**: p. 281-351.

76. Miethke, M. and M.A. Marahiel, *Siderophore-based iron acquisition and pathogen control.* Microbiology and Molecular Biology Reviews, 2007. **71**(3): p. 413-+.

77. Ferguson, A.D., et al., *Siderophore-mediated iron transport: Crystal structure of FhuA with bound lipopolysaccharide.* Science, 1998. **282**(5397): p. 2215-2220.

78. Marahiel, M.A., T. Stachelhaus, and H.D. Mootz, *Modular peptide synthetases involved in nonribosomal peptide synthesis.* Chemical Reviews, 1997. **97**(7): p. 2651-2673.

79. Stachelhaus, T., et al., *Peptide bond formation in nonribosomal peptide biosynthesis - Catalytic role of the condensation domain.* Journal of Biological Chemistry, 1998. **273**(35): p. 22773-22781.

80. Stachelhaus, T. and M.A. Marahiel, *Modular Structure of Genes Encoding Multifunctional Peptide Synthetases Required for Nonribosomal Peptide Synthesis.* Fems Microbiology Letters, 1995. **125**(1): p. 3-14.

81. Schneider, A. and M.A. Marahiel, *Genetic evidence for a role of thioesterase domains, integrated in or associated with peptide synthetases, in non-ribosomal peptide biosynthesis in Bacillus subtilis.* Archives of Microbiology, 1998. **169**(5): p. 404-410.

82. Hoegy, F., M.N. Gwynn, and I.J. Schalk, *Susceptibility of Pseudomonas aeruginosa to catechol-substituted cephalosporin is unrelated to the pyochelin-Fe transporter FptA.* Amino Acids, 2010. **38**(5): p. 1627-1629.

83. Serino, L., et al., *Biosynthesis of pyochelin and dihydroaeruginoic acid requires the iron-regulated pchDCBA operon in Pseudomonas aeruginosa.* Journal of Bacteriology, 1997. **179**(1): p. 248-257.

84. Gaille, C., P. Kast, and D. Haas, *Salicylate biosynthesis in Pseudomonas aeruginosa - Purification and characterization of PchB, a novel bifunctional enzyme displaying isochorismate pyruvate-lyase and chorismate mutase activities.* Journal of Biological Chemistry, 2002. **277**(24): p. 21768-21775.

85. Serino, L., et al., *Structural Genes for Salicylate Biosynthesis From Chorismate in Pseudomonas aeruginosa.* Molecular & General Genetics, 1995. **249**(2): p. 217-228.

86. Visca, P., et al., *Metal Regulation of Siderophore Synthesis in Pseudomonas aeruginosa and Functional Effects of Siderophore-Metal Complexes.* Applied and Environmental Microbiology, 1992. **58**(9): p. 2886-2893.

87. Visca, P., L. Serino, and N. Orsi, *Isolation and Characterization of Pseudomonas aeruginosa Mutants Blocked in the Synthesis of Pyoverdin.* Journal of Bacteriology, 1992. **174**(17): p. 5727-5731.

Chapter 2: PchB Introduction

2.1 General Enzymology

For a reaction to happen, reactant molecules must have enough energy to be able to cross a potential energy barrier (activation energy). Depending on a variety of factors (temperature, pressure, recent collision history)[1, 2], different populations of molecules possess varying levels of energy. Some, but not all, of these populations, will have enough energy to cross the energy barrier for the reaction to occur. The lower the potential energy barrier to reaction, the more reactants have sufficient energy and, hence, the faster the reaction will occur. Small reductions in the potential energy barrier may result in significant increases in the rate of reaction. Enzymes behave as catalysts: they accelerate reactions by lowering potential energy barrier, as compared to the uncatalyzed reaction, without altering the chemical equilibrium between reactants and products. This increase in the rate of reaction (which can be as high as 10^{20} fold), allows reactions in biological systems to occur at a short enough timescale to support life [3].

2.1.1 Transition State Theory

Enzymes are able to increase rates of reactions by providing a reaction pathway with a transition state whose free energy of activation is lower than that of the uncatalyzed reaction, through binding of the substrate to the active site, and promoting and stabilizing the transition state (**Figure 2-1**) [4]. In order to do so, enzymes (E) bind their substrates (S) in the active site to form an enzyme-substrate complex (*ES*). Formation of the ES complex promotes the transition towards an activated, high energy state (transition state, $TS^{\ddagger}$)[5]. As bond breaking and bond forming events

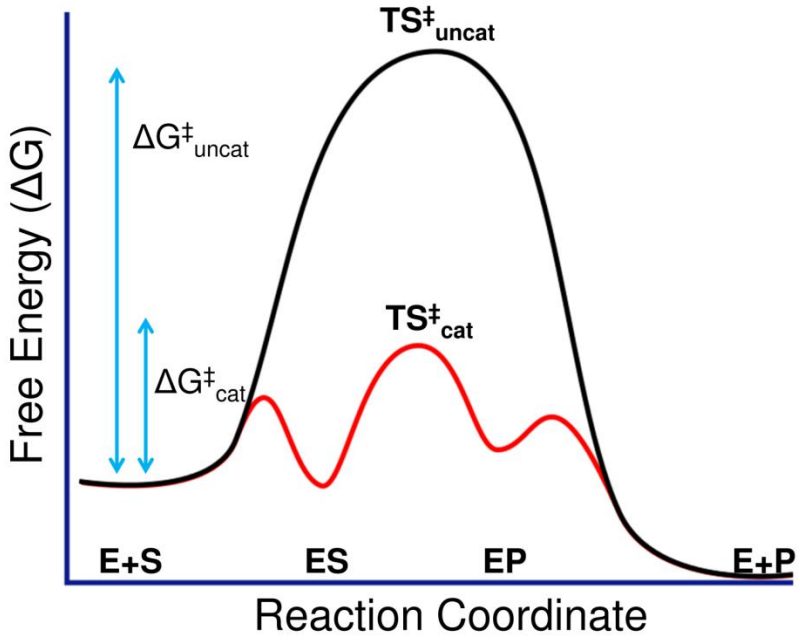

Figure 2-1: Reaction Coordinate. An example of a reaction coordinate diagram for the reaction

$$E + S \leftrightarrow ES \leftrightarrow TS^{\ddagger} \leftrightarrow EP \leftrightarrow E + P$$

The starting substrate is on the left, the product on the right. The free energy of the molecule is given by the black line (uncatalyzed reaction) and red line (catalyzed reaction). The transition state is the species with the highest free energy. The higher the free energy of the transition state, the slower the rate of the reaction. Formation of the ES complex through the binding of the substrate to the enzyme's active site promotes the formation of the transition state, lowering the free energy of activation.

occur, substrate converts into product in the active site (EP), which is then released (E + P). The enzyme-catalyzed reaction can thus be written as follows:

$$E + S \leftrightarrow ES \leftrightarrow TS^{\ddagger} \leftrightarrow EP \leftrightarrow E + P$$

2.1.2 Transition State

The transition state is the theoretical short lived, highest energy conformation of the molecule along the energy reaction coordinate [6]. It does not completely resemble substrate or product, as it is in a state in which bond breaking and bond forming events are simultaneously happening. Linus Pauling was the first to popularize Michael Polanyi's idea that enzymes lower the activation energy barrier by preferentially binding and stabilizing the transition state of a reaction [4]. The enzyme initially binds to the reactant through hydrophobic, electrostatic, or van der Waals interactions to form the ES complex. Binding of the substrate to the enzyme and the formation of the ES complex promotes the formation of the transition state by preorganizing the substrate, reducing entropy by reducing the degrees of freedom of the molecule, and bringing reactive groups closer to each other. Binding also involves the loss of the protective solvation sphere around the substrate, as hydrogen bonds between water and substrate are replaced by interactions with specific residues in the active site [4, 7-9].

2.1.3 Active Site

The reactive center of the enzyme, its active site, is the substrate binding pocket where residues are precisely positioned to provide specificity for the substrate as well as to

promote catalysis by providing reactive groups or by promoting the right microenvironment. Nucleophiles or acid/base residues provide chemically reactive groups, whereas hydrogen bond donors and acceptors, charged residues, and hydrophobic pockets create a microenvironment suitable to stabilize the transition state and promote catalysis. Shape and residue composition of the active site of the enzyme contribute to a set of mechanisms through which the enzyme is able to lower the energy of activation of the reaction. These mechanisms include entropy loss in ES formation, destabilization of ES due to strain, desolvation, or electrostatic effects; covalent catalysis; general acid or base catalysis; metal ion catalysis; and proximity and orientation. Usually, enzyme catalysis requires contributions from one or more of these mechanisms[10-12].

2.1.4 Mechanisms of Catalysis

2.1.4.1 Entropy loss and destabilization of ES complex

Raising the energy of the ES complex, either through a loss of entropy due to substrate binding or destabilizing the substrate due to strain, distortion or desolvation will increase the enzyme-catalyzed reaction rate[12]. The enzymatic rate is determined by the difference in energy between ES and $ES^{\ddagger}$. The smaller this difference, the faster the enzyme-catalyzed reaction [13]. The formation of the ES complex resulting from the binding of the substrate to the active site results in a highly organized complex as compared to E + S in solution (highly disordered), resulting in a net loss of entropy. Destabilization of the ES complex through structural strain, desolvation, or electrostatic effects is a consequence of the enzyme binding the transition state more

strongly than the substrate: because the substrate does not have the same shape as the transition state, when the substrate binds, the “induced fit” results in distortion or strain in the substrate, the enzyme, or both. Substrate binding in the active site results in desolvation of charged groups, which leads to higher reactivity of the substrate [12].

2.1.4.2 Covalent Catalysis

Enzymes are also able to derive catalytic power through formation of covalent bonds between enzyme and substrate[14].

For a given uncatalyzed reaction:

$$AX + Y \rightarrow AY + X$$

where “A” is the compound undergoing the reaction, “Y” is a nucleophillic attacking group and X is the leaving group, the theoretical enzymatic version of this reaction involving formation of a covalent intermediate would be described as:

$$E + AX \rightarrow EA + X + Y$$

$$EA + X + Y \rightarrow E + AY$$

where “E” is the enzyme, “AX” is one substrate of two chemical moieties (“A” and “X”), and “Y” is a second substrate. If the acceptor group on the enzyme is a better attacking group than Y and a better leaving group than X, the rate of the reaction will be increased [11, 14]. Typical nucleophilic centers for catalysis, such as amines, carboxylates, aryl and alkyl hydroxyls, imidazoles, and thiol groups, readily attack

electrophilic centers of substrates, forming covalently bonded enzyme-substrate intermediates (EA) [11, 13, 14]. Typical electrophilic centers in substrates would include phosphoryl groups, acyl groups, and glycosyl groups[13]. Covalent electrophilic catalysis usually involves coenzyme adducts that generate electrophilic centers[13].

2.1.4.3 Acid/Base Catalysis

There are two types of acid-base catalysis[13]. In specific acid-base catalysis, H+ and OH- ions accelerate the reaction[14]. In general acid-base catalysis, an acid or a base other than H+ or OH- accelerates the reaction. Side chains involved in acid-base catalysis are most commonly ionizable side chains with pKas near physiological pH values (*e.g.* histidine, which has an imidazole sidechain with a pKa of 6.1, is a good general acid or base) [14].

2.1.4.4 Metal Ion Catalysis

Metal-activated enzymes are enzymes that require a metal ion for catalysis. Metalloenzymes on the other hand are enzymes that require a metal ion for stability as well as for catalysis. Metal ions can be used by the enzyme as electrophilic catalysts, stabilizing an increased electron density or a developing negative charge during reactions. Metal ions also increase the acidity of a nucleophile, making it more reactive [11-13].

2.1.4.5 Proximity Effects

By bringing reactants closer together in the active site, enzymes are able to raise the reactants' "effective" concentration over that of the substrates in solution, resulting in an increased reaction rate. In addition to bringing reactants together, the enzyme also orients the reactive groups of the substrates, to encourage catalysis [11-13].

2.2 PchB

PchB is an accessory protein to the pyochelin biosynthetic pathway in *P. aeruginosa.* PchB is an isochorismate-pyruvate lyase, catalyzing the breakdown of isochorismate into salicylate and pyruvate[15].

2.2.1 Reactions Catalyzed by PchB

PchB catalyzes two pericyclic reactions (**Figure 2-2**). Physiologically, it catalyzes the breakdown of isochorismate into salycilate and pyruvate in a concerted but asynchronous pericyclic {1,5}-sigmatropic shift with a quantitative hydrogen transfer from C2 to C9 [16, 17] (**Figure 2-2, A**). PchB can also catalyze a non-physiological chorismate mutase reaction, a pericyclic Claisen rearrangement of chorismate to prephenate with a concerted but asynchronous {3,3}-sigmatropic transfer of the pyruvate tail from the C3 ether linkage to a C1-C9 linkage [18] (**Figure 2-2, B**). However, the chorismate mutase activity shows a much lower catalytic efficiency (isochorismate-pyruvate lyase k_{cat}/K_m of 4.11×10^4 $M^{-1}s^{-1}$ versus chorismate mutase k_{cat}/K_m of 1.96×10^2 $M^{-1}s^{-1}$ [19]).

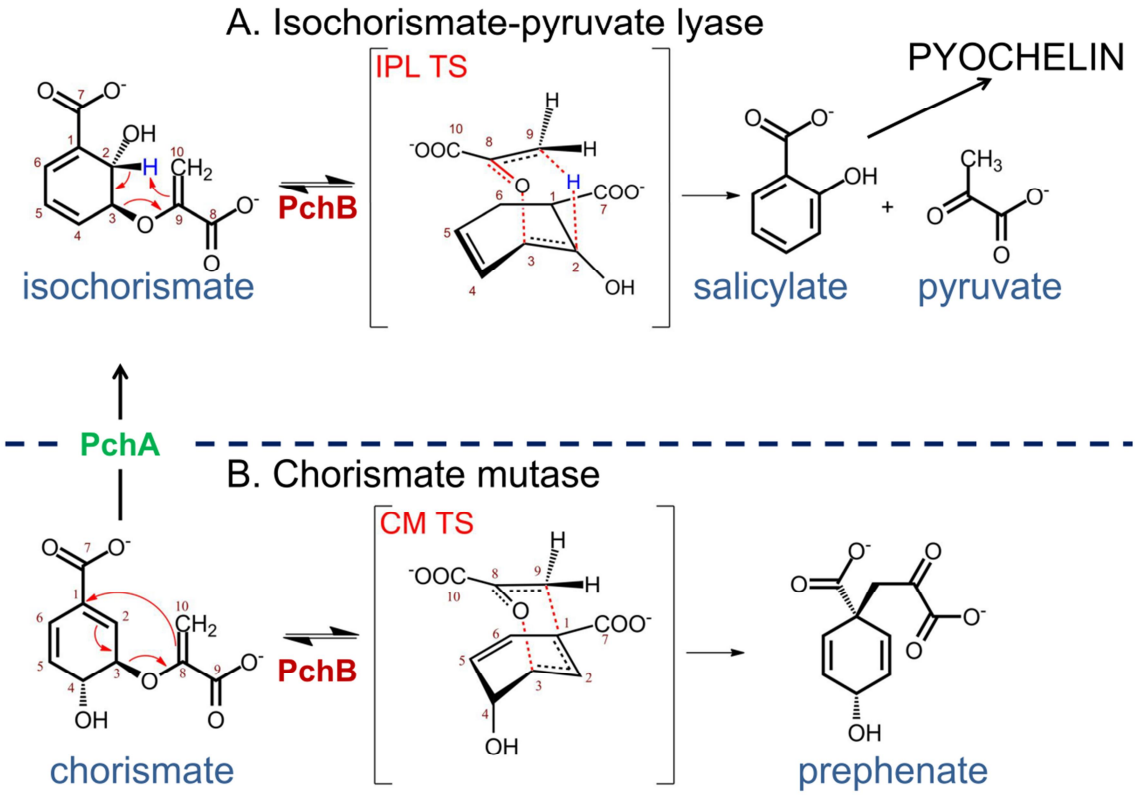

Figure 2-2: Reactions catalyzed by PchB. PchB catalyzes two pericyclic reactions: (A) an isochorismate-pyruvate lyase reaction, breaking down isochorismate to generate salicylate and pyruvate. The salicylate goes on as a precursor building block for pyochelin. (B) PchB is also able to catalyze a non-physiological chorismate mutase reaction, albeit significantly less efficiently than the lyase activity, generating prephenate from chorismate. The mutase pericyclic reaction and its transition state have been widely studied and are considered a standard reference in the field. However, the lyase transition state is somewhat unusual, in that it includes a hydrogen as part of the ring structure of the transition state. The chorismate precursor for both of these reactions is generated through the Shikimate pathway, part of the aromatic amino acid biosynthetic pathway [15]. Pericyclic reactions are unusual in nature, but PchB is able to catalyze two pericyclic reactions in the same active site, offering a unique opportunity for mechanistic enzymology.

2.2.2 Pericyclic Reactions

A pericyclic reaction is a type of reaction, usually a rearrangement, where the transition state of the molecule has a cyclic geometry, and the reaction progresses in a concerted (but not necessarily synchronous) fashion [20]. While pericyclic reactions are an important tool in organic synthetic chemistry [20], they are unusual in biological systems. Enzymatic pericyclic reactions do not require direct contribution from the enzyme [21, 22]. No protons or electrons are donated or accepted from enzyme or cofactors, and there are no covalent intermediates [21, 22]. Binding of the substrate to the active site leads to organization into a transition state, and product formation [22]. Since reactions do not require direct contribution from the enzyme, many traditional ideas (*e.g.* acid-base catalysis, covalent intermediates, metal ion catalysis) about enzyme catalysis do not apply.

Although the chorismate mutase reaction has been studied in detail, the isochorismate-pyruvate lyase reaction has a more unusual pericyclic transition state with a hydrogen atom forming part of the transition state cyclization event[23-25]. Traditional concepts regarding enzyme catalysis do not apply to pericyclic reactions, and there is an ongoing debate in the field regarding electrostatic stabilization of the transition state by the active site and the driving catalytic mechanism of the reaction. The ability of PchB to catalyze two pericyclic reactions in the same active site, makes this enzyme a very interesting candidate to study fundamental ideas of transition state theory. Moreover inhibitors for this class of enzymes have been found to be poor drug candidates due to low binding affinity[26]. Understanding the catalytic mechanism that underlies these reactions will help understand and improve drug design and development.

2.2.3 Structure of PchB

PchB is an intertwined alpha-helical dimer. Each monomer is composed of three alpha helices connected by loops [27] (**Figure 2-3**). There are two active sites per dimer and each active site contains catalytically important residues from both monomers [27] (**Figure 2-4**). PchB is a structural homolog of *E. coli* chorismate mutase and shares approximately 20% sequence similarity with the AroQ family of chorismate mutases [24] (**Figure 2-5**). In the only available structure of *E. coli* chorismate mutase an oxabicyclic transition state analog is bound in the active site[28]. This transition state analog is stabilized in the active site by eight charged or polar amino acids[28]. In PchB five of those residues (R14, R31, K42 R53 and Q90) are conserved [27, 28]. Therefore it is not surprising that PchB is able to catalyze the chorismate mutase reaction, albeit inefficiently.

One of these five residues, the lysine at position 42, homologous to lysine 39 in *E. coli* chorismate mutase, is located in the flexible active site loop that opens and closes upon substrate binding and product release[27]. This flexible loop has been found to be disordered in the crystal structures determined without ligand in the active site but ordered in structures were the ligand is bound in the active site [27] (**Figure 2-6**). Moreover, based on the ligand bound structures it has been hypothesized that the positive charge of the lysine at position 42 would be able to interact, and stabilize, the

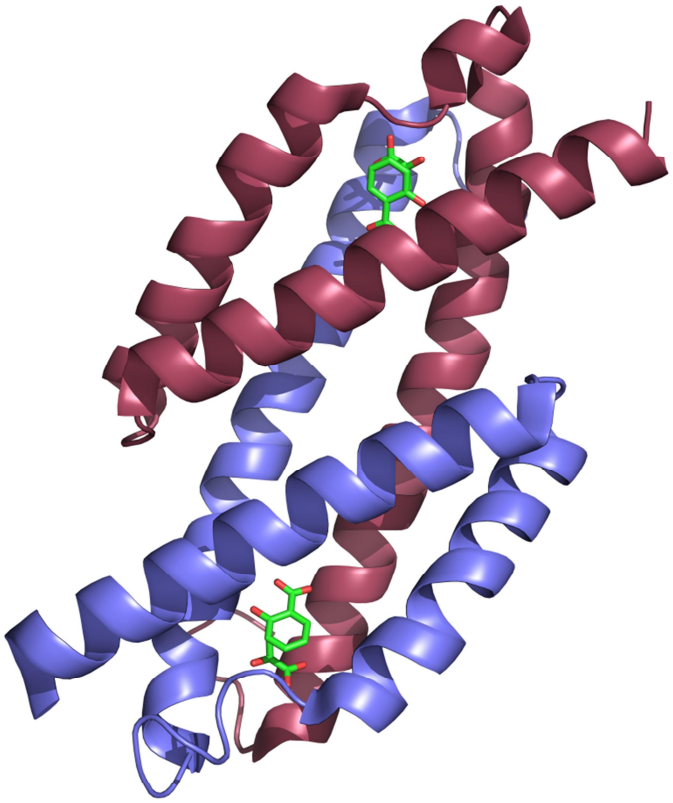

Figure 2-3: Structure of PchB with pyruvate and salicylate bound in the active site (PDB code 3REM, Olucha *et al Biochemistry, 2011*). PchB is an intertwined dimer, with monomers (displayed in raspberry red and purple) composed of 3 alpha helices connected by loops. There are two active sites per dimer containing residues from each monomer, and a flexible loop that has been proposed to open and close on the active site upon substrate binding and product release.

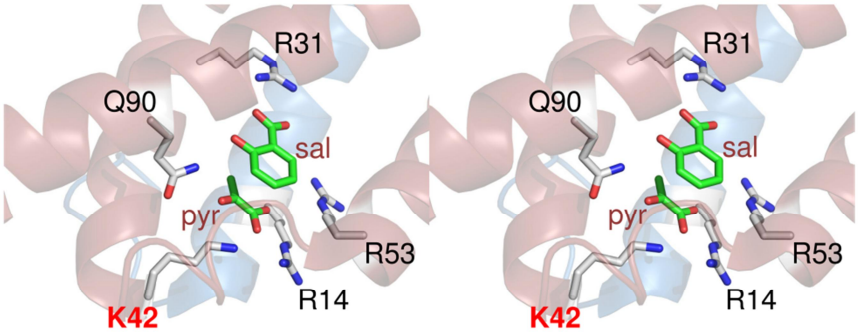

Figure 2-4. Stereo view of the PchB active site. There are 5 charged/polar residues in the PchB active site considered important for catalysis. Arginines 31, 53 and 14 from the second monomer, orient the substrate into the correct conformation in the active site, interacting with the carboxylates. The glutamine at position 90 and in particular the lysine at position 42 are poised to stabilize the developing negative charge of the ether oxygen at the transition state.

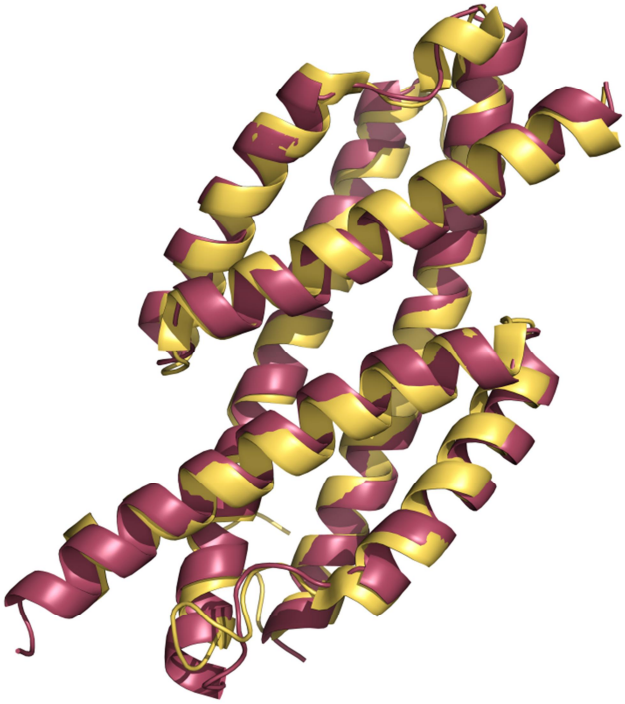

Figure 2-5: Overlay of *E. coli* Chorismate Mutase with PchB. *E. coli* chorismate mutase (*Ec*CM, PDB code 1ECM, burgundy red) shares about 20% sequence identity with PchB (PDB code 3REM, gold). A structural overlay of both enzymes shows that they are structurally also very similar, with an R.M.S.D. of 1.06 Å over 242 Cα (dimer).

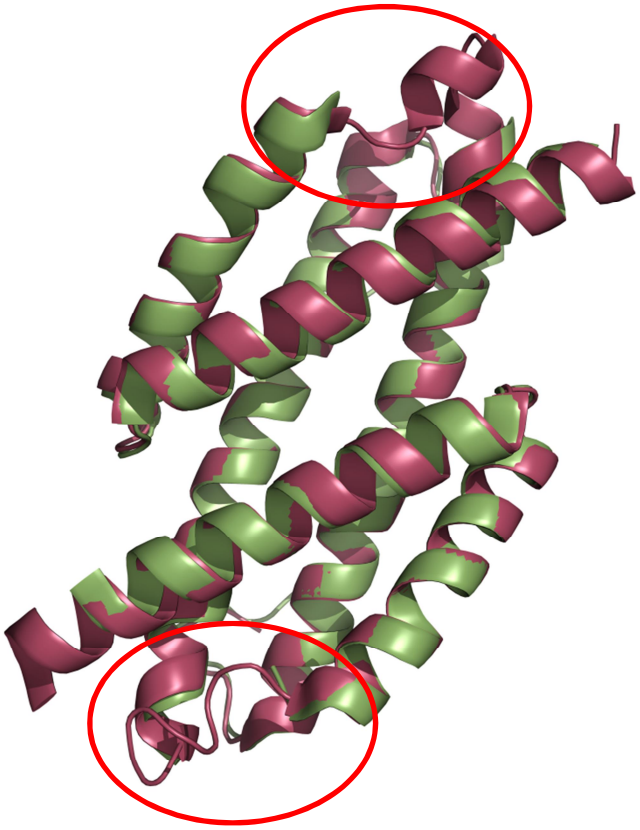

Figure 2-6: Overlay of structure of PchB without ligand in the active site and structure of PchB with salicylate and pyruvate in the active site. The active site flexible loop is flexible and highly mobile without ligand in the active site, but organizes upon ligand binding. Overlayed here are the “apo” (PDB code 2H9C, olive green) and salicylate and pyruvate bound (PDB code 3REM, burgundy red) wildtype PchB structures (without ligands for clarity). Circled in red, the active site loops. The active site loop of the “apo” structure (residues 42-49) could not be modeled for lack of density whereas it is very well defined and ordered in the ligand-bound structure.

partial negative charge of the ether oxygen at the transition state[24, 25, 27]. This hypothesis of electrostatic transition state stabilization juxtaposes to the hypothesis based on computational research done on *E. coli* chorismate mutase that suggests that only pre-organization of the substrate into a near attack conformation (NAC) is necessary for the reaction to occur. [29].

2.2.4 Electrostatic Transition State Stabilization.

Proponents of electrostatic transition state stabilization hypothesis argue that chorismate mutases, and by default PchB, derive their catalytic power from the stabilization of the transition state through complementary charges in the active site. One hypothesis to explain how chorismate mutases derive their catalytic power is electrostatic transition state stabilization (TSS). Biochemical and computational data from several chorismate mutases supports this hypothesis [18, 30-34]. Mutational and computational work performed on the chorismate mutase of the *Bacillus subtilis* supports this hypothesis. Removal of the positive charge of the arginine at position 90, homologous to the lysine at position 39 of *E. coli* chorismate mutase and the lysine at position 42 of PchB, severely impairs catalysis[30, 33, 34]. Proponents of the idea that this positive charge is not important for catalysis, argue that *Bacillus subtilis* chorismate mutase research is not relevant to *E. coli* chorismate mutase because they are not structurally homologous (belong to the AroH, not the AroQ family of chorismate mutases). Mutational analyses of position 39 in *E. coli* chorismate mutase also show abolishment or severe decrease in activity when the lysine positive charge is removed. However, circular dichroism spectra of these mutants shows a shoulder at 210nm,

indicating that the secondary structure of the enzyme is affected by these mutations[34, 35].

2.2.5 Near Attack Conformation

The near attack conformation hypothesis is supported by high level quantum mechanical/molecular mechanical (QM/MM) modeling simulations. This model predicts that the formation of a near attack conformation of the ligand while still at the substrate level is enough to lower the activation energy barrier and the reaction occurs spontaneously[36]. The near attack conformation is generally described as a structure in which the reacting atoms are within van der Waals contact and approach at an angle 15° to the bond that is formed, in an orientation in which the π-orbitals overlap[36]. This hypothesis predicts that once this conformation is achieved the reaction will occur spontaneously without electrostatic stabilization of the transition state or steric strain[36].

2.2.6 Combination of Both

A third hypothesis proposed by Dr. AJ Mulholland from the chemistry department at the University of Bristol suggests that neither model of electrostatic transition state stabilization nor near attack conformation is entirely correct but rather the catalytic power of chorismate mutases (his model was *B. subtilis* chorismate mutase) is derived from combination of both[37]. This hypothesis is supported by QM/MM calculations at high levels of QM theory and some of the mutational work performed in our lab. Our mutational work shows that the alanine mutant at position 42 of PchB still conserves 1% of both isochorismate-pyruvate lyase activity and chorismate mutase[38]. This indicates

that in spite of a lack of positive charge at that position catalysis can still happen. The research presented in this dissertation investigates the role of the positive charge at position 42 using mutational analysis, pH profiles, chemical rescue, and computational analyses.

2.3 References

1. Garcia-Viloca, M., et al., *How enzymes work: Analysis by modern rate theory and computer simulations.* Science, 2004. **303**(5655): p. 186-195.

2. van der Kamp, M.W. and A.J. Mulholland, *Computational enzymology: insight into biological catalysts from modelling.* Natural Product Reports, 2008. **25**(6): p. 1001-1014.

3. Jencks, W.P., *Catalysis in chemistry and enzymology*. McGraw-Hill series in advanced chemistry; Variation: McGraw-Hill series in advanced chemistry. 1969, New York: McGraw-Hill. xvi, 644 p. illus. 23 cm.

4. Pauling, L. and A.M. Soldate, *The Nature of the Bonds in the Iron Silicide Fesi and Related Crystals.* Acta Crystallographica, 1948. **1**(1-6): p. 212-216.

5. Andrews, P.R., G.D. Smith, and I.G. Young, *Transition-state stabilization and enzymic catalysis. Kinetic and molecular orbital studies of the rearrangement of chorismate to prephenate.* Biochemistry, 1973. **12**(18): p. 3492-8.

6. Schramm, V.L., *Enzymatic transition states and transition state analog design.* Annual Review of Biochemistry, 1998. **67**: p. 693-720.

7. Radzicka, A. and R. Wolfenden, *A Proficient Enzyme.* Science, 1995. **267**(5194): p. 90-93.

8. Radzicka, A. and R. Wolfenden, *Transition-State and Multisubstrate Analog Inhibitors.* Enzyme Kinetics and Mechanism, Pt D, 1995. **249**: p. 284-312.

9. Xiang, S.B., et al., *Transition-State Selectivity for a Single Hydroxyl Group during Catalysis by Cytidine Deaminase.* Biochemistry, 1995. **34**(14): p. 4516-4523.

10. Lehninger, A.L., *Biochemistry : the molecular basis of cell structure and function*. 2d ed. 1975, New York: Worth Publishers. xxiii, 1104 p.

11. Lehninger, A.L., *Principles of biochemistry*. 1982, New York, N.Y.: Worth Publishers. xxiv, 1011 p.

12. Voet, D.V.J.G., *Biochemistry*, 1995, J. Wiley & Sons.

13. Garret, R.H. and C.M. Grisham, *Biochemistry*. Second ed. 2004, Belmont, CA: Thomson Brooks/Cole.

14. Voet, D.V.J.G., *Biochemistry*, 2004, Hoboken, NJ : J. Wiley & Sons. p. xv, 1591 : ill. (some col.) ; 29 cm. + 1 CD-ROM (4 3/4 in.).

15. Gaille, C., P. Kast, and D. Haas, *Salicylate biosynthesis in Pseudomonas aeruginosa - Purification and characterization of PchB, a novel bifunctional enzyme displaying isochorismate pyruvate-lyase and chorismate mutase activities.* Journal of Biological Chemistry, 2002. **277**(24): p. 21768-21775.

16. DeClue, M.S., et al., *Isochorismate Pyruvate Lyase: A Pericyclic Reaction Mechanism?* J. Am. Chem. Soc., 2005. **127**(43): p. 15002-15003.

17. Marti, S., et al., *Mechanism and plasticity of isochorismate pyruvate lyase: a computational study.* J. Am. Chem. Soc., 2009. **131**(44): p. 16156-61.

18. Gustin, D.J., et al., *Heavy Atom Isotope Effects Reveal a Highly Polarized Transition State for Chorismate Mutase.* J. Am. Chem. Soc., 1999. **121**(8): p. 1756-1757.

19. Luo, Q., J. Olucha, and A.L. Lamb, *Structure-function analyses of isochorismate-pyruvate lyase from Pseudomonas aeruginosa suggest differing catalytic mechanisms for the two pericyclic reactions of this bifunctional enzyme.* Biochemistry, 2009. **48**: p. 5239-5245.

20. Pindur, U. and G.H. Schneider, *Pericyclic Key Reactions in Biological Systems and Biomimetic Syntheses.* Chemical Society Reviews, 1994. **23**(6): p. 409-415.

21. Acevedo, O. and W.L. Jorgensen, *Advances in Quantum and Molecular Mechanical (QM/MM) Simulations for Organic and Enzymatic Reactions.* Accounts of Chemical Research, 2010. **43**(1): p. 142-151.

22. Tantillo, D.J., J.G. Chen, and K.N. Houk, *Theozymes and compuzymes: theoretical models for biological catalysis.* Current Opinion in Chemical Biology, 1998. **2**(6): p. 743-750.

23. Ferrer, S., et al., *Molecular mechanism of chorismate mutase activity of promiscuos MbtI.* Theoretical Chemistry Accounts, 2011. **128**(4-6): p. 601-607.

24. Lamb, A.L., *Pericyclic Reactions Catalyzed by Chorismate-Utilizing Enzymes.* Biochemistry, 2011. **50**(35): p. 7476-7483.

25. Luo, Q.Y., K.M. Meneely, and A.L. Lamb, *Entropic and Enthalpic Components of Catalysis in the Mutase and Lyase Activities of Pseudomonas aeruginosa PchB.* Journal of the American Chemical Society, 2011. **133**(18): p. 7229-7233.

26. DeClue, M.S., et al., *Isochorismate pyruvate lyase: A pericyclic reaction mechanism?* Journal of the American Chemical Society, 2005. **127**(43): p. 15002-15003.

27. Zaitseva, J., et al., *Two crystal structures of the isochorismate pyruvate lyase from Pseudomonas aeruginosa.* Journal of Biological Chemistry, 2006. **281**(44): p. 33441-9.

28. Lee, A.Y., et al., *Atomic Structure of the Buried Catalytic Pocket of Escherichia coli Chorismate Mutase.* Journal of the American Chemical Society, 1995. **117**(12): p. 3627-3628.

29. Zaitseva, J., et al., *Two crystal structures of the isochorismate pyruvate lyase from Pseudomonas aeruginosa.* J. Biol. Chem., 2006. **281**(44): p. 33441-9.

30. Cload, S.T., et al., *Mutagenesis Study of Active Site Residues in Chorismate Mutase from Bacillus subtilis.* J. Am. Chem. Soc., 1996. **118**(7): p. 1787-1788.

31. Kast, P., et al., *Exploring the active site of chorismate mutase by combinatorial mutagenesis and selection: the importance of electrostatic catalysis.* Proc. Natl. Acad. Sci. U.S.A., 1996. **93**(10): p. 5043-8.

32. Kast, P., et al., *A strategically positioned cation is crucial for efficient catalysis by chorismate mutase.* J. Biol. Chem., 2000. **275**(47): p. 36832-8.

33. Kienhofer, A., P. Kast, and D. Hilvert, *Selective stabilization of the chorismate mutase transition state by a positively charged hydrogen bond donor.* J. Am. Chem. Soc., 2003. **125**(11): p. 3206-7.

34. Liu, D.R., et al., *Analysis of Active Site Residues in Escherichia coli Chorismate Mutase by Site-Directed Mutagenesis.* J. Am. Chem. Soc., 1996. **118**(7): p. 1789-1790.

35. Hur, S. and T.C. Bruice, *The mechanism of catalysis of the chorismate to prephenate reaction by the Escherichia coli mutase enzyme.* Proc. Natl. Acad. Sci. U.S.A., 2002. **99**(3): p. 1176-81.

36. Hur, S. and T.C. Bruice, *The near attack conformation approach to the study of the chorismate to prephenate reaction.* Proceedings of the National Academy of Sciences of the United States of America, 2003. **100**(21): p. 12015-12020.

37. Lyne, P.D., A.J. Mulholland, and W.G. Richards, *Insights Into Chorismate Mutase Catalysis From a Combined QM/MM Simulation of the Enzyme Reaction.* Journal of the American Chemical Society, 1995. **117**(45): p. 11345-11350.

38. Luo, Q., J. Olucha, and A.L. Lamb, *Structure-function analyses of isochorismate-pyruvate lyase from Pseudomonas aeruginosa suggest differing catalytic mechanisms for the two pericyclic reactions of this bifunctional enzyme.* Biochemistry, 2009. **48**(23): p. 5239-45.

Chapter 3: pH Dependence of PchB Catalysis

The work discussed in this chapter has been published as the following research articles:

Luo, Q., **J. Olucha**, and A.L. Lamb, *Structure-function analyses of isochorismate-pyruvate lyase from Pseudomonas aeruginosa suggest differing catalytic mechanisms for the two pericyclic reactions of this bifunctional enzyme.* Biochemistry, 2009. **48**: p. 5239-5245.

and

Olucha, J., et al., *pH Dependence of catalysis by Pseudomonas aeruginosa isochorismate-pyruvate lyase: implications for transition state stabilization and the role of lysine 42.* Biochemistry, 2011. **50**(33): p. 7198-207.

3.1 Introduction

PchB is an isochorismate-pyruvate lyase. Its physiological function is to catalyze the breakdown of isochorismate into salicylate and pyruvate[1]. As described in Chapter 2, the salicylate produced by PchB is incorporated into the siderophore pyochelin via non-ribosomal peptide synthetases [2]. PchB is also able to catalyze a second non-physiological chorismate mutase reaction, generating prephenate from chorismate [1], albeit at a much lower catalytic efficiency. Both of these reactions are pericyclic: bond breaking and bond forming happen in a concerted fashion, resulting in a partially aromatic transition state with cyclic geometry [3-7]. The lyase reaction in PchB catalyzes a quantitative hydrogen transfer from **C2** to **C9 (Figure 3-1a)**, resulting in a somewhat unusual pericyclic transition state with a hydrogen forming part of the cyclic structure **(Figure 3-1a, IPL TS)** [3]. The chorismate mutase pericyclic reaction on the other hand, is a Claisen rearrangement of chorismate to prephenate, transferring the

a. isochorismate-pyruvate lyase

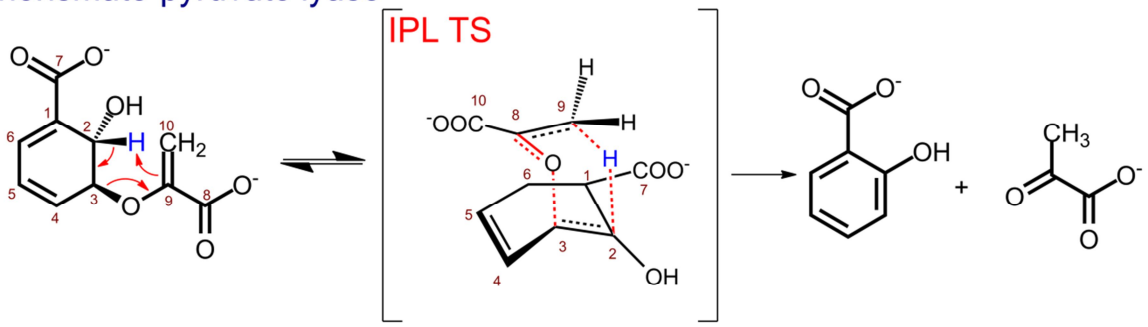

b. chorismate mutase

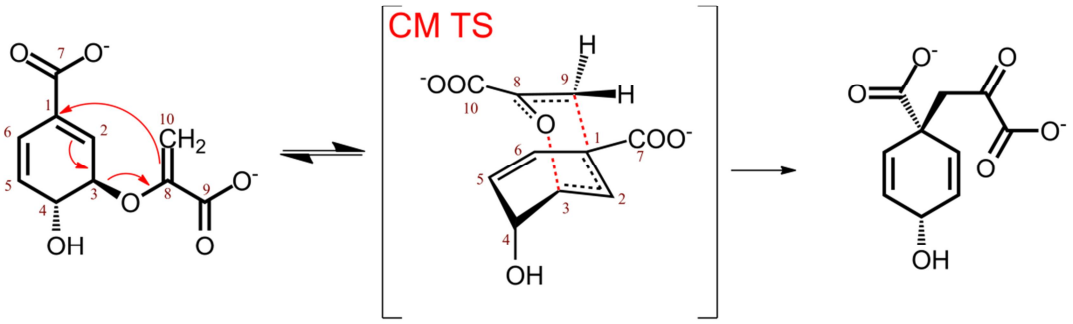

Figure 3-1: The two pericyclic reactions catalyzed by PchB: (a) isochorismate-pyruvate lyase is a quantitative hydrogen transfer from C2 to C9 and (b) chorismate mutase is a Claisen rearrangement with a shift of the enol-pyruvate tail from C3 to C1.

enolpyruvate tail from the C3 ether to a C1-C9 bond **(Figure 3-1b)**. The ability of PchB to catalyze two pericyclic reactions in the same active site makes this enzyme an interesting model to investigate the catalytic driving mechanism of pericyclic reactions.

As described in Chapter 2, there is an ongoing debate in the field regarding the mechanism driving pericyclic reactions. On one hand, it has been proposed that the enzyme's active site behaves as a vessel that orients the substrate into an orientation where reactive atoms are at van der Waals contact with each other and approach at an angle 15° to the bond that is to be formed, in an orientation in which the π-orbitals overlap[7-12]. On the other hand, it has also been proposed that it is not a near attack conformation but electrostatic stabilization of the transition state through the polar and charged residues in the active site which orient the substrate and stabilize the developing charges of the transition state **(Figure 3-2)** that drive the reaction forward [4-6, 13-19]**.** In *E. coli* chorismate mutase (EcCM), the structural homolog of PchB, lysine 39 was hypothesized to play such a role. In order to test the electrostatic transition state stabilization hypothesis, Liu and colleagues performed a mutational analysis of the active site in which mutations to the lysine 39 resulted in 106 fold loss in catalytic efficiency [16]. However, the mutation resulted in a circular dichroism spectrum slightly different from that of wild type, which indicated secondary structure was also affected by the mutation. Fortunately, mutations on the homologous residue in PchB (lysine 42) result in a similar loss of catalytic efficiency without disruption of secondary structure **(Figure 3-3a)** or active site architecture **(Figure 3-3b)** [20, 21]. Furthermore, the crystal

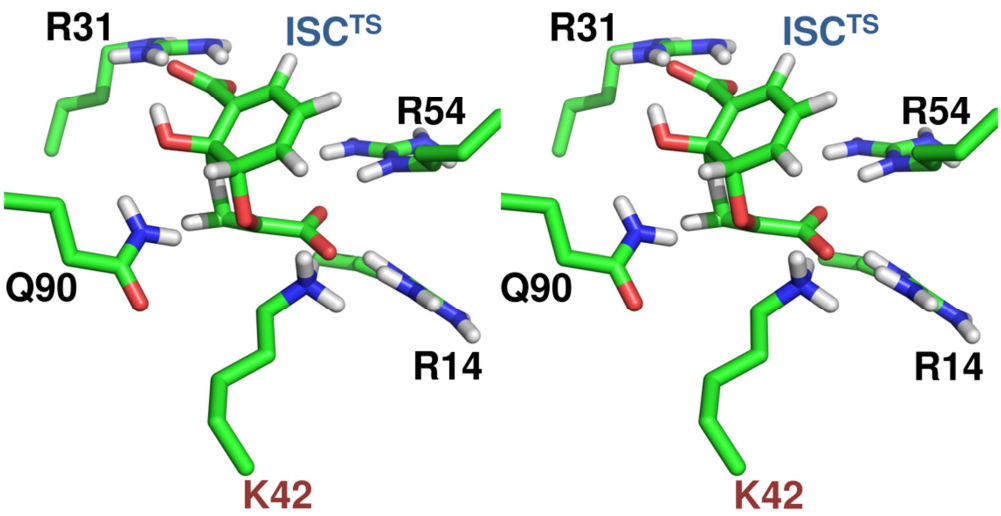

Figure 3-2: Stereo view of a snapshot of the PchB active site, from a QM/MM trajectory of the lyase reaction. The K42 is oriented such that the positive charge will stabilized the developing charge of the ether oxygen of the transition state. The QM/MM work will be presented in **Chapter 5**.

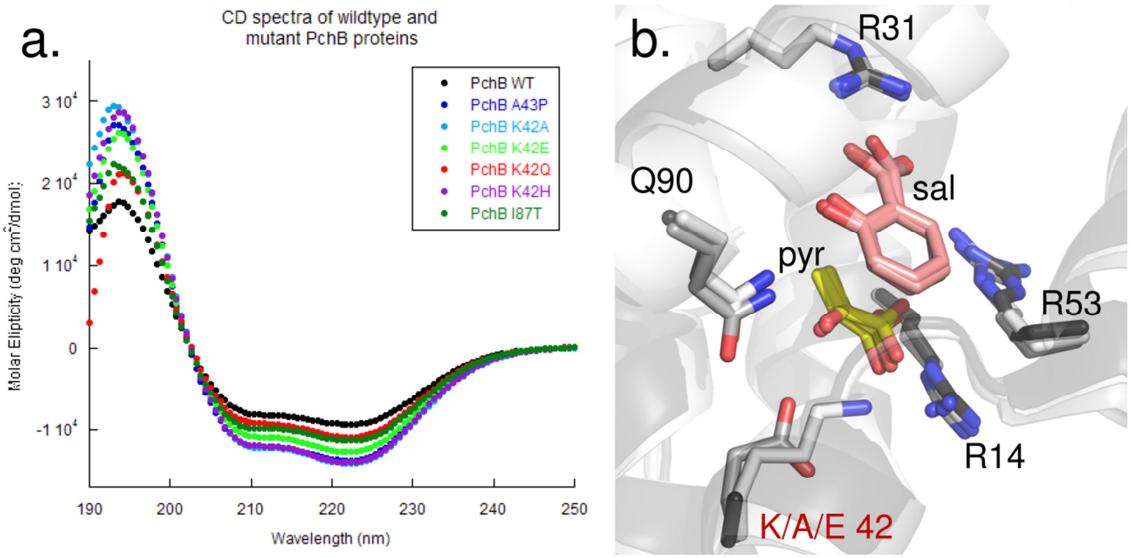

Figure 3-3: Mutations at position 42 do not affect secondary structure or architecture of the active site. (a) Circular dichroism spectra of mutants overlaid over wild type PchB [22]. All mutants display the same alpha-helical secondary structure. (b) Overlay of the active sites of wild type (white), K42E (light gray) and K42A (dark gray).

structure of wild type with two pyruvates in the active site shows lysine 42 hydrogen bonding with one of the pyruvate molecules and potentially poised to stabilize the developing negative charge of the ether oxygen in both lyase and mutase transition states **(Figure 3-3b)** [23]. For these reasons PchB is a good model to investigate the relative contributions of the near attack conformation and electrostatic transition state stabilization. In order to investigate the role of the positive charge of the lysine in both lyase and mutase activities, a lysine to histidine mutant was generated. Histidine is the only proteogenic amino acid with a side chain *pKa* value within physiological pH range (*pKa* = 6.1) [24]. Noting that the *pKa* value of the imidazole ring will be altered slightly depending on the environment [25], I hypothesized that below a pH value of 6, I would expect the histidine population shift towards both amino groups of the imidazole being protonated, and thus positively charged, whereas at pH value above 6, the histidine population would shift towards a neutral, unprotonated state **(Figure 3-4)** [24]. In PchB K42H, therefore I would expect to see pH indepence of both chorismate mutase and isochorismate-pyruvate lyase activites if charge-independent near attack conformation is a more important contributor to catalysis **(Figure 3-5a)**. On the other hand, if the contribution of the electrostatic transition state stabilization is more important for catalysis, I would expect to see pH dependence of both activities as pH increases above from the *pKa* value of histidine **(Figure 3-5b)**.

3.2 Materials and Methods

3.2.1 Protein preparation

Wild-type PchB without a histidine tag was prepared as previously described [26]. K42H-, K42A- and K42E-PchB were prepared as previously described [27].

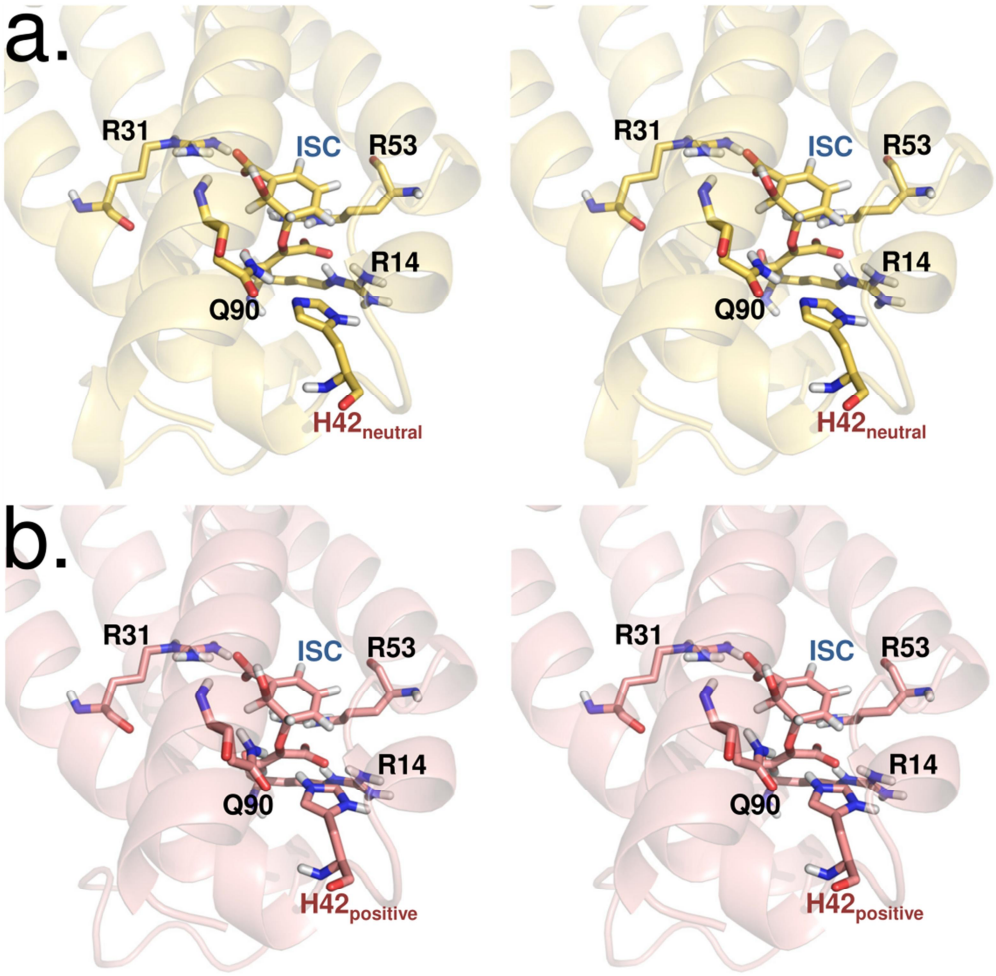

Figure 3-4: Stereo view of QM/MM model of PchB K42H active site. At higher pH, the deprotonated histidine will have a neutral charge (a). At lower pH, the histidine will be protonated and positively charged (b).

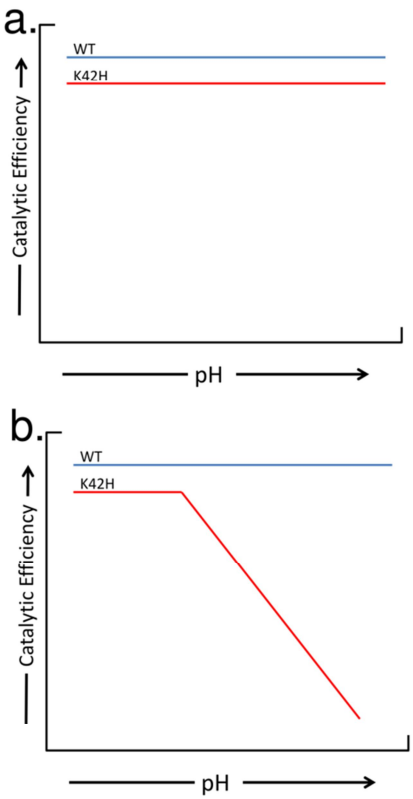

Figure 3-5 Hypothetical pH profiles of PchB K42H lyase and mutase activities. If the NAC is the prevalent contributor to catalysis both lyase and mutase activities will be independent of pH (a). If electrostatic transition state contributes more to catalysis both lyase and mutase reactions will show dependence to pH.

3.2.2 Preparation of isochorismate and chorismate

Isochorismate was isolated from *K. pneumoniae* 62-1 harboring the *entC* plasmid pKS3-02 [28] with only minor changes, as described previously [27]. Chorismate (Sigma, 60-80% pure) was recrystallized as previously described [29].

3.2.3 Measurement of isochorismate-pyruvate lyase initial velocities

Initial velocities for the production of salicylate were recorded at pH values from four to nine in steps of one pH unit for wild-type, K42H, K42A and K42E-PchB. A multicomponent buffer system was used to provide a constant ionic strength of 100 mM and to minimize salt effects: 50 mM formate, 50 mM MES, 100 mM TrisHCl, and adjusted to the appropriate pH with HCl or NaOH [30]. All reactions were carried out at room temperature (25 °C) with 5.3 μM enzyme (wild-type or mutant), incubated in buffer for 10 min, and initiated with the addition of 150 μM isochorismate (saturating conditions) with a total reaction volume of 100 μL. The reactions were monitored for 50 s by the increase in fluorescence using an excitation wavelength of 300 nm, and emission wavelength of 430 nm using Cary Eclipse fluorescence spectrometer (Varian). Data were plotted using Kaleidagraph (Synergy Software).

3.2.4 pH Dependence of the Kinetic Parameters for the Isochorismate-pyruvate Lyase Activity

Kinetic parameters for isochorismate-pyruvate lyase activity of wild type and K42H-PchB were determined at pH values from 3.5 to 9.5 in steps of 0.5 pH units using the formate/MES/TrisHCl buffer described above. All reactions were carried out at room

temperature with 1.5 μM enzyme (wild type or mutant) incubated in buffer for 10 min, and initiated with the addition of 0.1 mM – 0.4 mM isochorismate. Product formation (initial velocity) was linear over the course of the experiment for all pH values tested. k_{cat} and K_m were calculated using SigmaPlot (SSPS, Inc.) and Kaleidagraph (Synergy Software).

3.2.5 pH Dependence of the Kinetic Parameters for the Chorismate Mutase Activity

Kinetic parameters for chorismate mutase activity of wild type and K42H were determined in the formate/MES/TrisHCl buffer described above, at pH values ranging from 3.5 to 9.5 in steps of 0.5 pH units (however, there was no measurable activity over pH 8), and pH 7.0 to 8.0 in pH steps of 0.1. Protein concentrations varied per experiment from 90 μM to 900 μM per 100 μL run, with protein concentration increasing with pH, to optimize the signal-to-noise ratio. Reactions between pH 3.5 and 7 were carried out at room temperature. Temperature was kept constant for reactions from pH 7.0 to 8.0 using a Quantum Northwest TC 125 temperature controller set at 25° C. PchB wild-type and PchB K42H were incubated in the buffer for 10 minutes before each reaction. Reactions were initiated by the addition of the chorismate at concentrations ranging from 0.1 mM to 5.0 mM, and were mixed using a micropipette tip before placing the cuvette in the spectrophotometer. Initial velocities were determined by measuring the disappearance of chorismate at 310 nm (**Figure 3-6**, ε_{310} = 370 M^{-1} cm^{-1}) using a UV Spectrophotometer (Cary 50 Bio, Varian). Substrate consumption was linear over the course of the experiment for those pH values that showed detectable activity.

Michaelis-Menten kinetic data were fit by nonlinear regression. For experimental conditions at pH 7.5 and above, substrate concentrations were sub-saturating; therefore, kinetic constants were determined using Henderson and Dixon plots [31]. All data were fit using KaleidaGraph (Synergy Software) or SigmaPlot (SSPS, Inc.).

3.2.6 Data analysis for pH studies

pH profiles of k_{cat} and k_{cat}/K_M values for substrates were fit to equations 1-4. Plots for which the log of the parameter decreased at acidic pH with a slope of 1 were fit with equation 1:

$$\log Y = \log \left[\frac{C}{1 + \frac{H}{K_{a1}}} \right]$$

Profiles in which the log of the plotted parameter decreased with a slope of 1 at acidic pH and decreased with a slope of -1 to a lower plateau value at basic pH were fit to equation 2:

$$\log Y = \log \left[\frac{Y_L + Y_H \left(\frac{K_{a2}}{H} \right)}{1 + \frac{H}{K_{a1}} + \frac{K_{a2}}{H}} \right]$$

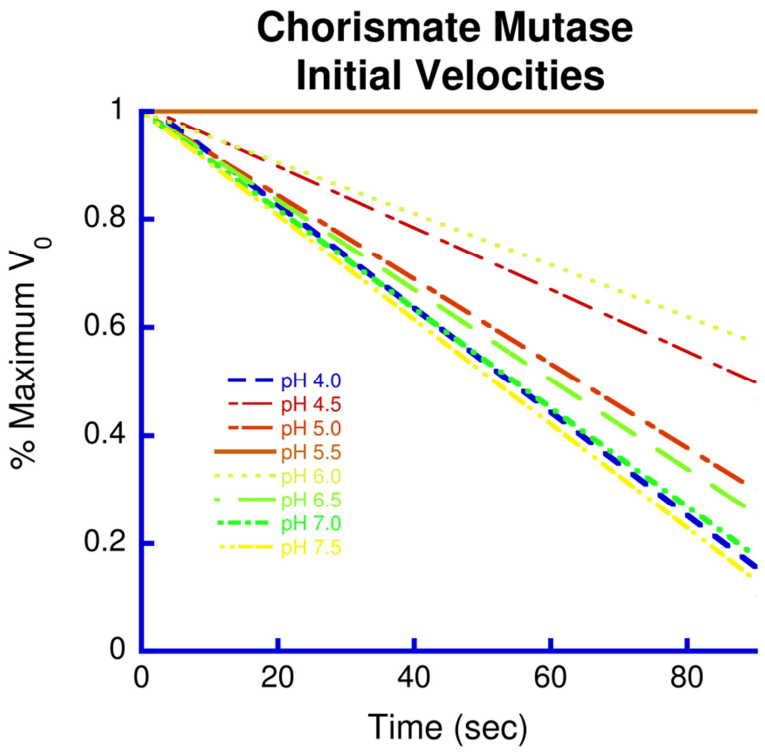

Figure 3-6: Sample Initial velocities of the chorismate mutase at selected pH values. PchB is a poor chorismate mutase, and in order to measure a linear initial velocity through a reasonable time period for all pH values, the assay conditions and buffer had to be optimized.

Profiles in which the log of the plotted parameter decreased at basic pH with a slope of 2 were fit to equation 3:

$$\log \mathrm{Y} = \log \left[\frac{c}{1 + \frac{K_{a1}}{H} + \frac{K_{a1}K_{a2}}{H^2}} \right]$$

Profiles in which the plotted parameter decreased at acidic pH with a slope of 1 and decreased at basic pH with a slope of 2 were fit to equation 4:

$$\log \mathrm{Y} = \log \left[\frac{c}{1 + \frac{H}{K_{a1}} + \frac{K_{a2}}{H} + \frac{K_{a2}K_{a3}}{H^2}} \right]$$

In equations 1-4, Y is the observed value (k_{cat} or k_{cat}/K_M), *c* is a pH independent plateau value of Y, Y_L is a plateau value of Y at low pH, Y_H is a plateau value of Y at high pH, *H* is the proton concentration, and K_{a1}, K_{a2} and K_{a3} are the apparent dissociation constants for groups on the enzyme or substrate. Any data represented as a straight line is a simple linear regression. The *pKa* values and kinetic constants can be seen in **Table 3-1**.

3.2.7 Calculation of $\Delta\Delta G^{\neq}$

The "mutational effect" was determined by dividing k_{cat}/K_m value of the mutant enzyme by that of the wild type, as done previously [27]. The $\Delta\Delta G^{\ddagger}$ was calculated from the equation:

$$\Delta\Delta G^{\ddagger} = -RT \ln (\text{mutational effect})$$

Table 3-1: pH profiles for wild type and mutant PchB[1]

Activity	Enzyme	Kinetic Parameter	p*K* values and kinetic constants		Titratable group
Lyase					
	WT	k_{cat}	c	0.90 ± 0.01	
			pKa_1	2.78 ±0.02	substrate
		k_{cat}/K_m	c	4.17 ±0.09	
			pKa_1	2.79 ± 0.08	substrate
	K42H	k_{cat}	Y_L	0.75 ± 0.02	
			Y_H	0.03 ± 0.07	
			pKa_1	3.04 ± 0.00	substrate
			pKa_2	6.65 ± 0.13	His 42
		k_{cat}/K_m	Y_L	3.40 ± 0.01	
			Y_H	1.90 ± 0.00	
			pKa_1	3.00 ± 0.01	substrate
			pKa_2	6.29 ± 0.00	His 42
Mutase					
	WT	k_{cat}/K_m	c	2.01 ± 0.1	
			pKa_1	2.7 ± 0.0	substrate
	K42H	k_{cat}	c	0.6 ± 0.1	
			pKa_1	3.6 ± 0.0	substrate
			pKa_2	7.7 ± 0.0	His 42
			pKa_3	8.5 ± 0.1	?
		k_{cat}/K_m	c	1.3 ± 0.2	
			pKa_1	9.0 ± 0.6	?
			pKa_2	6.1 ± 0.4	His 42

[1] Table adapted from Olucha et al, 2011 [21]

3.3 Results

3.3.1 Initial velocity of wild type, K42E, K42A and K42H

To determine the viability of the experiment I determined the overall pH profile of wild type PchB and mutants K42A K42E and K42H **(Figure 3-7)**. lyase activity was determined by fluorescence, measuring production of the salicylate (ex 310 em 430) at saturating concentrations of isochorismate over range of pH values from pH 4 to pH 9. As described in previous work the K42E mutant displayed no activity throughout the pH range. Wild type PchB and K42A mutant displayed pH independent initial velocities throughout the pH range. On the other hand, the K42H mutant displayed the pH dependence of initial velocities throughout pH range as expected from the theoretical *pKa value* of the histidine side chain.

3.3.2 pH dependence of lyase activity

To determine the catalytic constants of the lyase activity from a pH value of 3.5 to a pH value of 9.0, I used a multi-component buffer system that would allow me to buffer the solution at all the desired pHs as well as maintain a constant ionic strength along the pH range without interfering with the fluorescence of salicylate. Kinetic parameters for wild type and mutant enzymes were determined throughout pH range in steps of 0.5 pH units. The kinetic parameters were plotted as a function of pH and fitted to equation 2. **(Figure 3-8)**. As expected wild type PchB showed independent catalytic activity

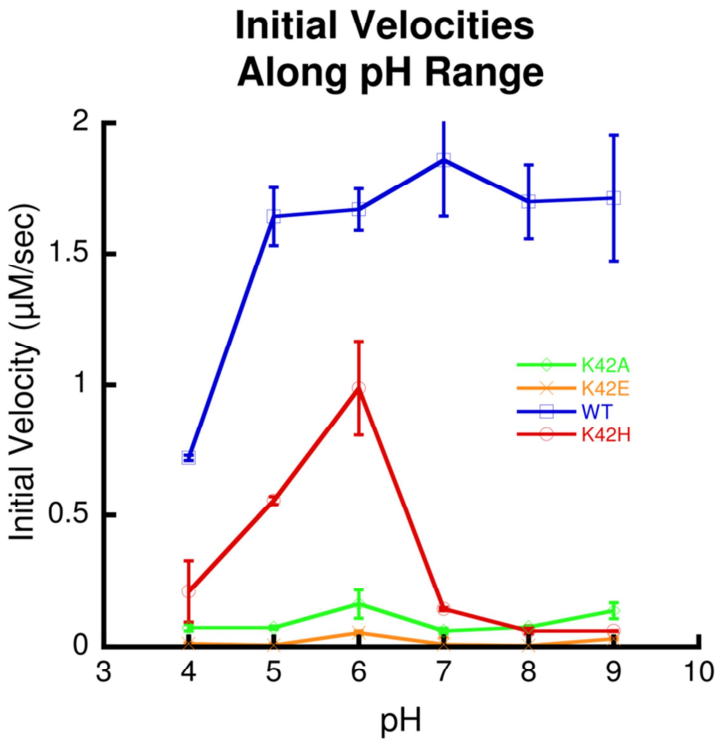

Figure 3-7: pH dependency of mutants K42A, K42E, and K42H overlayed over wild type PchB. Only PchB K42H displays pH dependency of catalytic activity along the whole pH range.

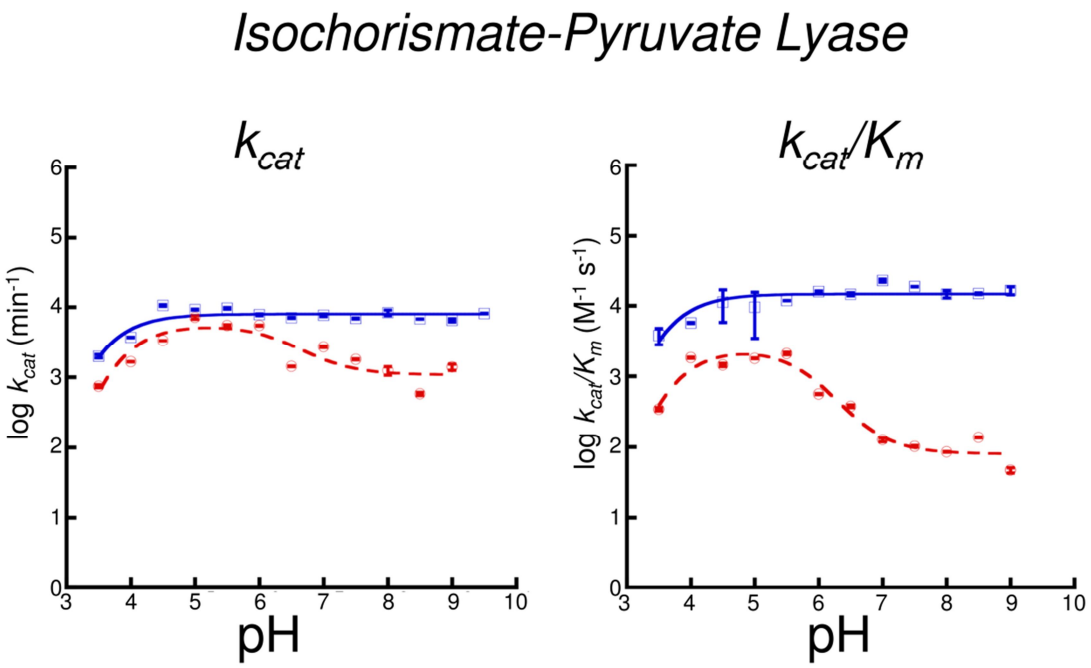

Figure 3-8: pH dependence of isochorismate-pyruvate lyase activity k_{cat} and k_{cat}/K_m. Both k_{cat} and k_{cat}/K_m show pH dependence. The decrease in activity at the lower pH values is most likely the result of an ionizable group in the substrate (*pKa value* ~3). Decrease in activity at higher pHs is indicative of a single ionizable group with a *pKa value* ~ 6.5, which agrees with the theoretical *pKa value* of the histidine. At higher pHs, the activity once again becomes pH independent, suggesting electrostatic transition state stabilization is not the only driving mechanism for the reaction.

throughout the pH range except for a decrease in activity at lower pH values with a slope of 1.0. This indicated a single protonation/deprotonation event with a calculated pKa values of 2.78 ± 0.02 or 2.79± 0.08 depending on whether k_{cat} or k_{cat}/K_m were used for the calculation. This pKa value can be attributed to the protonation of the isochorismate carboxylates which have a theoretical pKa value of approximately 3.6 [32]. The K42H mutant on the other hand while showing activity throughout the pH range showed pH dependent variability up to a pH value of 7, displaying the same decrease in activity as wild type PchB at pH values under 4.5, a peak in activity at pH value of 5.0 and a decrease with a slope of -1 to pH 7. Above pH 7 catalytic efficiency remain constant up to pH 9 albeit an order of magnitude less than the peak pH 5.0, and two orders of magnitude less than wild type . The decrease in activity at low pH values is comparable of that to wild type, again a single ionizable group (slope = 1) with a *pKa value* of 3.04± 0.00 (k_{cat}) or 3.00± 0.01(k_{cat}/K_m) corresponding to the carboxylates of the isochorismate. The decrease of slope -1 between pH values 5.0 and 7.0 corresponds to a second ionizable group with a calculated pKa value between 6.65 ± 0.13 it calculated from the k_{cat} or 6.29 ± 0.00 if calculated from the k_{cat}/K_m. This pH value dependent variation in catalytic activity is not observed either in wild type PchB or the other two mutants tested. This together with the calculated pKa values very close to the theoretical histidine *pKa value* of 6.1 indicate that we are observing a decrease in catalytic activity as we shift the population of enzyme from positively charged histidine at low pH values to neutral histidine at higher pH values. However in spite of the significant decrease in activity, activity is still observable at pH values where the

population of enzyme is almost completely shifted towards neutral charge, indicating catalysis independent of the positive charge at that position.

3.3.3 pH dependence of PchB mutase activity

Wild type PchB showed pH value independent mutase activity throughout the pH range from 3.5 to 9.5. As with the lyase activity the mutase catalytic efficiency of wild type PchB showed a decrease in activity at lower pH values with a slope of 1 at low pH values with a pKa value of 2.7 ± 0.0 **(Figure 3-9)**. This corresponds to the theoretical pKa value of the carboxylates of chorismate calculated at 3.6. This carboxylate needs to be deprotonated for efficient catalysis. PchB K42H mutase activity showed pH dependence at high pH values, and we were unable to detect activity at pH values above 7.8. Again turnover was highest at pH value 5.5. Unlike the lyase activity, fitting the turnover data to equation 4 indicated a decrease in activity with a slope of -2 as pH was increased, suggesting that we are observing not one but two ionizable groups, one with a pKa value value of 7.7 ± 0.0 and a second group with a *pKa value* value of 8.5 ± 0.1. The catalytic efficiency pH profile of the mutase activity also indicated two ionizable groups necessary for catalytic activity with pKa value's of 9.0 ± 0.6 and 6.1 ± 0.4. As in the lyase activity data, we can attribute the pKa with values of 7.7 (k_{cat}) and 6.1 (k_{cat}/K_m) to the histidine in the active site.

3.4 Discussion

Two models have been proposed to explain the molecular mechanism that drives pericyclic reactions in chorismate mutases and by extension PchB's lyase and mutase activities. On one hand, it has been proposed that two arginines buried within the active

site of the enzyme orient the substrate into the correct position, and the enzyme acts as a container, promoting the substrate to conform to a particular shape, the near attack conformation, or NAC. Once the substrate conforms to this shape, the reaction goes forward[7, 18]. On the other hand, it has been proposed that charged or polar residues in the active site stabilize the transition state by complementing the transition state's developing charges. Mutations of lysine 39 in EcCM abolished activity, but also disrupted secondary structure. Mutations of the homologous residue in PchB, lysine 42, also impair catalysis, but do not disrupt secondary structure, or alter the architecture of the active site, making PchB an excellent model to study the molecular mechanism in these enzymes. Mutating the lysine to a histidine at position 42 lowers the pKa value at that position. This enables us to observe the effects of shifting the H42 population from protonated (positively charged) to deprotonated (neutral) within a physiological pH range within the same enzyme. The model proposing that the formation of a NAC is enough to lower the energy barrier predicts that we would observe pH independent catalysis throughout the pH range, both for wild type PchB and the K42H mutant, because the charge at position 42 is not required for catalysis **(Figure 3-5a)**. However, the electrostatic transition state stabilization model predicts the opposite, a pH dependent decrease in catalytic activity as the H42 population is shifted to neutral **(Figure 3-5b)**.

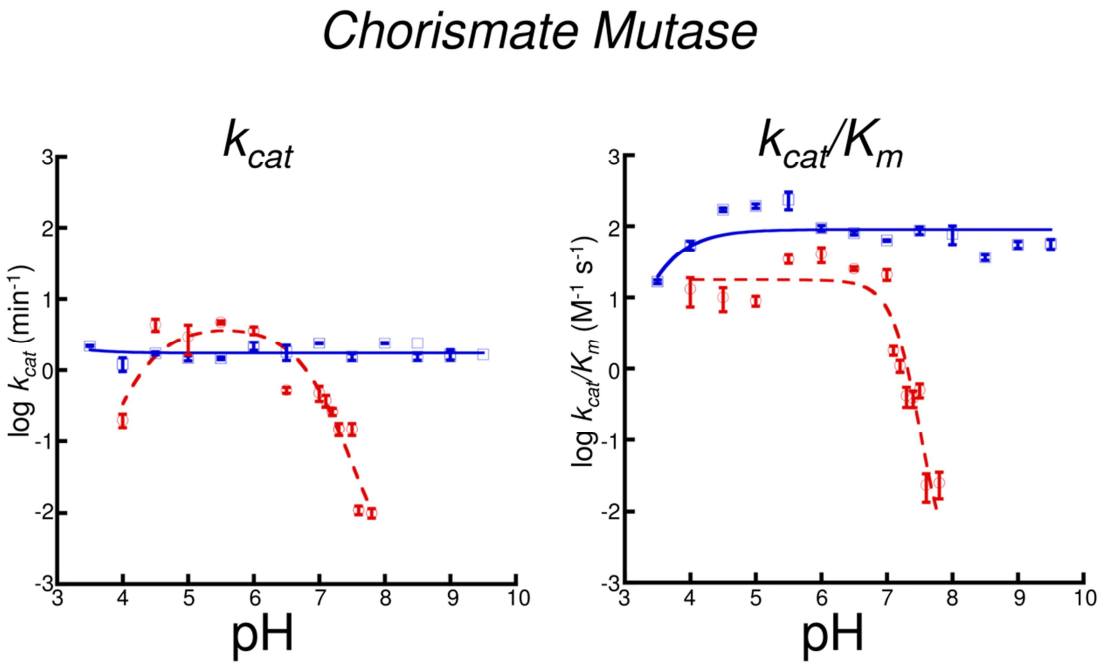

Figure 3-9: pH dependence of chorismate mutase activity k_{cat} and k_{cat}/K_m. Both k_{cat} and k_{cat}/K_m show pH dependence. Decrease in activity at the lower pH values most likely the result of an ionizable group in the substrate (*pKa value* ~3), comparable to that observed in the lyase activity. Decrease in activity at higher pH values is indicative of a two ionizable groups with *pKa value*s ~ 6.1-7.7 (whether determined from k_{cat}/K_m *or* k_{cat}*, respectively)*, and a second *pKa value* of ~9.0. The first *pKa value* agrees with the theoretical *pKa value* of the histidine. The second *pKa value* most likely corresponds to an ionizable group further away from the active site, with an effect small enough not to be observable in the physiological lyase activity, but clearly observable in the already poor mutase activity. Unlike the lyase activity, there is no observable mutase activity past pH value 7.8.

3.4.1 PchB Lyase activity

The isochorismate-pyruvate lyase activity of wild type PchB showed a constant, pH independent catalytic efficiency throughout the pH range, as expected. Only at pH values below 4.5 was a drop in activity observed. This would either correspond to the protein beginning to unfold, or a protonation/deprotonation event necessary for catalysis. The inflexion point of this event at pH value ~3, approximately corresponds to the pKa value of the carboxylates of the isochorismate (p*Ka* = 3.6). Protonation of these carboxylates would alter their interaction with the active site arginines that orient the substrate into its correct position for catalysis. This drop is observed for both, wild type and K42H mutant, indicating that the same protonation event is occurring for both enzymes. As predicted by the electrostatic transition state stabilization model, we observed a decrease in activity corresponding to a single protonation event (slope = -1) and a pKa value closely approximating the pKa value of the histidine. However, past pH value 7.5, catalysis becomes once again pH independent, albeit approximately an order of magnitude lower than at its peak at pH value 5. Although electrostatic transition state stabilization is necessary for efficient catalysis, another catalytic model, possibly the NAC formation, is sufficient for inefficient, but detectable catalysis.

3.4.2 Mutational effects and free energy contributions to lyase activity

In order to determine the individual contribution of the positive charge at position 42 to catalysis the data can also be interpreted in terms of mutational effects and differences in free energies of activation. To calculate the contribution of the positive charge to catalysis, we first need to determine the contributing effect of the mutation from lysine to

histidine. At the peak of K42H catalytic efficiency, (between pH values 5 and 5.5), the mutational effect **(**$(k_{cat}/K_m)_{mut}/(k_{cat}/K_m)_{WT}$**)** is approximately 0.2, representing a $\Delta\Delta G^{\ddagger}$ of 1.0 kcal/mol. This difference in energy can most likely be attributed to the difference in shape and size between the lysine in the wild type PchB and the histidine of the K42H. At pH value 9, when most of the K42H enzyme population is deprotonated, a mutational effect of 0.003 represents a $\Delta\Delta G^{\ddagger}$ of 3.4 kcal/mol. This number includes the contribution of the positive charge *and* sidechain shape and size. Subtracting the effect of the mutation (1.0 kcal/mol) results in a $\Delta\Delta G^{\ddagger}$ contribution of 2.4 kcal/mol, agreeing with the previously reported mutational effect for the K42A mutant of 2.7 kcal/mol [20].

3.4.3 PchB mutase activity

Chorismate mutase activity in PchB was not covariant with the lyase activity. As was observed in the lyase data, the mutase activity decreased with a slope of 1 at lower pH values, suggesting once again an ionizable group (a carboxylate) from the substrate affecting catalysis. At the peak of catalytic activity, between pH values 5 and 6, K42H exhibits higher turnover than wild type PchB. Unlike the lyase activity, there is no detectable activity past pH value 7.8, and the data fit a model with two ionizable groups, one at a *pKa value* 6.1 (k_{cat}) or 7.7 (k_{cat}/K_m) and the second with a *pKa value* of ~9. The first ionizable group agrees with the theoretical pKa value of the histidine sidechain, and agrees with the lyase activity. The second pKa value however might correspond to one of the arginines in the active site, (theoretical pKa value ~12, albeit lowered in the active site environment). The ionization state of these arginines would be essential for the correct orientation of the substrate in the active site, as they hydrogen-bond to the

substrates' carboxylates. Another option is that this phenomenon is not caused by an ionizable group in the active site, but a group further away, whose protonation state affects a hydrogen bond or a salt bridge. A small disruption in the enzyme's structure might not affect the physiological lyase activity (this observation is not observed in the lyase activity), but the poorer chorismate mutase activity might be more sensitive to such a small disruption.

3.5 Conclusions

Previous mutagenesis experiments showed that lysine 42 is important for catalysis, with evidence supporting electrostatic transition state stabilization as essential for efficient catalysis. However, the K42A mutant still displayed about 1% of wild type lyase activity, and the pH profile of K42H at high pH values shows similar activity, indicating that lyase catalysis still occurs at an observable rate *without a positive charge* at position 42. Electrostatic transition state stabilization is essential for efficient catalysis, but some other mechanism (a reactive substrate conformer?) is *sufficient* for (albeit inefficient) catalysis. As with the lyase activity, the data indicate that the positive charge at position 42 is important for catalysis, supporting the electrostatic transition state stabilization hypothesis. However, there is no observable catalysis at a point where the majority of the enzyme (>75%) population has lost the positive charge at that position. This would indicate that unlike the lyase activity, in PchB, electrostatic transition state stabilization is essential for observable catalysis.

Lyase and mutase activities had been suggested to be concomitant with electrostatically and geometrically similar transition states, based on mutational analyses of Q90 [3] in

which pH profiles showed a titration of activity with K_m not k_{cat}. If this were true, we would have observed the same trends in the lyase and mutase data for K42H, which is not the case. The positive charge of the lysine contributes differently to lyase and mutase reactions. Furthermore, observable lyase activity at high pH values indicates that there might be multiple catalytic pathways, at least two, for the lyase activity. This "catalytic network", already proposed for other enzymes by Benkovic, would indicate that instead of a two dimentional energy coordinate, there are multiple pathways in a three-dimentional energy landscape that would lead to catalysis. This leads to the hypothesis that protein motions are important for catalysis. This hypothesis will be explored in **Chapter 4** (Chemical Rescue) and **Chapter 5** (QM/MM Simulations).

3.6 References

1. Gaille, C., P. Kast, and D. Haas, *Salicylate biosynthesis in Pseudomonas aeruginosa - Purification and characterization of PchB, a novel bifunctional enzyme displaying isochorismate pyruvate-lyase and chorismate mutase activities.* Journal of Biological Chemistry, 2002. **277**(24): p. 21768-21775.

2. Serino, L., et al., *Structural Genes for Salicylate Biosynthesis From Chorismate in Pseudomonas aeruginosa.* Molecular & General Genetics, 1995. **249**(2): p. 217-228.

3. DeClue, M.S., et al., *Isochorismate pyruvate lyase: A pericyclic reaction mechanism?* Journal of the American Chemical Society, 2005. **127**(43): p. 15002-15003.

4. Gustin, D.J., et al., *Heavy atom isotope effects reveal a highly polarized transition state for chorismate mutase.* Journal of the American Chemical Society, 1999. **121**(8): p. 1756-1757.

5. Kast, P., et al., *Exploring the active site of chorismate mutase by combinatorial mutagenesis and selection: The importance of electrostatic catalysis.* Proceedings of the National Academy of Sciences of the United States of America, 1996. **93**(10): p. 5043-5048.

6. Kienhofer, A., P. Kast, and D. Hilvert, *Selective stabilization of the chorismate mutase transition state by a positively charged hydrogen bond donor.* Journal of the American Chemical Society, 2003. **125**(11): p. 3206-3207.

7. Hur, S. and T.C. Bruice, *The near attack conformation approach to the study of the chorismate to prephenate reaction.* Proceedings of the National Academy of Sciences of the United States of America, 2003. **100**(21): p. 12015-12020.

8. Bruice, T.C., *A view at the millennium: The efficiency of enzymatic catalysis.* Accounts of Chemical Research, 2002. **35**(3): p. 139-148.

9. Lau, E.Y. and T.C. Bruice, *Importance of correlated motions in forming highly reactive near attack conformations in catechol O-methyltransferase.* Journal of the American Chemical Society, 1998. **120**(48): p. 12387-12394.

10. Lightstone, F.C. and T.C. Bruice, *Ground state conformations and entropic and enthalpic factors in the efficiency of intramolecular and enzymatic reactions .1. Cyclic anhydride formation by substituted glutarates, succinate, and 3,6-endoxo-Delta(4)-tetrahydrophthalate monophenyl esters.* Journal of the American Chemical Society, 1996. **118**(11): p. 2595-2605.

11. Repasky, M.P., et al., *Investigation of solvent effects for the Claisen rearrangement of chorismate to prephenate: Mechanistic interpretation via near attack conformations.* Journal of the American Chemical Society, 2003. **125**(22): p. 6663-6672.

12. Torres, R.A. and T.C. Bruice, *Molecular dynamics study displays near in-line attack conformations in the hammerhead ribozyme self-cleavage reaction.* Proceedings of the National Academy of Sciences of the United States of America, 1998. **95**(19): p. 11077-11082.

13. Claeyssens, F., et al., *Multiple high-level QM/MM reaction paths demonstrate transition-state stabilization in chorismate mutase: correlation of barrier height with transition-state stabilization.* Chemical Communications, 2005(40): p. 5068-5070.

14. Cload, S.T., et al., *Mutagenesis study of active site residues in chorismate mutase from Bacillus subtilis.* Journal of the American Chemical Society, 1996. **118**(7): p. 1787-1788.

15. Kast, P., M. AsifUllah, and D. Hilvert, *Is chorismate mutase a prototypic entropy trap? Activation parameters for the Bacillus subtilis enzyme.* Tetrahedron Letters, 1996. **37**(16): p. 2691-2694.

16. Liu, D.R., et al., *Analysis of active site residues in Escherichia coli chorismate mutase by site-directed mutagenesis.* Journal of the American Chemical Society, 1996. **118**(7): p. 1789-1790.

17. Ranaghan, K.E. and A.J. Mulholland, *Conformational effects in enzyme catalysis: QM/MM free energy calculation of the 'NAC' contribution in chorismate mutase.* Chemical Communications, 2004(10): p. 1238-1239.

18. Strajbl, M., et al., *Apparent NAC effect in chorismate mutase reflects electrostatic transition state stabilization.* Journal of the American Chemical Society, 2003. **125**(34): p. 10228-10237.

19. Warshel, A., et al., *Electrostatic basis for enzyme catalysis.* Chemical Reviews, 2006. **106**(8): p. 3210-3235.

20. Luo, Q., J. Olucha, and A.L. Lamb, *Structure-function analyses of isochorismate-pyruvate lyase from Pseudomonas aeruginosa suggest differing catalytic mechanisms for the two pericyclic reactions of this bifunctional enzyme.* Biochemistry, 2009. **48**(23): p. 5239-45.

21. Olucha, J., et al., *pH Dependence of catalysis by Pseudomonas aeruginosa isochorismate-pyruvate lyase: implications for transition state stabilization and the role of lysine 42.* Biochemistry, 2011. **50**(33): p. 7198-207.

22. Luo, Q., *Mechanistic and Structural Studies of Salicylate Biosynthesis in Pseudomonas aeruginosa*, in *Molecular Biosciences Departmene*2009, University of Kansas: Lawrence, Kansas. p. 148.

23. Zaitseva, J., K.M. Meneely, and A.L. Lamb, *Structure of Escherichia coli malate dehydrogenase at 1.45 A resolution.* Acta Crystallogr Sect F Struct Biol Cryst Commun, 2009. **65**(Pt 9): p. 866-9.

24. Garret, R.H. and C.M. Grisham, *Biochemistry*. Second ed. 2004, Belmont, CA: Thomson Brooks/Cole.

25. Edgcomb, S.P. and K.P. Murphy, *Variability in the pKa of histidine side-chains correlates with burial within proteins.* Proteins-Structure Function and Genetics, 2002. **49**(1): p. 1-6.

26. Zaitseva, J., et al., *Two crystal structures of the isochorismate pyruvate lyase from Pseudomonas aeruginosa.* J. Biol. Chem., 2006. **281**(44): p. 33441-9.

27. Luo, Q., J. Olucha, and A.L. Lamb, *Structure-function analyses of isochorismate-pyruvate lyase from Pseudomonas aeruginosa suggest differing catalytic mechanisms for the two pericyclic reactions of this bifunctional enzyme.* Biochemistry, 2009. **48**: p. 5239-5245.

28. Schmidt, K. and E. Leistner, *Microbial Production of (+)-trans-Isochorismic Acid.* Biotech. & Bioeng., 1995. **45**: p. 285-291.

29. Rieger, C.E. and J.L. Turnbull, *Small scale biosynthesis and purification of gram quantities of chorismic acid.* Prep Biochem Biotechnol, 1996. **26**(1): p. 67-76.

30. Gondry, M., et al., *Cyclic dipeptide oxidase from Streptomyces noursei. Isolation, purification and partial characterization of a novel, amino acyl alpha,beta-dehydrogenase.* Eur. J. Biochem., 2001. **268**(6): p. 1712-21.

31. Segel, I.H., *Enzyme Kinetics: Behavior and Analysis of Rapid Equilibium and Steady State Enzyme Systems*. 1975, New York: John Wiley & Sons.

32. Solaris, *Advanced Chemistry Development Software*, 2009.

Chapter 4: Chemical Rescue of Isochorismate-Pyruvate Lyase Activity of PchB

4.1 Introduction

Chemical rescue is a widely accepted enzymology tool that allows a more detailed analysis of specific sidechains in an active site [1-6]. The most commonly used chemical rescue technique involves non-covalent rescue **(Figure 4-1)**; an alanine mutant is generated at the position the researcher is interested in and excess compound mimicking the lost side chain (*e.g.* propylamine to mimic a lysine in **Figure 4-2b** [5, 6] or imidazole to mimic a histidine [7]). In excess, the compound will fill the void left by the mutated residue in a percentage of the enzyme, thus rescuing lost catalytic activity in that enzyme population.

Alternatively, mutation of the residue of interest to cysteine allows for covalent chemical modification [2, 3] via alkylating agents (chemical reaction in **Figure 4-3** *e.g.* bromoethylamine to generate γ-thio lysine, **Figure 4-2c** ; This scheme shows the modification by bromoethanol in **Figure 4-2d**, which will also be used in this work). Covalent modification allows for better control over the position and orientation of the rescue mimetic, with the caveat that any other reactive cysteines may be modified as well.

Previous work on *E. coli* chorismate mutase [8-13] suggest that a positive charge at position 42 is not essential for efficient catalysis, as long as the substrate organizes into

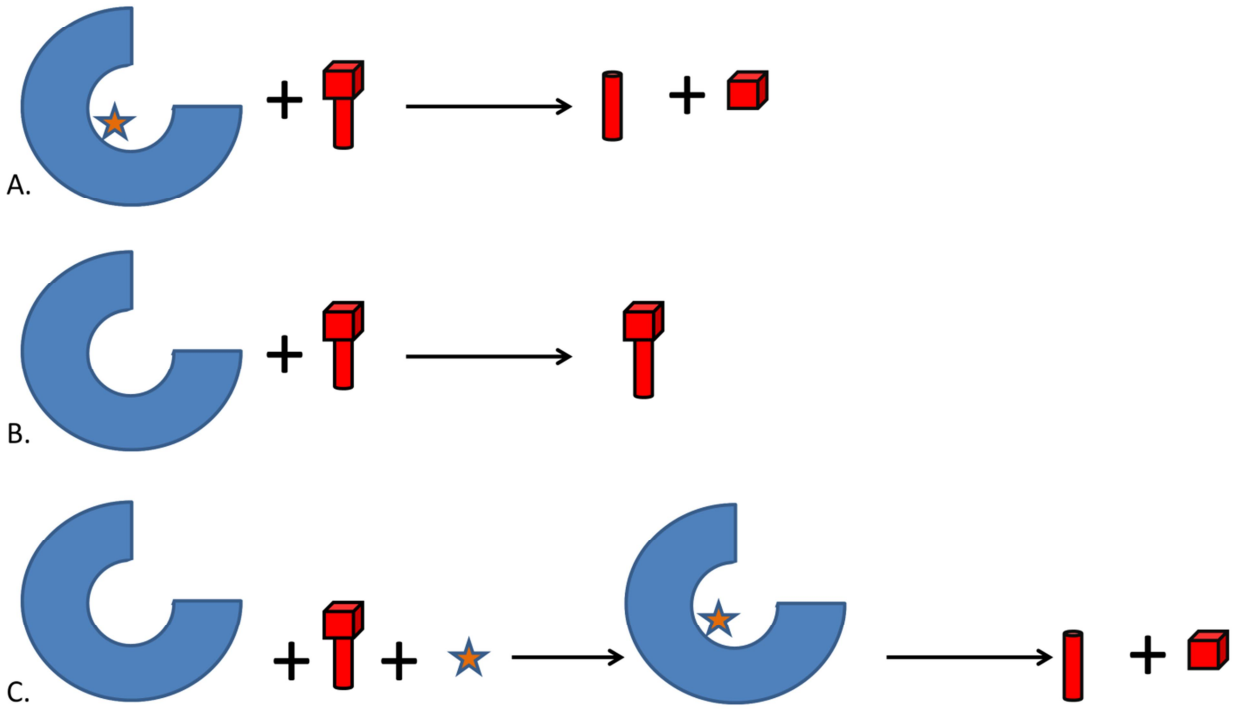

Figure 4-1: Chemical Rescue Overview. (A) Enzyme (blue C-shape) has residue of interest buried in the active site (star shape). This particular enzyme catalyzes a lyase reaction breaking down a compound (red cylinder-cube shape) into its components. (B) A mutant generated without the residue of interest is no longer able to catalyze the reaction. (C) If an exogenous compound mimicking the missing side chain is added to the solution in high enough excess, a percentage will find its way to the void left by the missing catalytic side chain, restoring catalytic activity, at least partially in this population of enzyme.

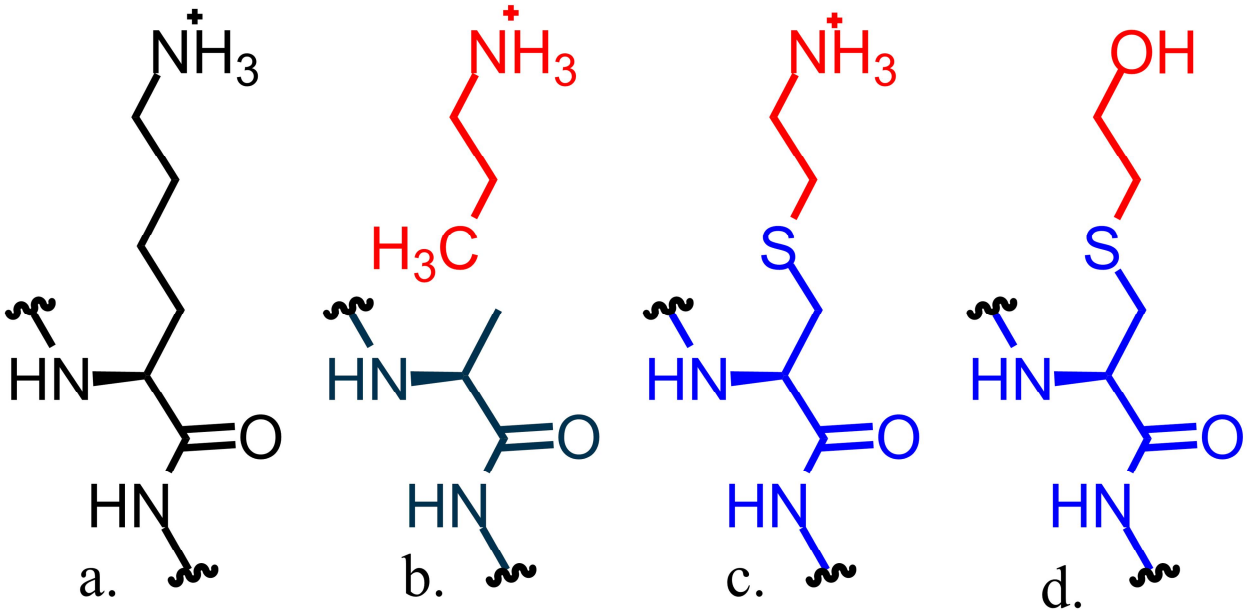

Figure 4-2: Comparison scheme of the different chemical rescues as compared to wild type lysine. Wild type lysine (a); propylamine rescue of the K42A mutant (b), and γ-thiolysine, and 3-(2-*hydroxy*ethyl)-thio-cysteine (d) rescue of the K42C mutants.

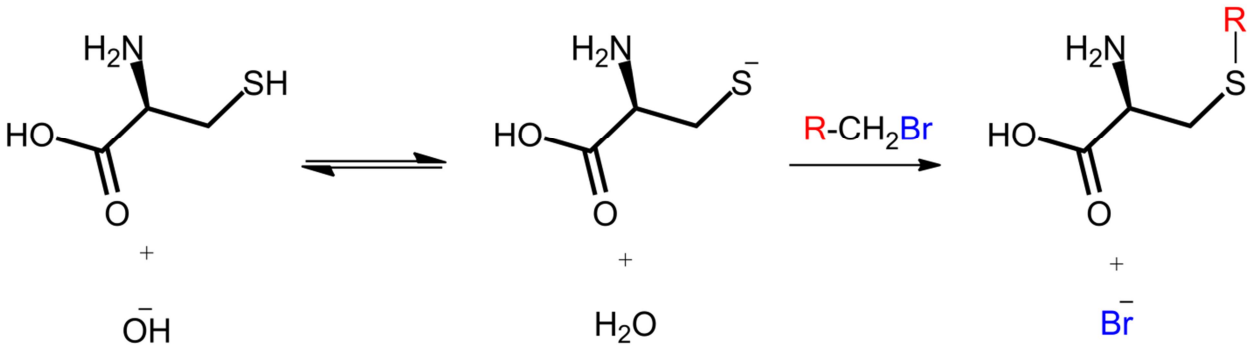

Figure 4-3: Cysteine alkylation reaction. In a high pH environment, SH is in equilibrium with the deprotonated form (S^-). The S^- performs a nucleophillic attach on the bromoethylamine, with a release of the Br^- as the leaving group.

a near attack conformation via interaction of its carboxylates with two buried arginine residues. However, mutational analyses and pH dependence studies of PchB have shown the positive charge at position 42 is necessary for efficient salicylate production (previous chapter and references [14, 15]) In these studies, the positive charge is hypothesized to stabilize the developing negative ether oxygen at the transition state, [16-19] analogous to work with *E. coli* chorismate mutase [18, 20, 21] . Crystal structures of PchB with and without product in the active site [22] reveal that K42 is located in a flexible loop that closes the active site upon substrate binding and opens as product is released. In addition, thermodynamic experiments have led to the hypothesis that organization of the loop is an energetically important step in catalysis [23]. The chemical rescue experiments described here provide further evidence that the positive charge at position 42 is important for catalysis and provide validation for the hypothesis that loop organization is also important: only covalent modifications of PchB variants with lysine mimetic alkyl-amines are able to rescue catalytic efficiency.

4.2 Materials and Methods

4.2.1 Protein Preparation.

Wild Type PchB was prepared as previously described [22]. Site directed mutants of PchB were prepared using the plasmid used for wild type PchB overexpression as the template and Quickchange II (Agilent) mutagenesis kit, protocol as per manufacturer's instructions. K42C mutation was generated using primer of sequence:

5'-GGCGTCGCGCTTCTGCGCCAGCGAGGCGG-3'

and its reverse complement. C07A mutation was generated using primer of sequence:

5'-AACTCCGAAGACGCCACCGGCCTGGCG-3'

and its reverse complement.

In order to prevent disulfide bond formation and aggregation of the mutants during purification, 20mM β mercapto-ethanol was added to the resuspension buffer. All buffers used in the purification process, including 30Q and gel filtration buffers contained 1mM TCEP (Sigma).

4.2.2 Enzymatic Assays.

All assays were performed using a TgK Scientific Stopped Flow device, with a xenon lamp emitting at 310 nm, and a 360 nm cutoff filter. Equal 50µl volumes of enzyme and substrate were injected into a 22 µl cell and initial velocity of salicylate production was measured as an increase in fluorescence at 430 nm for 30 seconds (during which the reaction was linear). Pre-injection enzyme and substrate concentrations were twice the final enzyme/substrate concentration in the cell (post mixing). Unless otherwise specified, all concentrations reported are final post-mixing concentrations. Both substrate and enzyme were prepared in the same buffer system to prevent buffer dilution effects post mix. Substrate was prepared from a stock of 4.8 mM isochorismate into 0 µM to 400 µM concentrations. Enzyme concentration ranged from 100 nM for Wild Type PchB experiments to 1 µM for PchB K42C and C07A/K42C experiments.

Michaelis-Menten kinetic data were fit using Kaleidagraph (Synergy Software) using non-linear regression. All catalytic constants can be seen on **Table 4-1**

4.2.3 Chemical Rescue of K42A by Propylamine

PchB K42A (1 μM) was incubated for 45 minutes on ice in 50 mM Tris HCl pH 8.0, 150mM NaCl, 10% Glycerol, 1mM TCEP buffer, with and without 500 mM chemical rescue agents of varying carbon chain length **(Figure 4-4)**. Substrate used for either of the experiments was prepared with the same buffer components, including 500 mM propylamine (to maintain propylamine concentration post-mix).

4.2.4 Covalent Chemical Rescue of single and double PchB cysteine mutants with Bromo-ethylamine and Bromo-ethanol.

PchB mutants and controls were incubated for 22-24 hrs at 18° C in 10 mL of 1 M Tris pH 8.8, 150mM NaCl, 10% Glycerol, 1mM TCEP buffer, with and without 1 mM bromoacylating reagent added. After the incubation period, enzyme was concentrated using microcon centrifuge concentrators, and enzyme buffer was exchanged to 50 mM Tris HCl pH 8.0, 150mM NaCl, 10% Glycerol, 1mM TCEP to remove alkylating agent using a PD-10 desalting column (GE Healthcare) as per manufacturer's specifications. Concentration measured via Bradford. Enzyme was added to 10 mL of reaction buffer without bromoacylating agent to final concentration of 200 nM – 20 uM (2X post-mix enzyme concentration). Substrate was prepared with the same buffer components.

Table 4-1: Catalytic constants

	Sample	k_{cat} ($x10^3$ s^{-1})	K_m (μM)	k_{cat}/K_m (M^{-1} s^{-1})
WT	*Control*	390 ± 10	1.5 ± 0.3	258,000 ± 5000
	PrA	110 ± 1	14.0 ± 0.1	7,700 ± 100
	BrEA	180 ± 1	9.7 ± 0.1	19,000 ± 100
	BrEtOH	85 ± 1	35.0 ± 0.1	2,500 ± 100
K42A	*Control*	23 ± 1	28.0 ± 0.4	850 ± 10
	PrA	39 ± 1	40.0 ± 0.1	970 ± 10
K42C	*Control*	1.0 ± 0.01	62.0 ± 0.7	15 ± 1
	BrEA	96 ± 1	63.0 ± 0.7	1,500 ± 20
C7A,K42C	*Control*	3.2 ± 0.1	63.0 ± 1.4	51 ± 1
	BrEA	98 ± 0	27.0 ± 0.7	3,700 ± 100
	BrEtOH	3.2 ± 0.2	98.0 ± 0.6	32 ± 1
C7A	*Control*	140 ± 1	2.1 ± 0.2	67,000 ± 6000
	BrEA	120 ± 1	1.6 ± 0.2	79,000 ± 2000
	BrEtOH	120 ± 1	2.9 ± 0.7	40,000 ± 2000

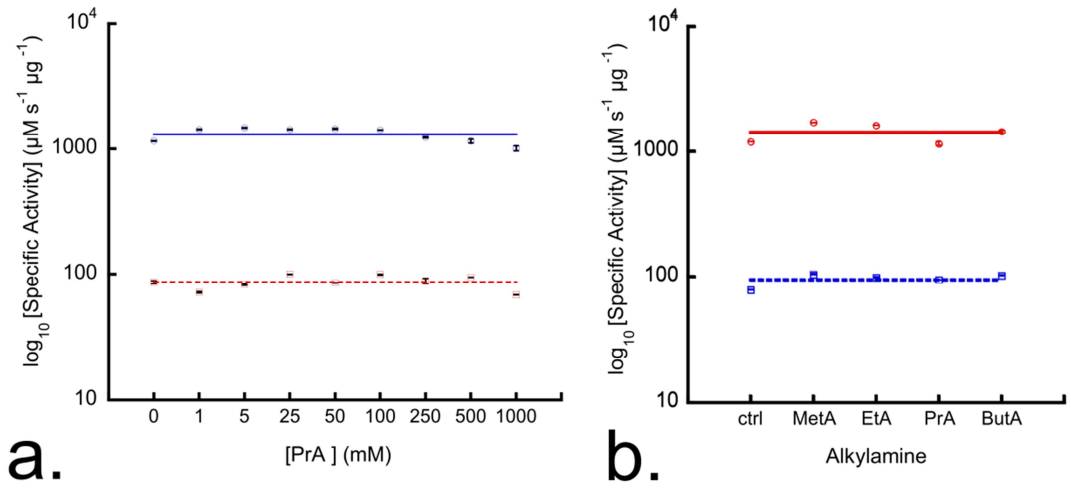

Figure 4-4: Chemical rescue of isochorismate-pyruvate lyase activity by the addition of exogenous alkylamine compounds of differing carbon chain length. No rescue of K42A activity was observed **(red data, in plot a)** with the addition of increasing concentrations of propylamine to the solution. Shorter or longer rescuing agent did not rescue catalytic activity either **(b)**

4.2.5 Ellman's Reagent competition assay

In order to determine whether the cysteine at position 7 was solvent accessible and thus alkylatable, 1 mL of 1mM protein sample (PchB WT; K42C; C7A or C7A,K42C, concentration determined by measuring absorbance at 280 nm) were incubated for 24 hours at 18°C in the same buffer used in the alkylation process as described above, but without alkylating reagent.

A volume of 100 µl of each of the samples was then allowed to react with 1 mM DTNB reagent in 300 mM Tris pH 8.0, 25 mM Sodium Acetate buffer for 5 minutes at room temperature. Absorbance was measured at 412 nm and concentration of NTB^{-2} was determined (ε=13600 cm^{-1} l^{-1}) [24] . This concentration corresponds at a 1:1 ratio with the solvent accessible cysteines in solution.

PchB WT and C7A mutant showed no change increase absorbance, indicating no cysteines are solvent accessible in these enzymes **(Table 4-2)**.

K42C and C7A,K42C both showed a similar absorbance change corresponding to only one cysteine (the cysteine at position 42) per protein molecule being solvent accessible.

Table 4-2: Percentage derivatization at position 42

	Sample	% alkyl-amination at pos. 42*
WT	*Control*	*0%*
	PrA	*0%*
	BrEA	*0%*
	BrEtOH	*0%*
K42A	*Control*	*-*
	PrA	*-*
K42C	*Control*	*0%*
	BrEA	*82%*
C7A/K42C	*Control*	*0%*
	BrEA	*98%*
	BrEtOH	*100%*
C7A	*Control*	*0%*
	BrEA	*0%*
	BrEtOH	*0%*

Samples of each enzyme were then incubated at the same concentration and the same incubation buffer as described above for the controls but with excess alkylating agent (10 mM). DTNB competition assay was performed as described above for the controls and percent alkylation for each of the alkylating agents (bromoethylamine and bromoethanol) was determined as

$$1 - \frac{[sample\ with\ alkylated\ agent]_{DTNB}}{[sample\ without\ alkylated\ agent]_{DTNB}}$$

Using the concentrations as determined by DTNB assay (Table S3).

4.2.6 Calculation of ΔΔG‡

In order to quantify chemical rescue more effectively, variant effects were calculated in terms of changes in energies of activation:

$$\Delta\Delta G^{\ddagger} = -RT \ln[\frac{(k_{cat}/K_m)_1}{(k_{cat}/K_m)_2}]$$

Propagation of the error of k_{cat}/K_m *to the* $\Delta\Delta G^{\ddagger}$ was calculated as

$$\partial ratio = \frac{\sqrt{\left[\frac{(\partial kcat/Km\ )_1}{(kcat/Km\ )_1}\right]^2 + \left[\frac{(\partial kcat/Km\ )_2}{(kcat/Km\ )_2}\right]^2}}{\ln(ratio)}$$

4.3 Results and Discussion

A lysine to alanine (K42A) mutation reduces catalytic efficiency to 1% of wild type (**Table 4-3** and ref. 1). Similar (K→A) mutations in enzymes where the residue of interest is found deep within the active site have been successfully rescued using non-covalent binding of alkyl amines.[6, 25, 26] In other words, the non-covalent rescue agent, at high molar excess, binds in the void left by the alanine mutation and is properly situated when substrate binds to promote catalysis. The inability of propylamine at 10^5 molar excess to chemically rescue PchB K42A activity **(Figures 4-5 and 4-6 and Table 4-2)** suggests that the propylamine is not preorganized in the site of the K42A variant prior to substrate binding. On the other hand, covalently modification of the K42C-variant of PchB with bromoethylamine to generate a lysine mimetic **(Figures 4-5, 4-7 and Table 4-2)** successfully rescued catalytic activity by two orders of magnitude. In this case, the positive charge of the lysine mimetic is carried along during active site loop closure, thereby properly organizing the active site to stabilize the developing negative charge at the ether oxygen of the transition state. Finally, to test whether the lysine sidechain is instead important in a steric sense, promoting loop organization and closure, as opposed to the necessity of a positive charge to promote efficient catalysis, the K42C-varaint was modified with bromoethanol (Scheme 1D). This variant is isosteric with the K42C-bromoethylamine but has the neutral alcohol instead of the charged amine terminating the sidechain. This variant also provides a hydrogen bond that may

Table 4-3: Variational effects

Rescue Agent	Variational Effect	$\Delta\Delta G^{\ddagger}$ (kcal mol^{-1}) (-RT*ln* [mut. effect])	% Rescue
Controls			
	C7A/WT	0.78 ± 0.07	
	K42A/WT	3.32 ± 0.01	
	K42C/WT	5.66 ± 0.01	
	(C7A,K42C)/C7A	4.16 ± 0.03	
Propylamine (PrA)	(K42A+PrA)/K42A	-0.08 ± 0.07	2%
Bromoethylamine (BrEA)	(K42C+BrEA)/K42C	-2.68 ± 0.02	48%
	(C7A,K42C + BrEA)/ (C7A-K42C)	-2.49 ± 0.01	60%
Bromoethanol (BrEtOH)	(C7A,K42C + BrEtOH)/ (C7A,K42C)	0.3 ± 0.2	-6%

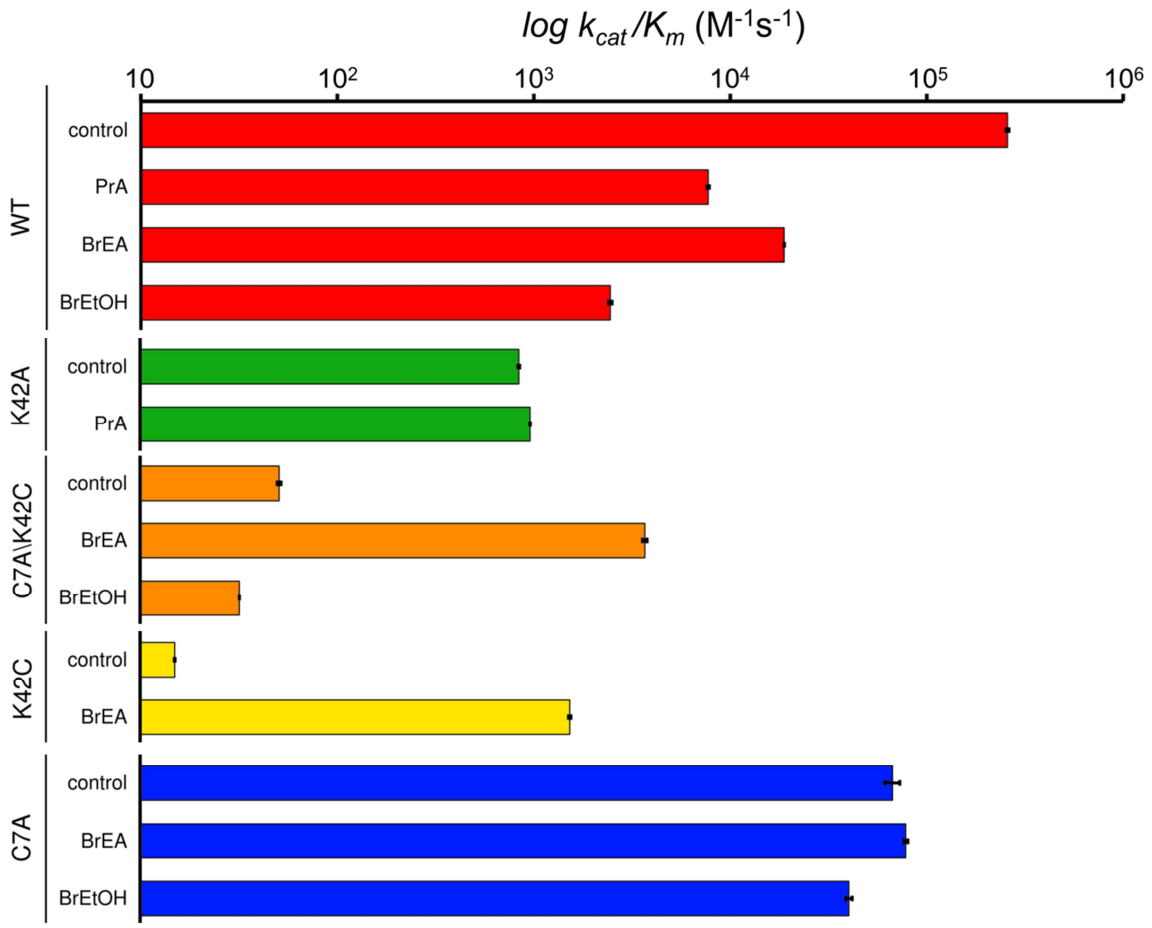

Figure 4-5: Catalytic Efficiencies of the Chemical Rescues. PchB wild type (WT) controls in red, K42A experiment in green. Cysteine mutants C7A/K42C and K42C (in orange and yellow respectively). Addition of rescue agents to WT enzyme assays results in decrease activity, most likely due to unexpected interaction of the propylamine (PrA) with WT enzyme due to the excess PrA present in solution, or alkylation of the cysteine at position 7 by bromoethylamine (BrEA) and bromoethanol (BrEtOH). Propylamine did not rescue catalytic efficiency in K42A mutant (green bars). However, covalent modification of the K42C to generate a lysine mimetic rescued 10^2 fold activity (top orange bar vs orange middle bar). In contrast bromoethanol (bottom orange bar), did not rescue activity. The C7A mutant was not significantly affected by the addition of the rescue agents.

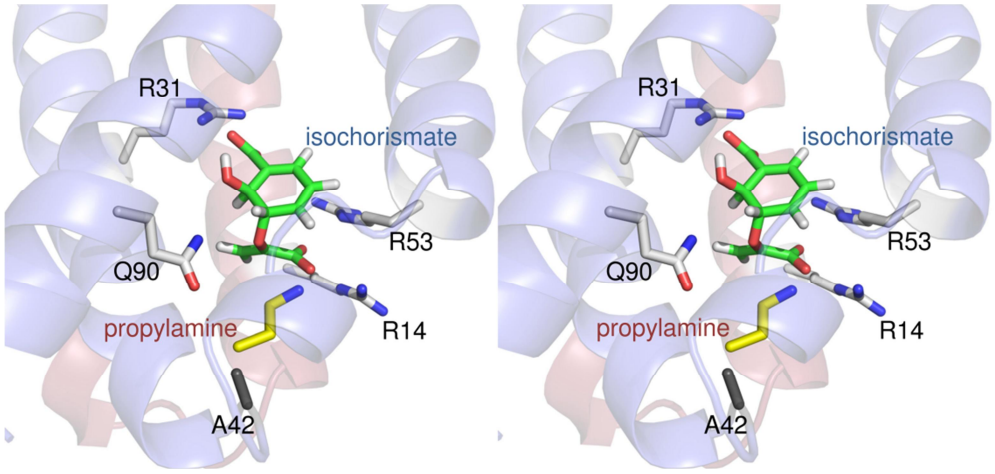

Figure 4-6: Stereo view of propylamine K42A chemical rescue. The model of the active site with isochorismate is based on QM/MM minimized wild type PchB active site.

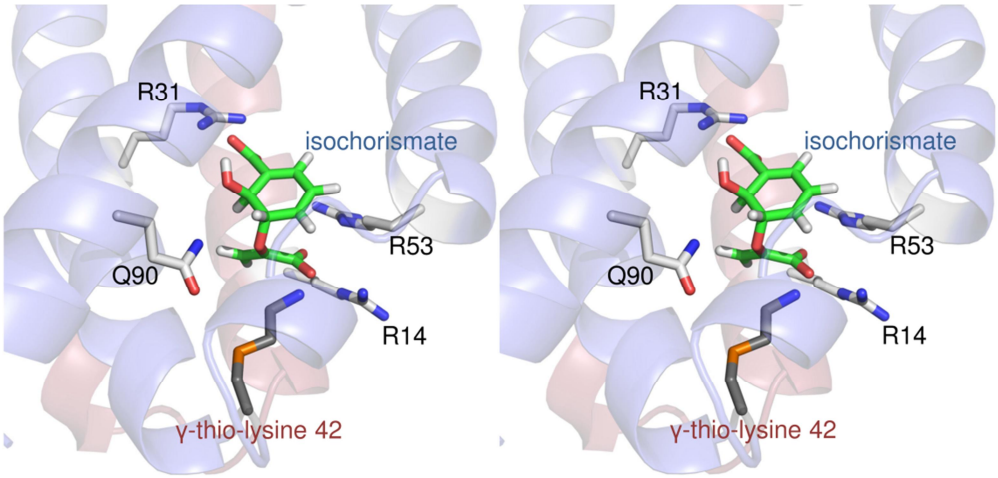

Figure 4-7: Stereo view of bromoethylamine K42C derivative (γ-thio-lysine). The model of the active site with isochorismate is based on QM/MM minimized wild type PchB active site.

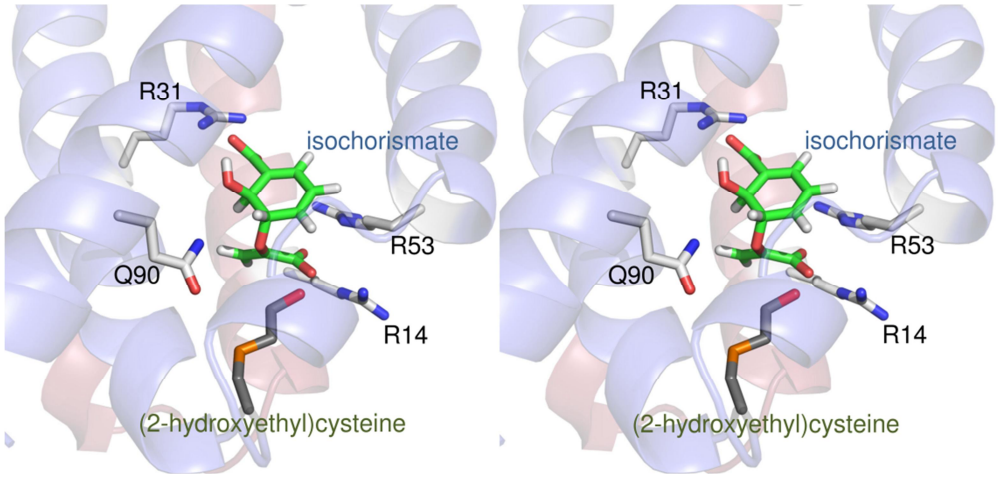

Figure 4-8: Stereo view of bromoethanol K42C derivative (3-(2-hydroxyethyl)-thiocysteine). The model of the active site with isochorismate is based on QM/MM minimized wild type PchB active site.

alternatively be important in catalysis (as opposed to charge). This variant did not rescue lyase activity **(Figure 4-5, 4-8 and Table 4-3**.

In order to quantify chemical rescue more effectively, mutational effects can be calculated in terms of changes in energies of activation ($\Delta\Delta G^{\ddagger}$, **Table 4-3**):

$$\Delta\Delta G^{\ddagger} = -RT \ln[\frac{(k_{cat}/K_m)_{var}}{(k_{cat}/K_m)_{ctrl}}]$$

where R is the gas constant (1.98×10^{-3} kcal K^{-1} M^{-1}) and T is the experimental temperature, 293 K (20°C).The mutational effect resulting from replacing the wild type lysine for an alanine at position 42 increases the free energy of activation by 3.32 kcal mol^{-1}. This number represents the maximum that any chemical rescue agent could promote activity in this variant. Adding 10^5 molar excess of propylamine does not significantly rescue activity (0.08 kcal mol^{-1} or 2% rescue of the mutational effect). As stated before, this value suggests that the propylamine positive charge is not organized in the active site such that upon loop closure there is no rescue of catalysis.

Replacing the wild-type lysine for a cysteine at position 42 contributes an additional 5.66 kcal mol^{-1} to the free energy of activation as compared to wild type PchB. Covalent modification of the cysteine with bromoethylamine to form a lysine mimetic however, rescues by 2.68 kcal mol^{-1}, which represents 48% rescue of the mutational effect. In other words, the covalently modified lysine mimetic is able to rescue the lyase activity because the positive charge contributing to catalysis is part of the active site loop that re-organizes with loop closure.

The decrease in catalytic efficiency of PchB WT treated with bromoethylamine as compared to PchB WT and may be due to the alkyl-amination of the cysteine at position 7. In order to control for the effects of modification at the naturally occurring cysteine in PchB, the C7A mutant was generated. The K42C mutation over the C7A background (double mutant C7A,K42C) resulted in a mutational effect energy gain of 4.16 kcal mol^{-1}. Treatment with BrEA of the double mutant C7A,K42C rescued 2.49 kcal mol^{-1}, 60% of the mutational effect. These results confirm the chemical rescue observed in the single mutant, K42C: covalent modification to generate a lysine mimetic at position 42 on the mobile active site loop rescues catalytic activity.

In order to determine whether we could rescue catalytic activity through hydrogen bonding alone, and no positive charge at position 42, we generated a variant with a hydroxyl group in place of the amine at position 42, by treating the C7A,K42C double mutant with bromoethanol instead of bromoethylamine. Treatment with bromoethanol resulted in the opposite effect as observed with bromoethylamine treatment; an additional 0.27 kcal mol^{-1} increase in activation energy. A hydrogen bond donor at position 42 does not rescue catalytic activity as does the positive charge of the lysine mimetic.

Previous mutagenesis[14] and pH dependence[15] experiments provided evidence that the positive charge at position 42 is important for efficient catalysis. The ability to rescue catalytic activity of the K42C variant through the generation of a γ-thio-lysine at position 42, but not through the generation of the hydroxyl derivative, gives further support to the importance of electrostatic transition state stabilization in the isochorismate-pyruvate lyase reaction. Structural[22] and thermodynamic[23] experiments have led to the

hypothesis that loop dynamics are important for catalysis. Indeed, this is supported by the ineffectiveness of the propylamine as a non-covalent chemical rescue reagent; the positive charge must be organized with the loop for efficient catalysis. In sum, these results indicate that a positive charge at position 42 AND correct loop organization lead to efficient lyase catalysis, and give further support to the idea that electrostatic transition state stabilization and loop dynamics work in concert for catalysis.

4.4 References

1. Colleluori, D.M., et al., *Probing the role of the hyper-reactive histidine residue of arginase.* Archives of biochemistry and biophysics, 2005. **444**(1): p. 15-26.

2. Kim, D.W., et al., *Studies of the active-site lysyl residue of thermostable aspartate aminotransferase: combination of site-directed mutagenesis and chemical modification.* J Biochem, 1994. **115**(1): p. 93-7.

3. Planas, A. and J.F. Kirsch, *Reengineering the catalytic lysine of aspartate aminotransferase by chemical elaboration of a genetically introduced cysteine.* Biochemistry, 1991. **30**(33): p. 8268-76.

4. Smith, H.B. and F.C. Hartman, *Restoration of activity to catalytically deficient mutants of ribulosebisphosphate carboxylase/oxygenase by aminoethylation.* J Biol Chem, 1988. **263**(10): p. 4921-5.

5. Toney, M.D. and J.F. Kirsch, *Direct Bronsted analysis of the restoration of activity to a mutant enzyme by exogenous amines.* Science, 1989. **243**(4897): p. 1485-8.

6. Toney, M.D. and J.F. Kirsch, *Bronsted analysis of aspartate aminotransferase via exogenous catalysis of reactions of an inactive mutant.* Protein science : a publication of the Protein Society, 1992. **1**(1): p. 107-19.

7. Adelroth, P., et al., *Identification of the proton pathway in bacterial reaction centers: decrease of proton transfer rate by mutation of surface histidines at H126 and H128 and chemical rescue by imidazole identifies the initial proton donors.* Biochemistry, 2001. **40**(48): p. 14538-46.

8. Hur, S. and T.C. Bruice, *The mechanism of catalysis of the chorismate to prephenate reaction by the Escherichia coli mutase enzyme.* Proceedings of the National Academy of Sciences of the United States of America, 2002. **99**(3): p. 1176-81.

9. Hur, S. and T.C. Bruice, *Comparison of formation of reactive conformers (NACs) for the Claisen rearrangement of chorismate to prephenate in water and in the E. coli mutase: the efficiency of the enzyme catalysis.* Journal of the American Chemical Society, 2003. **125**(19): p. 5964-72.

10. Hur, S. and T.C. Bruice, *Enzymes do what is expected (chalcone isomerase versus chorismate mutase).* Journal of the American Chemical Society, 2003. **125**(6): p. 1472-3.

11. Zhang, X. and T.C. Bruice, *The proficiency of a thermophilic chorismate mutase enzyme is solely through an entropic advantage in the enzyme reaction.* Proceedings of the National Academy of Sciences of the United States of America, 2005. **102**(51): p. 18356-60.

12. Zhang, X. and T.C. Bruice, *A definitive mechanism for chorismate mutase.* Biochemistry, 2005. **44**(31): p. 10443-8.

13. Zhang, X. and T.C. Bruice, *Temperature dependence of the structure of the substrate and active site of the Thermus thermophilus chorismate mutase E x S complex.* Biochemistry, 2006. **45**(28): p. 8562-7.

14. Luo, Q., J. Olucha, and A.L. Lamb, *Structure-function analyses of isochorismate-pyruvate lyase from Pseudomonas aeruginosa suggest differing catalytic mechanisms for the two pericyclic reactions of this bifunctional enzyme.* Biochemistry, 2009. **48**(23): p. 5239-45.

15. Olucha, J., et al., *pH Dependence of catalysis by Pseudomonas aeruginosa isochorismate-pyruvate lyase: implications for transition state stabilization and the role of lysine 42.* Biochemistry, 2011. **50**(33): p. 7198-207.

16. Claeyssens, F., et al., *Multiple high-level QM/MM reaction paths demonstrate transition-state stabilization in chorismate mutase: correlation of barrier height with transition-state stabilization.* Chemical Communications, 2005(40): p. 5068-5070.

17. Cload, S.T., et al., *Mutagenesis study of active site residues in chorismate mutase from Bacillus subtilis.* Journal of the American Chemical Society, 1996. **118**(7): p. 1787-1788.

18. Gustin, D.J., et al., *Heavy atom isotope effects reveal a highly polarized transition state for chorismate mutase.* Journal of the American Chemical Society, 1999. **121**(8): p. 1756-1757.

19. Warshel, A., et al., *Electrostatic basis for enzyme catalysis.* Chemical Reviews, 2006. **106**(8): p. 3210-3235.

20. Kast, P., et al., *Exploring the active site of chorismate mutase by combinatorial mutagenesis and selection: the importance of electrostatic catalysis.* Proceedings of the National Academy of Sciences of the United States of America, 1996. **93**(10): p. 5043-8.

21. Kast, P., et al., *A strategically positioned cation is crucial for efficient catalysis by chorismate mutase.* The Journal of biological chemistry, 2000. **275**(47): p. 36832-8.

22. Zaitseva, J., et al., *Two crystal structures of the isochorismate pyruvate lyase from Pseudomonas aeruginosa.* The Journal of biological chemistry, 2006. **281**(44): p. 33441-9.

23. Luo, Q., K.M. Meneely, and A.L. Lamb, *Entropic and enthalpic components of catalysis in the mutase and lyase activities of Pseudomonas aeruginosa PchB.* Journal of the American Chemical Society, 2011. **133**(18): p. 7229-33.

24. Sedlak, J. and R.H. Lindsay, *Estimation of total, protein-bound, and nonprotein sulfhydryl groups in tissue with Ellman's reagent.* Analytical biochemistry, 1968. **25**(1): p. 192-205.

25. Arnett, S.O., B. Gerratana, and C.A. Townsend, *Rate-limiting steps and role of active site Lys443 in the mechanism of carbapenam synthetase.* Biochemistry, 2007. **46**(32): p. 9337-9345.

26. Zheng, R. and J.S. Blanchard, *Identification of active site residues in E. coli ketopantoate reductase by mutagenesis and chemical rescue.* Biochemistry, 2000. **39**(51): p. 16244-51.

Chapter 5: Computational Enzymology of PchB

5.1 Introduction

Computational chemistry is a branch of chemistry that uses principles of computer science to assist in solving chemical problems. Experimental and theoretical chemistry results are incorporated into *in silico* models to calculate the structures and properties of molecules and trajectories (calculated reaction pathway) of enzymatic reactions. Necessity for computational enzymology arises from the idea that some enzymology questions cannot be solved analytically. Most often, computational results complement the information obtained by chemical experiments, but in some cases virtual experiments are also able to predict unobserved chemical phenomena. Computational enzymology is widely used in the design of new drugs and materials. Properties such as the structure of a transition state (i.e. the expected positions of the constituent atoms), interaction energies, electronic charge distributions, dipoles and vibrational frequencies, reactivity or other spectroscopic quantities can be determined using computational methods [1].

The combination of quantum mechanics and molecular mechanics (QM/MM), was first introduced by Warshel and Levitt in 1976 [2]. This hybrid technique combines a classical molecular mechanical definition of the biological system (atom positions and bond distances and types are defined), together with a quantum-mechanical definition of the region of interest (*e.g.* active site, substrate). The quantum-mechanical region is defined by approximating the atomic nuclei as point charges, and the electronic wave-

function as a set of Gaussian approximations. In contrast to the regions defined with classical molecular mechanics, this allows bond breaking and bond forming to be modeled in reaction trajectories. Increased computational power of modern parallel and vector-parallel platforms has for the first time allowed simulations of realistic large systems, including biomolecular structures and reactions [3]. This entirely new branch of biological chemistry is able to complement traditional *in vivo* and *in vitro* experiments, offering the possibility of performing with great accuracy virtual experiments on computers.

A significant amount of *in silico* work has been carried out on chorismate mutases, including *E. coli* chorismate mutases from E. coli (EcCM) [4-12] and *Bacillus subtillis* (BsCM) [1, 6, 9, 13-16], as well the isochorismate-pyruvate lyase from *P. aeruginosa* (PchB)[5, 17]. Indeed, The near attack conformation hypothesis (NAC), which proposes that the correct substrate conformation is enough to drive the reaction forward [8-12], was developed based on theoretical and computational work done on EcCM. Computational work on BsCM proposed that in addition to the NAC, electrostatic transition state stabilization is also required for the mutase reaction [4, 16]. In PchB, Marti *et al.* looked at the mutase and lyase activities and the effect of the A37I mutation on catalytic activity [17].

The data obtained from the mutational [18], pH [19] and chemical rescue experiments described in **chapters 2, 3, and 4** of this dissertation, identified the catalytic importance of the positive charge on the active site loop at position 42 (in the form of a lysine), *and* the importance of position and orientation of the positive charge with loop closure for efficient catalysis. Computational enzymology is the ideal tool to investigate these ideas,

since it enables us to observe the active site in more detail to measure angles and distances, as well as allowing us to test experimental conditions impossible to test in wet systems.

5.2 Materials and Methods

5.2.1 Model Building

The initial structure used to generate the QM/MM model is the X-ray structure of PchB (Protein Data Bank entry 3REM) containing salicylate and pyruvate in the active site. For K42H mutant, the K to H mutation was performed using COOT [20]. The original substrates were replaced by isochorismate, overlaying the molecule over the electron density map to fit the ring over the salicylate density and the enolypyruvyl tail to over the pyruvate density using COOT [20]. The hydrogen atoms were incorporated into the structure and minimized using CHARMM [21]. The model was placed in a sphere of waters 25 Å in diameter and minimized using QM at the AM1 level (**Figure 5-1**). Atoms beyond the sphere of water were removed, and the full system was relaxed by successive QM/MM minimization steps, equilibrated at 300 K with a time step of 1.0 fs during a total time of 500 ps. The geometry of the substrate was maintained by means of harmonic restraints applied to internal coordinates.

5.2.2 Single Coordinate Reactions

Single coordinate trajectories were carried out using CHARMM using QM at AM1 level, in a sphere of TIP3P waters 25 Å in diameter. Coordinate was calculated as:

$$C = R - Q$$

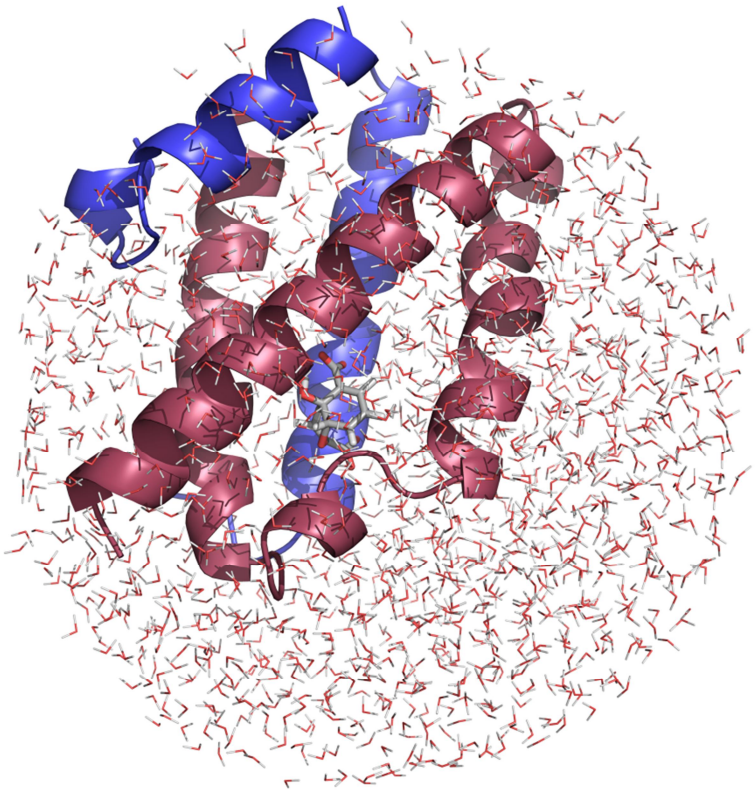

Figure 5-1: overall structure of PchB models: The PchB dimer is placed in a sphere of water molecules with 25 Å radius, with the isochorismate molecule at the center of the model. Any atoms beyond the 25 Å, are removed from the model.

where R and Q define bond breaking and bond forming events (**Figure 5-2**):

$$R = \left[d_{(C2-H21)-(C3'-H21)}\right]$$

and

$$Q = \left[d_{(C3-O3')}\right]$$

where structures were calculated for values of C between -2.0 Å and 2.5 Å in 0.1 Å steps.

Two Coordinate Trajectories

Two coordinate trajectories were calculated by separating R and Q coordinates, and running the trajectories sequentially; first running R values from -2.0 to 2.5 Å in steps of 0.1 while maintaining Q coordinates constant and subsequently running Q values from 1.4 Å to 3.1 Å in steps of 0.1Å for every generated R structure. Energies were calculated and extracted for each structure using CHARMM and plotted as contour plots.

5.3 Results and Discussion

5.3.1 Energies of activation

Single coordinate trajectories have been performed on wild type and K42H PchB (both protonated and unprotonated states of K42, reflecting conditions well above and well

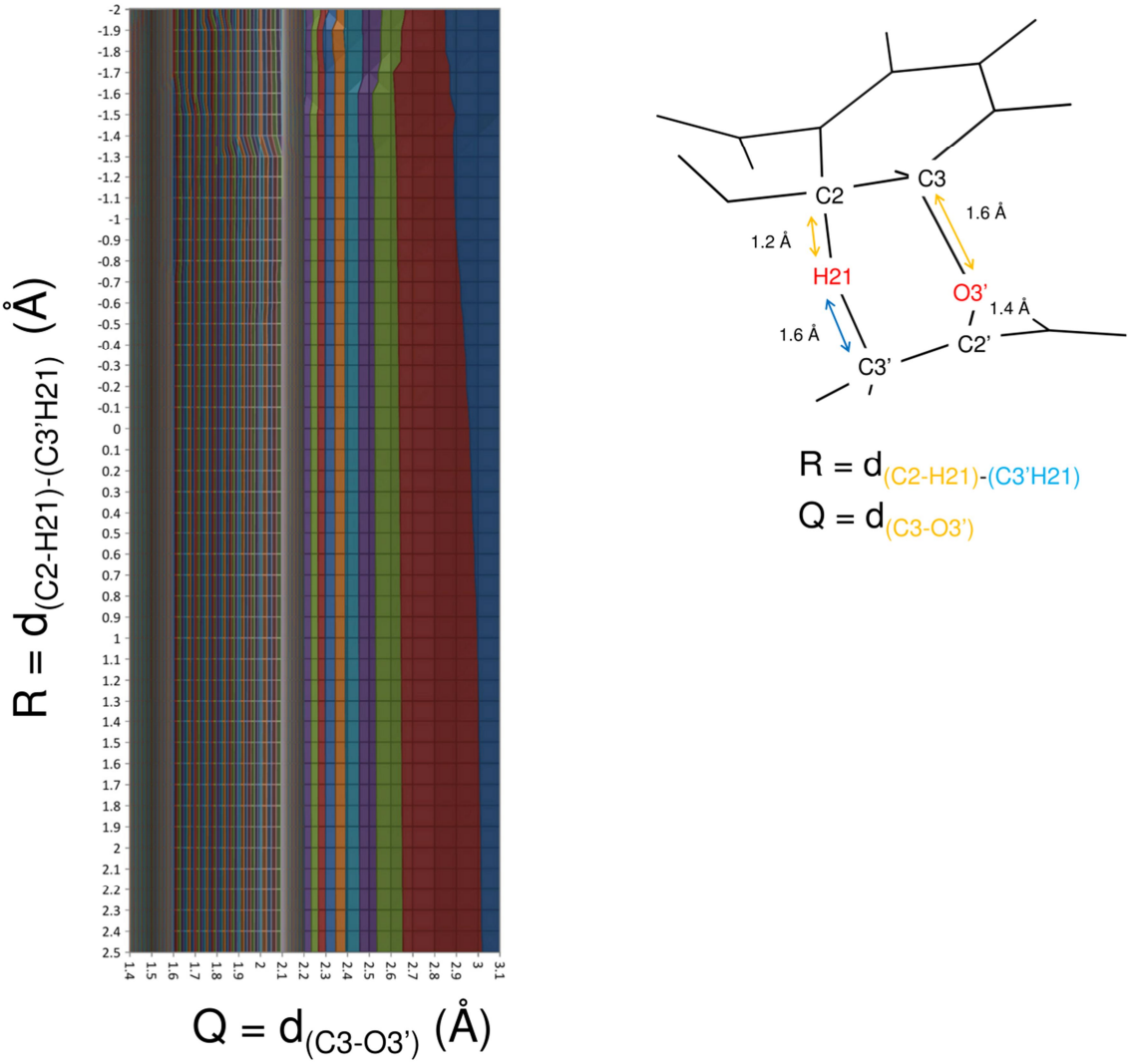

Figure 5-2: Trajectory analysis. To the left, sample double coordinate trajectory model, showing wild type PchB data, with energies at each point plotted in a colored surface plot (highest energy red, lowest energy blue). Double trajectories have to be optimized to improve the resolution of the plot. To the right, model of the transition state as determined by single coordinate trajectory. In red, are the H21 and O3' atoms, at the center of the bond braking and forming. Marked with double orange arrows, the bonds that break to form products, and in blue, the bond generated upon product formation.

below the pKa of histidine). However, in order to determine energies thoughout the trajectories, 2 coordinate trajectories have to be carried out. This work is currently underway to test the proposed “energy landscape” hypothesis [19], proposed by Benkovic and colleagues[22, 23], and states that rather than a two-dimentional reaction coordinate, catalysis occurs through a series of interconnected catalytic networks, influenced among other factors by protein motions and shape[22, 23]. A trajectory determined by 2 coordinates (**as in figure 5-2, left surface plot**) would determine if I can identify different pathways for catalysis that agree with energies calculated experimentally [24].

5.3.2 Transition State

Single trajectory experiments enabled us to determine the lengths of the bonds breaking and forming at the transition state (**Figure 5-2, right**). The breaking **C2-H21** bond is the shortest upon formation of the transition state, at 1.2 Å, stretching until it breaks at 1.8 Å, while the **C3’-H21** bond is 1.6 Å at the transition state and shortens to 1.1 Å (in agreement with theoretical 1.09 Å C-H bond length [25]. The ether oxygen bond (**C3-O3’**) stretches to 1.6 Å at the transition state and breaks at 1.8 Å, and the O3’ C2’ bond remains at 1.4 Å throughout the reaction trajectory. Interestingly, the transition state maintains the same overall structure in the wild type active site and the histidine mutants (both with the protonated and unprotonated histidines) as seen in **figure 5-3, middle column.** However, the difference in shape and size between the lysine and the

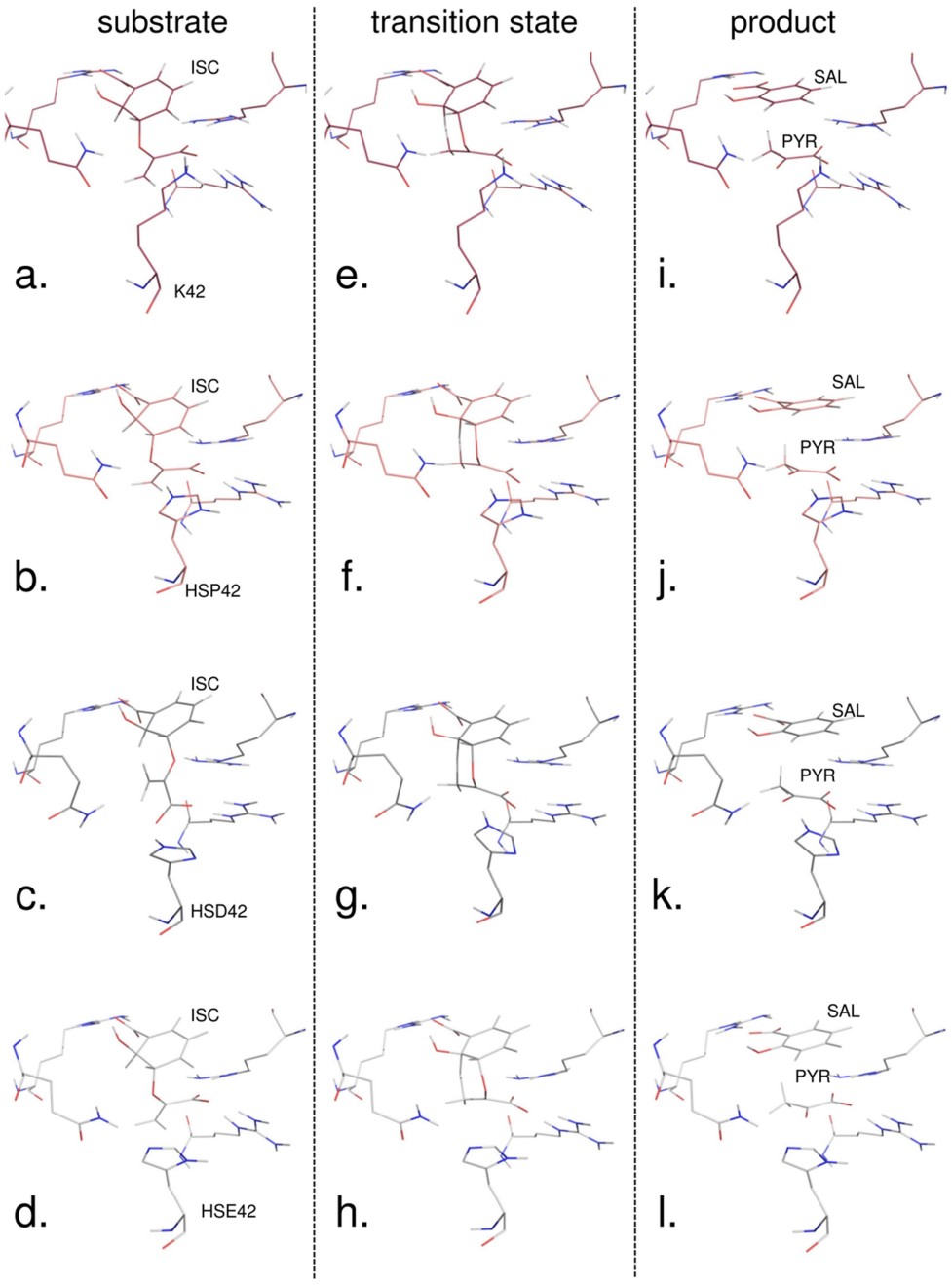

Figure 5-3: Active sites of tested models: wild type (a, e, i), protonated histidine mutant (b, f, j) and deprotonated histidine mutants (HSD in c, g, and k and HSE in d, h, l). showing substrate (column to the left) transition state (middle column) and product (column to the right).

histidine (the histidine is shorter) causes a 0.3 Å shift in the active site. The shift, which can be clearly seen in **figure 5-5,** a comparison between the wild type and protonated histidine (HSP histidine conformer, as diagramed in **figure 5-4**) is not caused by incorrect alignment of the structures, but rather it is caused by a rearrangement in order to accommodate the differences in shape and length of the sidechain (lysine vs. histidine) at position 42, while maintaining the distance between the ether oxygen and the positively charged nitrogen at approximately 3 Å. This small conformational change, would explain the mutational effect observed between the wild type PchB and K42H in the pH experiments [19] at pH 5.5 where the maximal activity of PchB was observed. More interestingly, this shift could explain the higher mutase activity of the K42H mutant at its peak activity as compared to wild type [19], if this small shift is enough to better accommodate the mutase reaction. Further analysis of the transition state is necessary to identify the effect of this shift in catalysis.

The two unprotonated histidine conformers (**Figure 5-6 and 5-6**) show different interactions with the transition state, with the most drastic being the HSD conformer, at a drastically different angle and 1 Å further away from the O3' than any of the other conformers. Indeed preliminary single-coordinate experiments seem to indicate a higher energy barrier for this conformer, in agreement with previous pH and mutational experiments which showed the positive charge at position 42 is important for catalysis [18, 19]. Albeit just preliminary evidence, these trajectories indicate multiple binding modes in the histidine mutant, that would still lead to catalysis if the right conditions are met and the energy barrier is overcome by the enzyme.

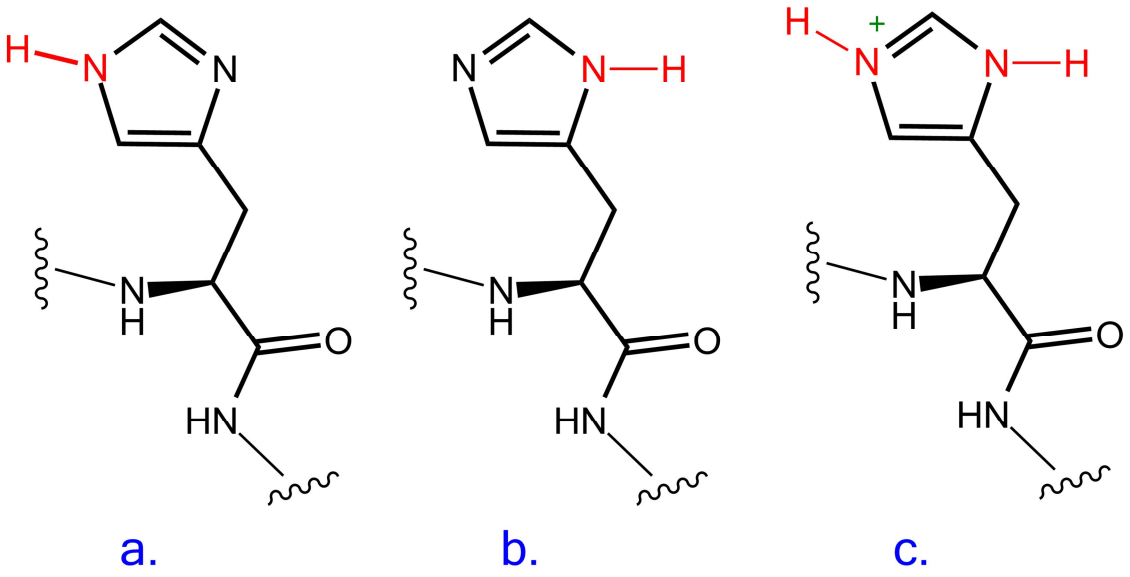

Figure 5-4: Histidine conformers tested: Neutral charge conformers HSE (a) and HSD (b) may have one of two amino groups protonated. On the positively charged conformer (HSP, c) BOTH amino groups are protonated.

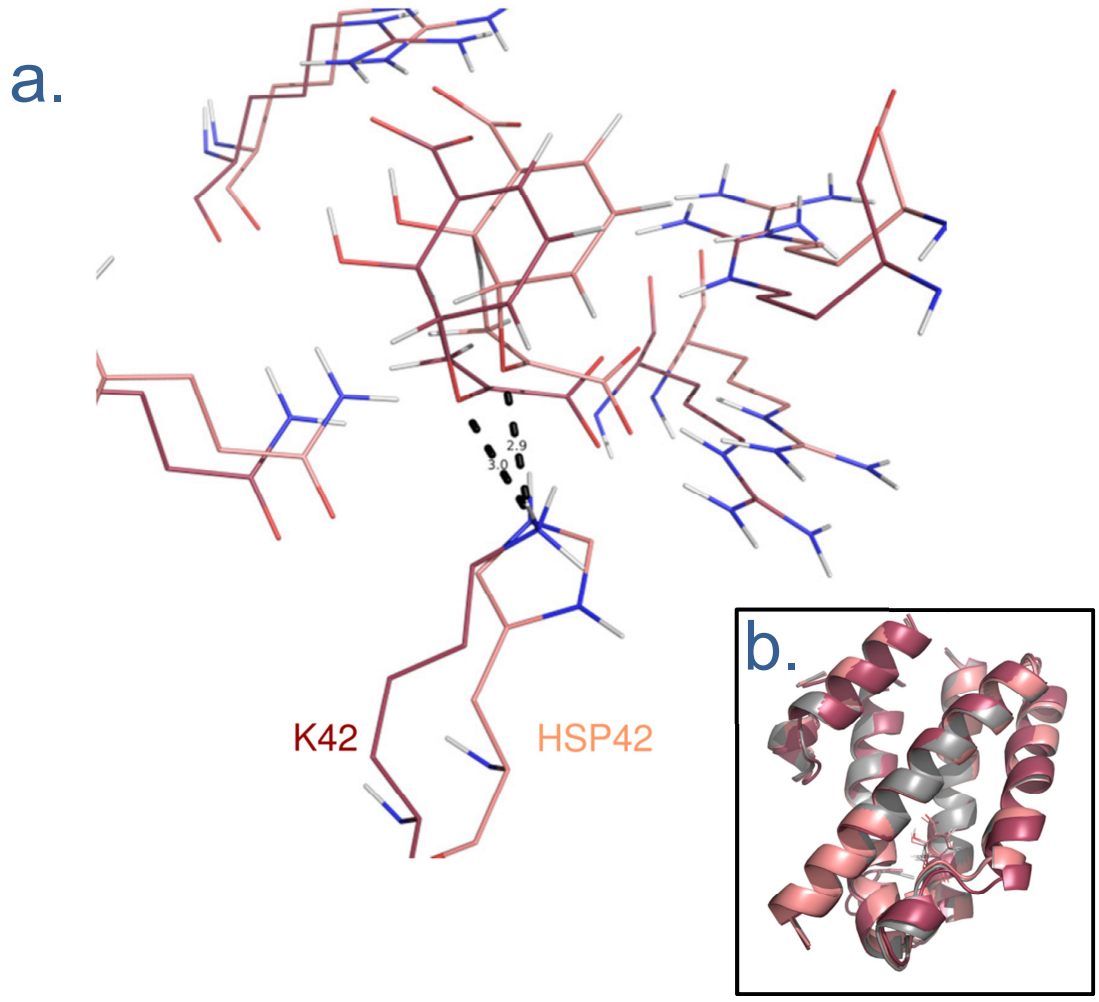

Figure 5-5: Overlay of wild type PchB (dark pink) and protonated histidine mutant (light pink). On **(a)** The positively charged groups are within 0.1 A of each other, (black dashed line) but the overall architecture of the active site is slightly shifted in the histidine mutant as compared to the wild type. This is not due to an improper alignment of the models as can be seen in the cartoon overlay of all four models **(b)** where wild type is dark pink, protonated histidine model is pink and the two unprotonated conformers are colored in shades of grey.

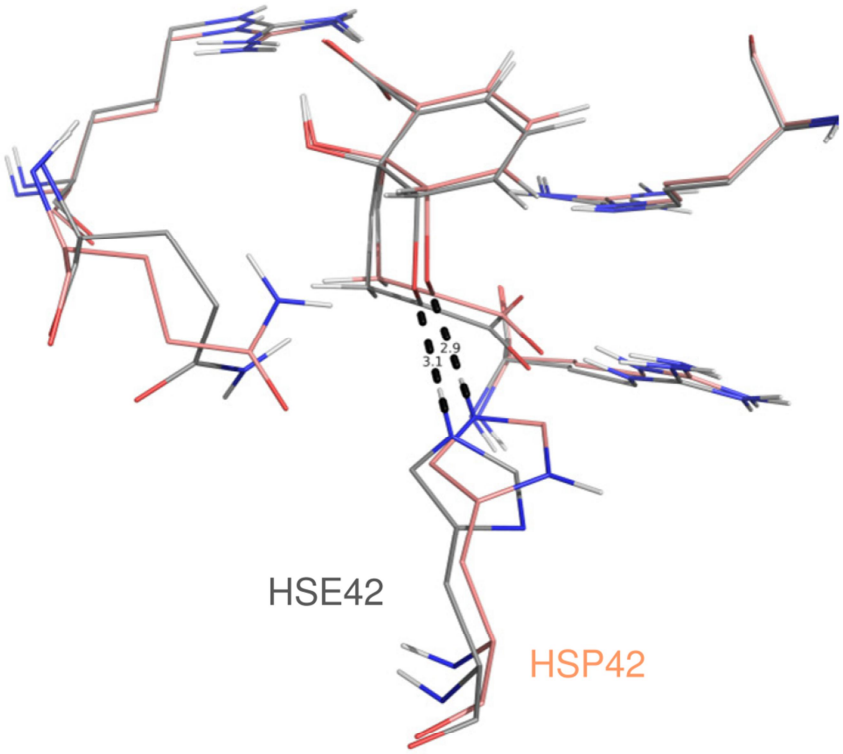

Figure 5-6: Overlay of HSE unprotonated histidine conformer (gray) and protonated histidine mutant (light pink). Although slightly shifted, both imidazole groups are within 0.2 A of each other with respect to the ether oxygen, (black dashed line).

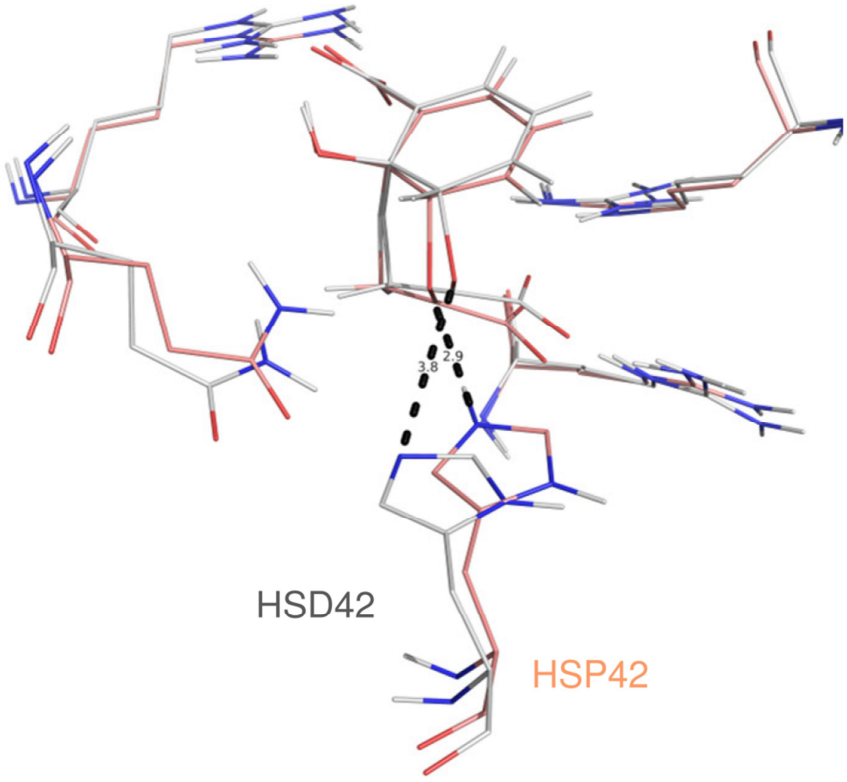

Figure 5-7: Overlay of HSD unprotonated histidine conformer (white) and protonated histidine mutant (light pink). The imidazole groups are positioned at different angles and 0.9 Å of each other with respect to the ether oxygen, (black dashed line).

5.3.3 Substrate binding and Product release

All trajectories, both for wild type and K42H mutant, show the same binding mode for substrate and products, except for the HSD conformer (**figure 5-3 c**), where the enolpyruvyl tail of the isochorismate is interacting with the histidine instead of with one of the argininines. This results in a slightly different trajectory, with preliminary single coordinate experiments indicating a higher energy barrier required to overcome the less optimal binding mode. More detailed two-coordinate trajectories are currently underway, nevertheless, the data shown here is further evidence for a network of catalytic pathways: alternate binding modes of the substrate still lead to product formation, if the energy requirements are met by the enzyme through energetically favorable protein motions.

5.4 Conclusions

Although the computational virtual experiments are still underway, preliminary results are already yielding valuable information. In a more pragmatic sense, a more detailed structure of the transition state and its interactions with residues in the active site can be important for future development of inhibitors, especially in light of the fact that current endo-oxabicyclic transition state analogs cannot be considered good inhibitors because of their low binding affinity [26, 27]. A better understanding of the charge distribution in the transition state could lead to a better rational design approach. In terms of theoretical contributions, the preliminary results agree with the previous mutational, pH, and chemical rescue experiments: **1.)** The positive charge at position 42 is important for efficient catalysis; **2.)** orientation and position of the positive charge at position 42 is

also important, as it affects position of the substrate molecule *and* shape of the active site; and **3.)** Histidine mutant trajectories support the hypothesis of multiple reaction pathways interwoven in a network that forms a three-dimentional catalytic landscape. Further higher level trajectories and molecular dynamics experiments are necessary to understand the preliminary results in more detail. The information obtained in these experiments will be invaluable to develop new testable hypotheses and will provide shed new light on the mutational, pH, and chemical rescue experiments.

5.5 References

1. van der Kamp, M.W. and A.J. Mulholland, *Computational enzymology: insight into biological catalysts from modelling.* Natural Product Reports, 2008. **25**(6): p. 1001-1014.

2. Warshel, A. and M. Levitt, *Theoretical Studies of Enzymic Reactions - Dielectric, Electrostatic and Steric Stabilization of Carbonium-ion reaction of Lysozyme.* Journal of Molecular Biology, 1976. **103**(2): p. 227-249.

3. Senn, H.M. and W. Thiel, *QM/MM Methods for Biomolecular Systems.* Angewandte Chemie-International Edition, 2009. **48**(7): p. 1198-1229.

4. Claeyssens, F., et al., *Multiple high-level QM/MM reaction paths demonstrate transition-state stabilization in chorismate mutase: correlation of barrier height with transition-state stabilization.* Chemical Communications, 2005(40): p. 5068-5070.

5. Ferrer, S., et al., *Molecular mechanism of chorismate mutase activity of promiscuos MbtI.* Theoretical Chemistry Accounts, 2011. **128**(4-6): p. 601-607.

6. Kast, P., M. AsifUllah, and D. Hilvert, *Is chorismate mutase a prototypic entropy trap? Activation parameters for the Bacillus subtilis enzyme.* Tetrahedron Letters, 1996. **37**(16): p. 2691-2694.

7. Lamb, A.L., *Pericyclic Reactions Catalyzed by Chorismate-Utilizing Enzymes.* Biochemistry, 2011. **50**(35): p. 7476-7483.

8. Bruice, T.C., *A view at the millennium: The efficiency of enzymatic catalysis.* Accounts of Chemical Research, 2002. **35**(3): p. 139-148.

9. Hur, S. and T.C. Bruice, *The near attack conformation approach to the study of the chorismate to prephenate reaction.* Proceedings of the National Academy of Sciences of the United States of America, 2003. **100**(21): p. 12015-12020.

10. Lau, E.Y. and T.C. Bruice, *Importance of correlated motions in forming highly reactive near attack conformations in catechol O-methyltransferase.* Journal of the American Chemical Society, 1998. **120**(48): p. 12387-12394.

11. Lightstone, F.C. and T.C. Bruice, *Ground state conformations and entropic and enthalpic factors in the efficiency of intramolecular and enzymatic reactions .1. Cyclic anhydride formation by substituted glutarates, succinate, and 3,6-endoxo-Delta(4)-tetrahydrophthalate monophenyl esters.* Journal of the American Chemical Society, 1996. **118**(11): p. 2595-2605.

12. Torres, R.A. and T.C. Bruice, *Molecular dynamics study displays near in-line attack conformations in the hammerhead ribozyme self-cleavage reaction.* Proceedings of the National Academy of Sciences of the United States of America, 1998. **95**(19): p. 11077-11082.

13. Cload, S.T., et al., *Mutagenesis study of active site residues in chorismate mutase from Bacillus subtilis.* Journal of the American Chemical Society, 1996. **118**(7): p. 1787-1788.

14. Lyne, P.D., A.J. Mulholland, and W.G. Richards, *Insights Into Chorismate Mutase Catalysis From a Combined QM/MM Simulation of the Enzyme Reaction.* Journal of the American Chemical Society, 1995. **117**(45): p. 11345-11350.

15. Martin, N.I., et al., *Isolation, structural characterization, and properties of mattacin (Polymyxin M), a cyclic peptide antibiotic produced by Paenibacillus kobensis* Journal of Biological Chemistry, 2003. **278**(15): p. 13124-13132.

16. Ranaghan, K.E. and A.J. Mulholland, *Conformational effects in enzyme catalysis: QM/MM free energy calculation of the 'NAC' contribution in chorismate mutase.* Chemical Communications, 2004(10): p. 1238-1239.

17. Marti, S., et al., *Mechanism and Plasticity of Isochorismate Pyruvate Lyase: A Computational Study.* Journal of the American Chemical Society, 2009. **131**(44): p. 16156-16161.

18. Luo, Q., J. Olucha, and A.L. Lamb, *Structure-function analyses of isochorismate-pyruvate lyase from Pseudomonas aeruginosa suggest differing catalytic mechanisms for the two pericyclic reactions of this bifunctional enzyme.* Biochemistry, 2009. **48**(23): p. 5239-45.

19. Olucha, J., et al., *pH Dependence of catalysis by Pseudomonas aeruginosa isochorismate-pyruvate lyase: implications for transition state stabilization and the role of lysine 42.* Biochemistry, 2011. **50**(33): p. 7198-207.

20. Emsley, P. and K. Cowtan, *COOT: model-building tools for molecular graphics.* Acta Crystallographica Section D-Biological Crystallography, 2004. **60**: p. 2126-2132.

21. Brooks, B.R., et al., *CHARMM: The Biomolecular Simulation Program.* Journal of Computational Chemistry, 2009. **30**(10): p. 1545-1614.

22. Benkovic, S.J., G.G. Hammes, and S. Hammes-Schiffer, *Free-energy landscape of enzyme catalysis.* Biochemistry, 2008. **47**(11): p. 3317-3321.

23. Benkovic, S.J. and K.D. Raney, *Mechanisms: molecular machines.* Current Opinion in Chemical Biology, 2011. **15**(5): p. 577-579.

24. Luo, Q., K.M. Meneely, and A.L. Lamb, *Entropic and enthalpic components of catalysis in the mutase and lyase activities of Pseudomonas aeruginosa PchB.* Journal of the American Chemical Society, 2011. **133**(18): p. 7229-33.

25. Bartell, L.S., et al., *Electron-Diffraction Study of the Structures of C_2H_4 and C_2D_4.* Journal of Chemical Physics, 1965. **42**(8).

26. Bartlett, P.A., et al., *Chorismate Mutase Inhibitors - Synthesis and Evaluation of Some Potential Transition-State Analogs.* Journal of Organic Chemistry, 1988. **53**(14): p. 3195-3210.

27. Nakagawa, Y., et al., *Chorismate Mutase Inhibitors - Design, Synthesis, and Evaluation of Some Potential Transition-State Analogs.* Abstracts of Papers of the American Chemical Society, 1989. **197**: p. 126-AGRO.

Chapter 6: Conclusions from PchB Experiments.

6.1 How PchB derives its catalytic power is a matter of debate

Two competing hypothesis propose different models as to how PchB derives its catalytic power. The electrostatic transition state stabilization hypothesis proposes that a positive charge, in the form of K42 in PchB or K39 in EcCM, stabilizes the developing negative charge at the ether oxygen [1-6]. A second model based on quantum mechanical/molecular mechanical (QM/MM) simulations [7-12], proposes that a substrate conformation (near attack conformation or NAC) in which the reacting atoms are within van der Waals contact distance and at an orientation in which the π-orbitals overlap [8, 10]. The model proposes that once this conformation forms, the reaction occurs spontaneously, without the need for electrostatic stabilization of the transition state [7-10, 12].

6.2 pH Experiments suggest multiple reaction pathways and three-dimentional free-energy landscape rather than 2-dimentional free energy coordinate

The pH experiments described in **Chapter 3** build upon mutational and thermodynamic analyses of PchB [13] that indicated that neither NAC formation or electrostatic transition state stabilization completely account for catalysis [13].

The pH experiments allowed me to test the contribution of both electrostatic transition state stabilization and near attack conformations, for both lyase and mutase activities in a single mutant enzyme. The results indicate that rather than one or the other catalytic mechanism, both contribute to lowering of the energy barrier to drive catalysis, resulting not in a 2 dimensional free energy trajectory but rather a free energy landscape resulting from a network of different possible pathways, similar to those proposed by Benkovic [14-17].

6.3 Chemical Rescue experiments suggest active site loop has to be organized for effective lyase catalysis

The mutagenesis and pH dependence [18] experiments provided evidence that the positive charge at position 42 is important for efficient lyase catalysis, but some other mechanism (possibly the formation of a NAC) was sufficient for lyase catalysis. This suggested a network of catalytic mechanisms contributing to catalysis. Thermodynamic data [19], suggested that loop motions are also important for catalysis. The next question to ask was whether enzyme movements also contribute to catalysis, as has been proposed by Benkovic [27], and if so, how. Prior to the chemical rescue experiments described in **Chapter 4**, we hypothesized that the closing of the active site loop was important for catalysis, in particular because the K42, required for efficient catalysis, is in said loop. The ability to rescue catalytic activity of the K42C variant through the generation of a γ-thio-lysine at position 42, but not through the generation of the hydroxyl derivative, gives further support to the importance of electrostatic transition

state stabilization in the isochorismate-pyruvate lyase reaction. The ineffectiveness of the propylamine as a non-covalent chemical rescue reagent indicates that the positive charge must be organized *with the loop* for efficient catalysis: correct loop organization leads to efficient lyase catalysis. This once again points to a catalytic network with multiple contributors to catalysis: substrate shape in the active site, electrostatic stabilization of the transistion state, and loop organization all contribute to catalysis.

6.4 Computational enzymology experiments agree with and shed new light on previous experimental results

QM/MM experiments are still ongoing. However, some valuable information has been extracted from these first sets of experiments. Preliminary results agree with the previous mutational, pH, and chemical rescue experiments, indicating that the positive charge at position 42 is important for efficient lyase catalysis *and* the orientation and position of the positive charge is very important. Snapshots of the active site throughout the reaction trajectory suggest that the position of the positive charge affects position of the substrate molecule *and* shape of the active site when substrate binds. This accounts for the mutational effect seen in the pH experiments between wild type PchB and K42H at maximal K42H activity – the shape and orientation of the positive charge is not optimal for catalysis. Unexpectedly, histidine mutant trajectories support the hypothesis of multiple reaction pathways interwoven in a network that forms a three-dimentional catalytic landscape: protonated and unprotonated mutant active sites show different modes of binding substrate and transition state, yet these modes may all lead to

turnover, given the right conditions. Further higher level trajectories and molecular dynamics experiments are necessary to understand these preliminary results in more detail. These experiments are also yielding more detailed structure of the transition state and its interactions in the active site. This information may lead to future rational design of transition state analog inhibitors. Further higher level QM/MM computational experiments are needed to understand the lyase chemistry in more detail, but preliminary results have already yielded valuable information.

Taken together, these three different lines of experimentation all point to the conclusion that a positive charge at the 42 position must be organized within the active site for efficient catalysis.

6.5 References

1. Cload, S.T., et al., *Mutagenesis Study of Active Site Residues in Chorismate Mutase from Bacillus subtilis.* J. Am. Chem. Soc., 1996. **118**(7): p. 1787-1788.

2. Gustin, D.J., et al., *Heavy Atom Isotope Effects Reveal a Highly Polarized Transition State for Chorismate Mutase.* J. Am. Chem. Soc., 1999. **121**(8): p. 1756-1757.

3. Kast, P., et al., *Exploring the active site of chorismate mutase by combinatorial mutagenesis and selection: the importance of electrostatic catalysis.* Proc. Natl. Acad. Sci. U.S.A., 1996. **93**(10): p. 5043-8.

4. Kast, P., et al., *A strategically positioned cation is crucial for efficient catalysis by chorismate mutase.* J. Biol. Chem., 2000. **275**(47): p. 36832-8.

5. Kienhofer, A., P. Kast, and D. Hilvert, *Selective stabilization of the chorismate mutase transition state by a positively charged hydrogen bond donor.* J. Am. Chem. Soc., 2003. **125**(11): p. 3206-7.

6. Liu, D.R., et al., *Analysis of Active Site Residues in Escherichia coli Chorismate Mutase by Site-Directed Mutagenesis.* J. Am. Chem. Soc., 1996. **118**(7): p. 1789-1790.

7. Hur, S. and T.C. Bruice, *The mechanism of catalysis of the chorismate to prephenate reaction by the Escherichia coli mutase enzyme.* Proc. Natl. Acad. Sci. U.S.A., 2002. **99**(3): p. 1176-81.

8. Hur, S. and T.C. Bruice, *The near attack conformation approach to the study of the chorismate to prephenate reaction.* Proc. Natl. Acad. Sci. U.S.A., 2003. **100**(21): p. 12015-20.

9. Hur, S. and T.C. Bruice, *Just a near attack conformer for catalysis (chorismate to prephenate rearrangements in water, antibody, enzymes, and their mutants).* J. Am. Chem. Soc., 2003. **125**(35): p. 10540-2.

10. Hur, S. and T.C. Bruice, *Comparison of formation of reactive conformers (NACs) for the Claisen rearrangement of chorismate to prephenate in water and in the E. coli mutase: the efficiency of the enzyme catalysis.* J. Am. Chem. Soc., 2003. **125**(19): p. 5964-72.

11. Schowen, R.L., *How an enzyme surmounts the activation energy barrier.* Proc. Natl. Acad. Sci. U.S.A., 2003. **100**(21): p. 11931-2.

12. Zhang, X., X. Zhang, and T.C. Bruice, *A definitive mechanism for chorismate mutase.* Biochemistry, 2005. **44**(31): p. 10443-8.

13. Luo, Q., J. Olucha, and A.L. Lamb, *Structure-function analyses of isochorismate-pyruvate lyase from Pseudomonas aeruginosa suggest differing catalytic mechanisms for the two pericyclic reactions of this bifunctional enzyme.* Biochemistry, 2009. **48**: p. 5239-5245.

14. Benkovic, S.J., G.G. Hammes, and S. Hammes-Schiffer, *Free-energy landscape of enzyme catalysis.* Biochemistry, 2008. **47**(11): p. 3317-3321.

15. Benkovic, S.J. and K.D. Raney, *Mechanisms: molecular machines.* Current Opinion in Chemical Biology, 2011. **15**(5): p. 577-579.

16. Bhabha, G., et al., *A Dynamic Knockout Reveals That Conformational Fluctuations Influence the Chemical Step of Enzyme Catalysis.* Science, 2011. **332**(6026): p. 234-238.

17. Hammes, G.G., S.J. Benkovic, and S. Hammes-Schiffer, *Flexibility, Diversity, and Cooperativity: Pillars of Enzyme Catalysis.* Biochemistry, 2011. **50**(48): p. 10422-10430.

18. Olucha, J., et al., *pH Dependence of catalysis by Pseudomonas aeruginosa isochorismate-pyruvate lyase: implications for transition state stabilization and the role of lysine 42.* Biochemistry, 2011. **50**(33): p. 7198-207.

19. Luo, Q.Y., K.M. Meneely, and A.L. Lamb, *Entropic and Enthalpic Components of Catalysis in the Mutase and Lyase Activities of Pseudomonas aeruginosa PchB.* Journal of the American Chemical Society, 2011. **133**(18): p. 7229-7233.

Chapter 7: PvdA introduction

7.1 Classification of Flavoprotein Monooxygenases

Flavoprotein monooxygenases are enzymes that use flavins an electron rich organic cofactor, to transfer molecular oxygen to organic compounds[1]. As shown on **Table 7-1** flavoprotein monooxygenases have been categorized into 6 classes ([2] A-F, Table 1). Class A and Class B enzymes are single component monooxygenases (encoded by a single gene), that use FAD as redox center, bound in a Rossmann-like, dinucleotide-binding domain [3]. Class A enzymes use either NADH or NADPH, which is released immediately upon FAD reduction, while Class B flavoproteins use exclusively NADPH as electron donor, which remains bound in the active site throughout the oxidative half reaction[3]. Classes C-F of flavoprotein monooxygenase on the other hand encompass two component enzymes (a flavin reductase and an oxidase), that use either FMN (Class C), or FAD (D-F), and interchangeably use NADH or NADPH as electron donor[3]. As opposed to the Rossman-like domains of the class A's and B's, class C monooxygenases are characterized by a TIM-barrel fold[3]. There are no structures available for Class D or E monooxygenases but are believed to contain Rossmann-like folds, and class F enzymes are mostly alpha helical[3].

7.2 PvdA is a Class B Flavoprotein

PvdA, the ornithine monooxygenase from Pseudomonas aeruginosa is the subject of the second half of this dissertation. PvdA catalyzes an FAD dependent hydroxylation of ornithine to hydroxyornithine using molecular oxygen and NADPH as electron donor [4].

Table 7-1: Classification of Flavoprotein Monooxygenases[1]

Class	Subclass	Reaction	Representative	Genes	Coenzyme	Cofactor
A	-	hydroxylation epoxidation	*para*-Hydroxy-benzoate hydroxylase	1	FAD	NAD(P)H
B	Flavin Dependent	heteroatom hydroxylation	yeast FMO			
	Baeyer Villiger	ketone to ester	Hyclohexanone monooxygenase	1	FAD	NADPH
	N-Hydroxylating	primary amine hydroxylation	PvdA			
C	-	light emission S-oxidation ketone to ester	Luciferase	2- reductase and oxidase	FMN	NAD(P)H
D	-	hydroxylation	*para*-Hydroxy-phenylacetate hydroxylase	2- reductase and oxidase	FAD	NAD(P)H
E	-	epoxidation	Styrene monooxygenase	2- reductase and oxidase	FAD	NAD(P)H
F	-	halogenation	Tryptophan 7-halogenase	2- reductase and oxidase	FAD	NAD(P)H

[1] Table adapted from van Berkel *et al.* 2006 [3]

PvdA is a member of the class B family of flavin dependent monooxygenases (FDMOs)[5, 6]. As mentioned above, class B monooxygenases share a common set of characteristics, albeit catalyzing a wide variety of reactions: **1.)** They are single component enzymes encoded by a single gene, **2.)** They have Rossmann-like dinucleotide binding domains to bind flavin and electron donor, **3.)** They use FAD as the redox center, which is stably bound to the enzyme, **4.)** They use NADPH exclusively as the electron donor (never NADH and finally, **5.)** the NADP+ remains bound in the active site throughout the oxidative half reaction [3].

7.3 Class B Flavoprotein Monooxygenases

The class B family of monooxygenases is subdivided into 3 subclasses: flavin containing monooxygenases (FMOs), microbial N-hydroxylating monooxygenases, and Baeyer Villager monooxygenases (BVMOs) [3].

7.3.1 Flavin Containing Monooxygenases

Flavin Containing Monooxygenases (FMOs), were originally named “mixed-function oxidases” because of their ability to hydroxylate a wide variety of xenobiotics in liver microsomes [7]. FMOs are found in all mammals, including humans, other eukaryotic organisms, including plants and yeast, and some bacteria [8-11]. Mammalian FMOs play a similar role to that of cytochrome P450 system in detoxification of drugs and other xenobiotics[12-18]. Mammalian FMOs catalyze the monooxygenation of carbon-bound reactive heteroatoms nitrogen, sulfur, phosphorus, selenium, and iodine **(Figure 7-1 b)** [19]. In plants, FMOs have been found to be involved in the tryptophan-

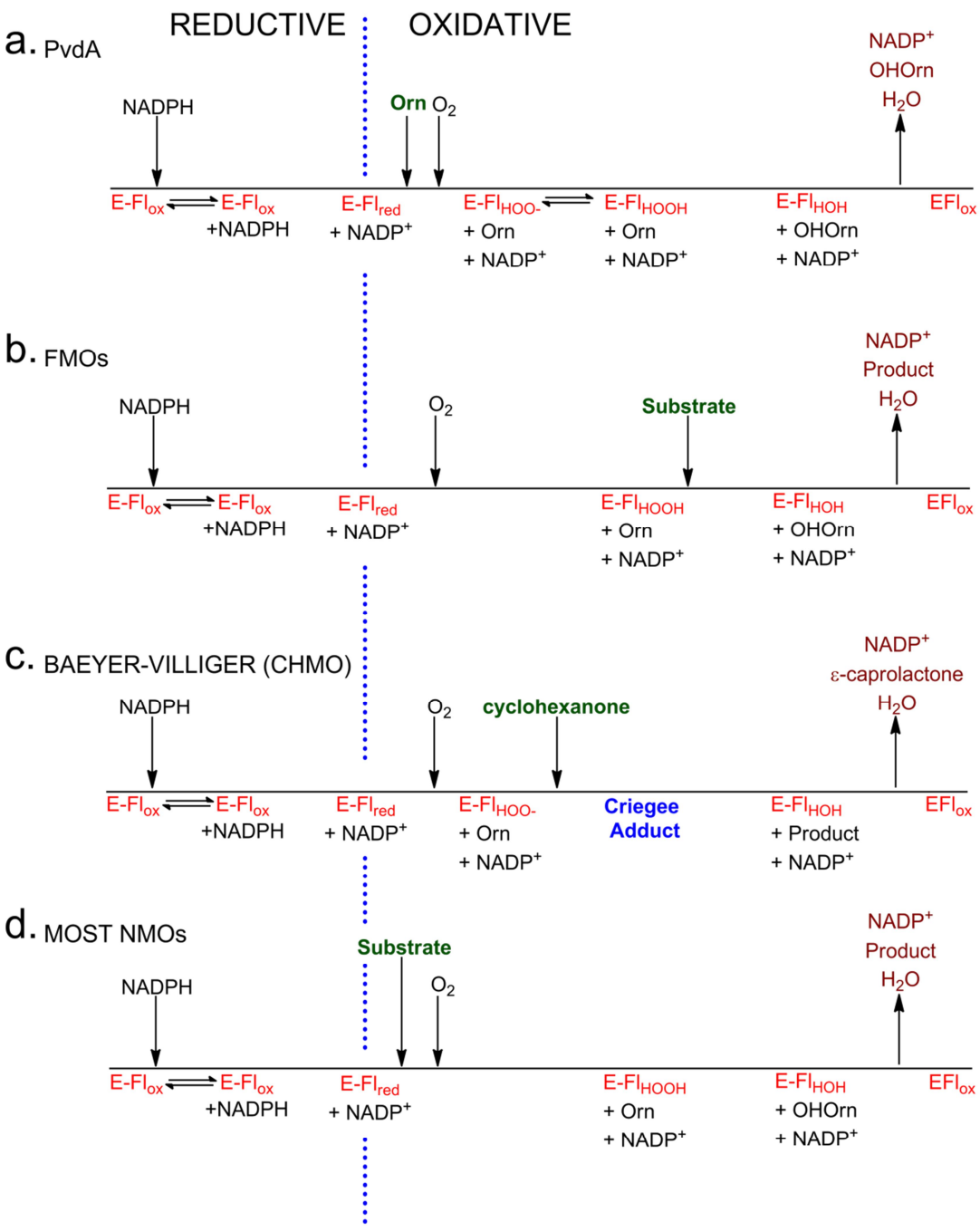

Figure 7-1: Comparison of Catalytic cycles of the Class B Flavoprotein monooxygenases. PvdA (a) catalytic cycle is unique from FMOs (b) in regards to the timing of the binding of the substrate and the formation of a relatively stable peroxyflavin. Baeyer-Villiger Monooxygenases' catalytic cycle (c) is characterized by the formation of the Criegee adduct necessary for the insertion of the oxygen atom. Unlike most N-hydroxylating monooxygenases' cycle (d) and FMOs, PvdA stabilizes the peroxyflavin intermediate long enough to be observable through pre-steady state kinetic experiments [5]. Figure adapted from [20]

dependent biosynthesis of plant development hormone auxin, catalyzing N-hydroxylation of tryptamine [21]. In contrast to mammalian and plant FMOs, yeast FMO does not hydroxylate nitrogen-containing compounds; it is only active with biological thiol [10], and is required for proper disulphide bond formation in some proteins by generating an oxidizing environment in the endoplasmatic reticulum [22]. Bacterial FMOs (bFMOs) are relatively rare as only a few representatives have be identified [23]. Of the known bFMOs, the FMO from *Methylophaga aminosulfidivorans* is the best characterized [9]. It is known that it is able to oxidize a number of amines, and indole is readily oxidized by the enzyme to produce indigo by recombinant *E. coli* cells expressing the bacterial FMO, but physiological substrates are yet to be identified [24].

7.3.2 Baeyer-Villiger Monooxygenases

Class B Baeyer-Villiger Monooxygenases (Type I BVMOs) are FAD, NADPH dependent monooxygenases with the ability to catalyze the incorporation of one atom of molecular oxygen into a substrate while reducing the second atom to water[25-28]. Baeyer-Villiger monooxygenases catalyze a variety of monooxygenation reactions[26] including synthesis of iridoids and steroids in plants, aflatoxin synthesis in fungi [29] and metabolism of aliphatic methyl ketones, tarpenes, alicyclic hydrocarbons and aromatic compounds in bacteria [26, 30-32]. The two best studied BVMOs are phenylacetone monooxygenase (PAMO) from *Thermobifida fusca* [33] and cyclohexanone monooxygenase (CHMO) from *Acinobacter* spp [34-36]. PAMO catalyzes the monoxygenation of phenylacetone to benzyl acetate, while CHMO catalyzes the insertion of an oxygen in the cyclohexanone ring to form ε-caprolactone **(Figure 7-1 c)**[25, 31, 37, 38].

7.3.3 N-Hydroxylating Monooxygenases

PvdA belongs to the N-hydroxylating subclass of class B FDMOs [6, 39, 40]. However, it shares functional characteristics of both class A and class B enzymes, and was hypothesized to share structural characteristics of both as well **(Figure 7-2)** As the name implies, this subclass catalyzes the hydroxylation of primary amines **(Figure 7-1 a and d)**. The best studied of the *N*-hydroxylating flavoprotein monooxygenase proteins are the ornithine hydroxylases from *Pseudomonas aeruginosa* (PvdA) and that from *Aspergillus fumigatus* (SidA) and the lysine hydroxylase from *Escherichia coli* (IucD) [41]. Unlike the other two subclasses, class B enzymes have only begun to be studied biochemically in detail recently. The structure of PvdA presented in **Chapter 8** is the first structure of an enzyme in this subclass.

7.4 Mechanism of Catalysis of Flavoproteins.

At the core of the catalytic mechanism of all flavin dependent monooxygenases lies the redox chemistry of the flavin adenine dinucleotide (FAD), and its ability to cycle through reactive redox states and permit nucleophillic attacks that lead to active oxygen species necessary for monooxygenation.

7.4.1 General Flavin Chemistry

Flavins are a group of redox cofactors produced from vitamin B_2 (riboflavin) and characterized by a catalytically important isoalloxazine hetero-tricyclic ring structure with a central diene, diimine moiety conjugated to electron withdrawing carbonyl groups[42]. The Flavin Adenine Dinucleotide (FAD) molecule required for PvdA catalysis consists

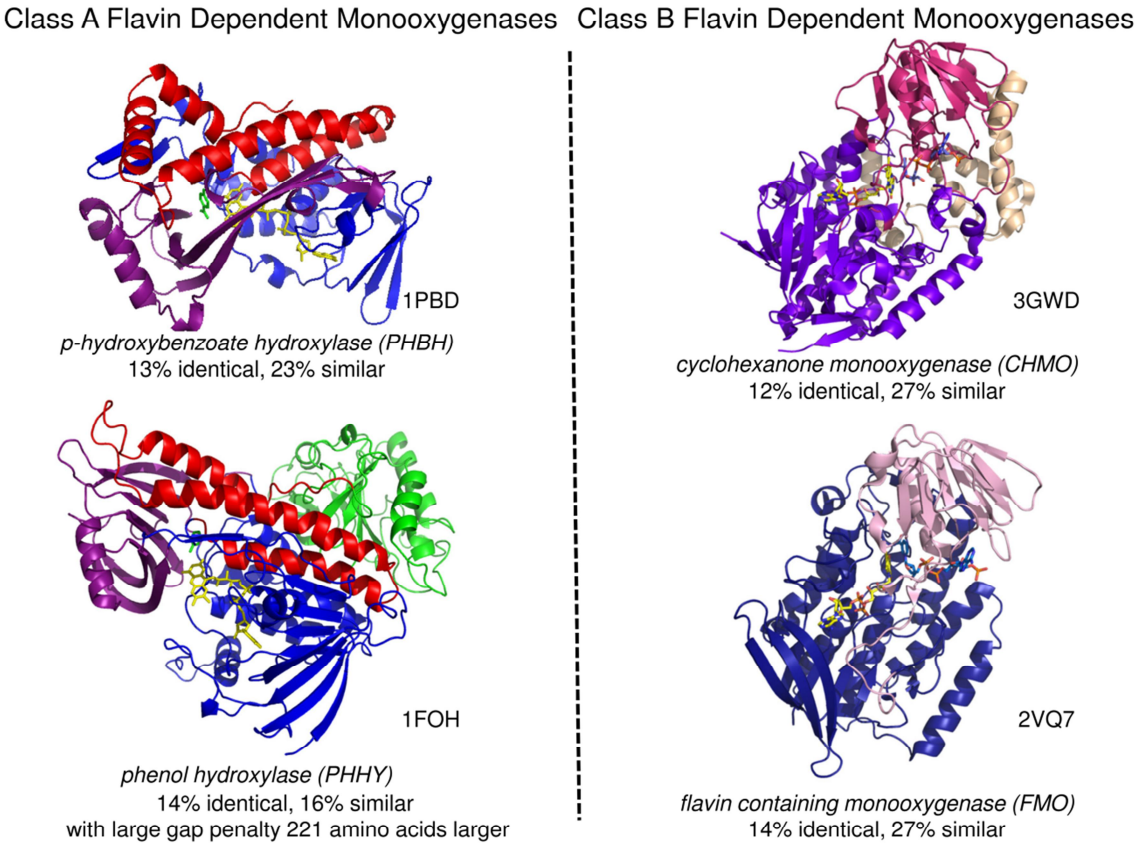

Figure 7-2: Comparison of the closest PvdA hypothesized homologs with known structures. Prior to the solution of the structure of PvdA, it had been proposed that it would share features of both Class A and Class B enzymes, albeit the low sequence identity. The FAD binding domains have been colored in different tones of blue. NAD(P)H binding domains in tones of red and pink and substrate binding domains in purple on the Class A structures, and wheat color on CHMO. Note that the FMO does not have a substrate binding domain, and PHHY has an additional domain, in green, of unknown function.

of a riboflavin moiety containing the catalytically relevant isoalloxazine ring, bound to the phosphate group of an adenine diphosphate molecule **(Figure 7-3)**. The electronic configuration of the isoalloxazine ring permits the FAD to readily accept or donate electrons and convert between two different redox states [43]. In its fully oxidized quinone form, the flavin is an aromatic ring system, whereas the fully reduced form (hydroquinone) is not aromatic, and in a higher energy conformation [44]. The flavin can be fully reduced by accepting two hydrogen atoms (a net gain of two electrons) becoming a hydroquinone, or partially reduced (semiquinone) by accepting one electron and one proton from the quinone redox state, or by donating an electron and a proton from the fully reduced hydroquinone state[44]. In its reduced form, the flavin ring can undergo nucleophillic attacks at either the N5 or the C4a [44]. In the case of flavoprotein monooxygenases, the reduced flavin undergoes a nucleophillic attack by molecular oxygen, resulting in the reactive oxygen species necessary for catalysis.

7.4.2 Overview of the Flavin Redox Cycle (Figure 7-4)

In order for the flavin to react with molecular oxygen, it has to be in its reduced (quinone or semiquinone) form. Most commonly the electron transfer happens either between other redox centers such as hemes or iron-sulfur centers and the flavin, or reducing molecules such as NAD(P)H. The reduced (electron rich) flavin is able to transfer an electron to molecular oxygen, generating a complex between the newly formed superoxide and the flavin radical [23, 24]. A spin inversion results in formation of reduced oxygen, generating a reactive $C_{(4a)}$-hydroperoxyflavin species adduct between the $C_{(4a)}$ of the flavin and molecular oxygen[45]. The peroxyflavin is unstable, decaying

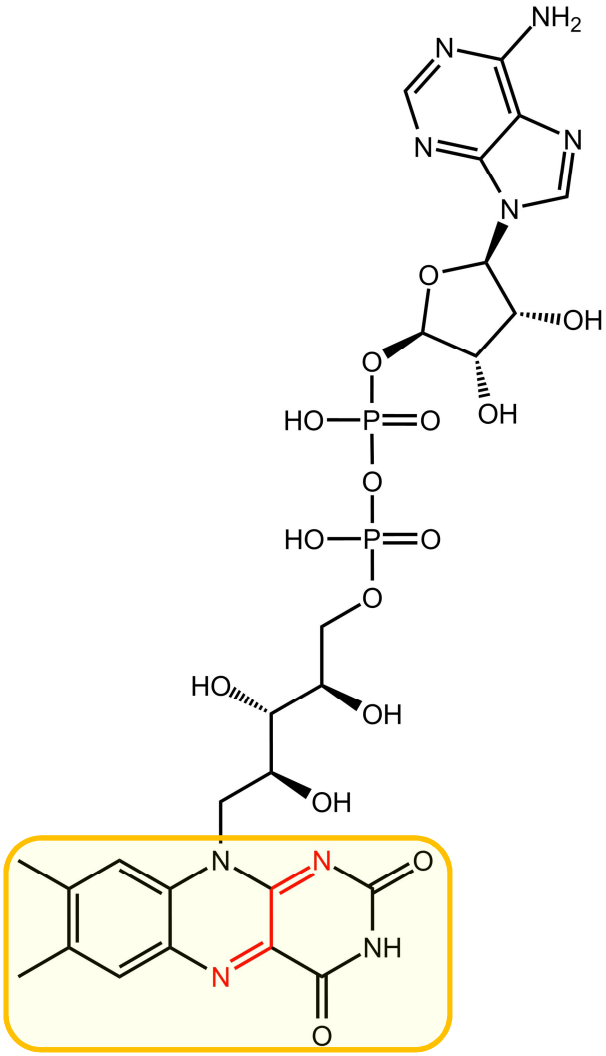

Figure 7-3: Structure of Flavin Adenine Dinucleotide. The Isoalloxazine ring in the yellow rectangle, is the catalytic functional group of the FAD. The diene-diimine moiety, in red, is able to accept one or two electrons (semiquinone and hydroquinone states) and react with oxygen molecules to form reactive oxygen species.

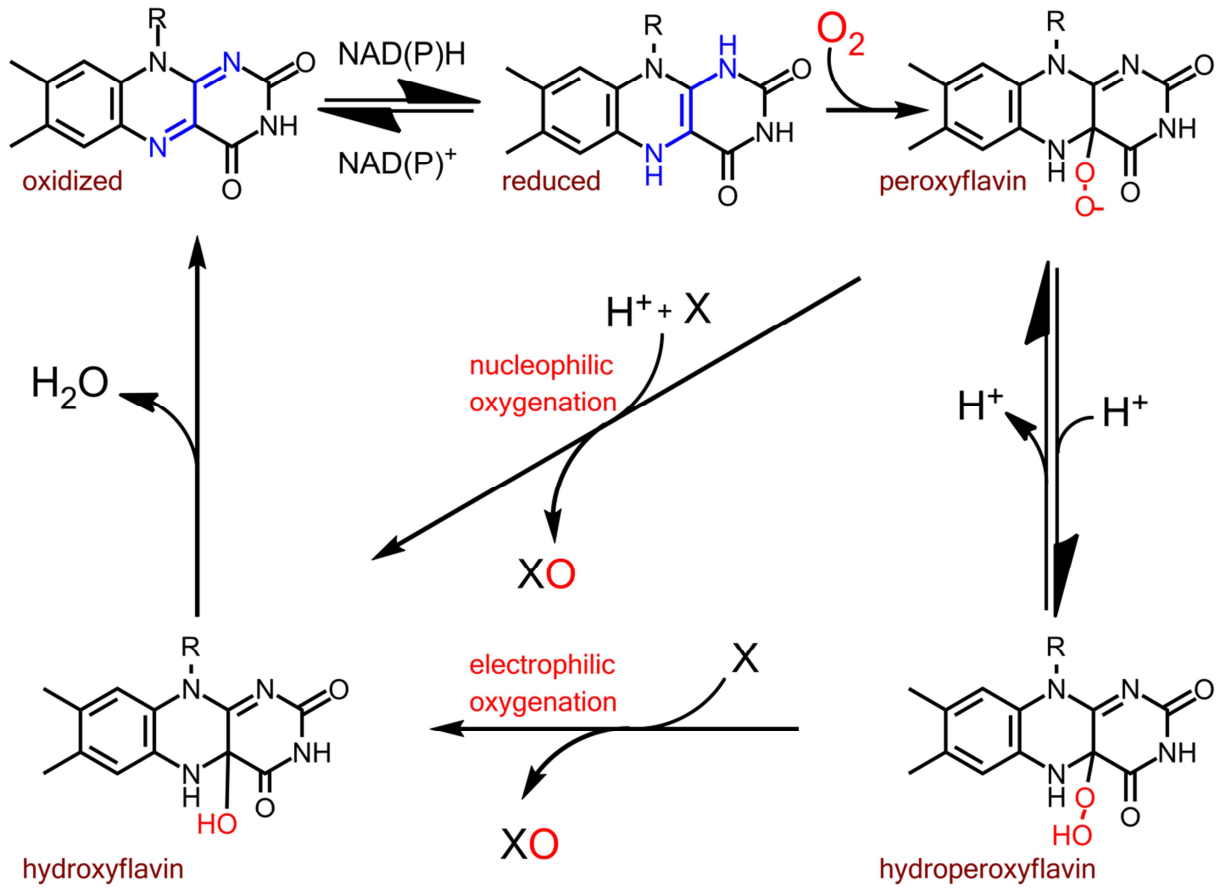

Figure 7-4: General Flavin Redox Cycle. A reducing molecule (most commonly NAD(P)H, reduces the flavin (a), changing the electronic structure of the diene diimine group of isoalloxazine ring (in blue). This allows reactivity with molecular oxygen (b) to form a very reactive peroxyflavin. Some enzymes, including Baeyer-Villiger monooxygenases, stabilize the peroxyflavin, allowing nucleophilic oxygenation of the substrate (d). Other enzymes stabilize the hydroperoxyflavin intermediate, which reacts with the substrate via electrophilic oxygenation (e). Both mechanisms, nucleophilic or electrophilic oxygenations generate an unstable hydroxyflavin (f) that degrades back to the oxidized isoalloxazine ring and a water molecule. If no substrate is present to accept the oxygen, uncoupling occurs, forming toxic hydrogen peroxides as the isoalloxazine ring re-oxidizes. Figure adapted from van Berkel *et al.* 2006 [6]

to form hydrogen peroxide and an oxidized flavin. However, the flavoprotein is able to stabilize the hydroperoxyflavin long enough to oxygenate the substrate. Depending on the protonation state of the flavin intermediate (peroxy COO-, or hydroperoxy (COOH), either a nucleophilic or electrophilic attack on the substrate is performed and a single atom of molecular oxygen is incorporated into the substrate, while the other oxygen atom is reduced to water [46].

7.4.3 PvdA catalytic cycle (Figure 7-5)

The C4a-peroxy and hydroperoxyflavin intermediates are highly unstable intermediates which, uncoupled from substrate oxidation generate highly toxic peroxides with the regeneration of the oxidized flavin [47]. In order to prevent uncoupling, flavoprotein monooxygenases use a variety of methods to stabilize and protect these reactive intermediates[44]. In the case of Class A flavoprotein monooxygenases, such as para-hydroxybenzoate hydroxylase (PHBH) and phenol hydroxylase (PHHY), reduction of the flavin by NAD(P)H is coupled to binding of the substrate: NAD(P)H oxidation (and flavin reduction) rates are significantly accelerated by the binding of the substrate to the active site[44]. In Class B FMOs, BVMOs, and some NMOs, the reduction of the flavin is independent of substrate binding, but the reactive oxygen intermediate is stabilized awaiting substrate binding[44]. For FMOs, the hydroperoxyflavin intermediate is stabilized, as there is no detectable peroxyflavin intermediate [48]. In BVMOs however, the peroxyflavin is stabilized, and coexist in equilibrium the hydroperoxyflavin [49, 50]. Based on pre-steady state kinetic analyses, unlike primary sequence homologs SidA and IucD **(Figure 7-6)** that behave more like FMOs, there is evidence that PvdA forms a stable peroxyflavin intermediate awaiting ornithine binding[4, 5] (**Figure 7-5 b**). Once

the ornithine binds, it has been hypothesized that the N5-amino group of the ornithine donates a proton to the peroxyflavin to generate the hydroperoxyflavin and the reactive ornithine ready to be hydroxylated[4, 5] (**Figure 7-5 c**). **Chapter 8** includes the work solving the structure of PvdA.

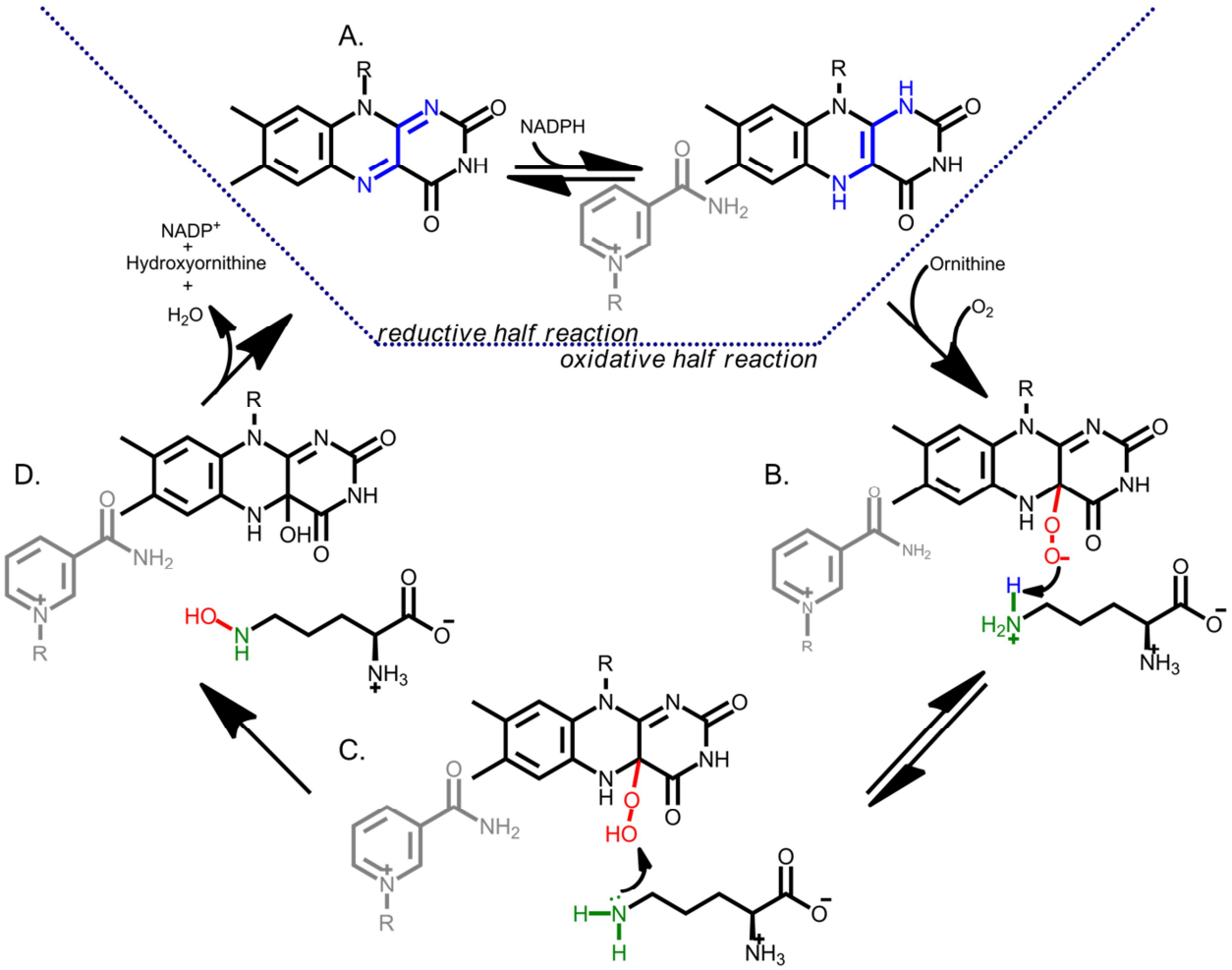

Figure 7-5 PvdA Catalytic cycle. (A) The reductive half reaction in PvdA involves the reduction of the flavin (FAD) by a molecule of NADPH. (B) Molecular oxygen reacts with the reduced FAD forming a peroxyflavin, as ornithine binds to the active site, donating a hydrogen to the peroxyflavin reactive oxygen species, forming a hydroperoxyflavin while activating the N^5amino group of the ornithine. (C) The activated amino group of the ornithine attacks the hydroperoxyflavin, generating the product, hydroxyornithine, and hydroxyflavin (D). The hydroxyflavin oxidizes, releasing a water molecule and the products, the hydroxyornithine and $NADP^+$. This mechanism was first proposed by Meneely *et al*. (2009) [5] Figure adapted from Olucha and Lamb 2011 [51]

a. Dinucleotide binding (FAD-binding) motif.

```
SIDA MEPLQRKSELDFQSYRKMPLAQQRTQRLKPTSPEELHDLICVGFGPASLAIAIALHDALD  60
PVDA ----------------------------MTQATATAVVHDLIGVGFGPSNIALAIALQERAQ  34
IUCD ------------------------------MKKSVDFIGVGTGPFNLSIAALSHQIE-  27
```

b. Dinucleotide binding (NADPH-binding) motif.

```
SIDA KDNNEPYNIAVLGSGQSAAEIFHDLQKRYP--NSRTSLIMRDTAMRPSDDSPFVNEVFNP 295
PVDA CSSGKPMKIAIIGGGQSAAEAFIDLNDSYP--SVQADMILRASALKPADDSPFVNEVFAP 259
IUCD RPDLSGKRITVVGGGQSGADLFLNALRGEWGEAAEINWVSRRNNFNALDEAAFADEYFTP 235
```

c. Ornithine binding motif.

```
SIDA SRKITRVEHYGPNKRMRVHVRAVKDGKDSLIGDGKEVLEVDALMVATGYNRNAHEQLLS- 414
PVDA ERATATAQG------IELALRDAGSGE-------LSVETYDAVILATGYERQLHRQLLEP 366
IUCD SRSVTTLESSGPG-WKLLMEHHLDQGR--------ESLESDVVIFATGYR-SALPQILPS 342
```

Figure 7-6: Sequence alignment between N-hydroxylating monooxygenases. Ornithine hydroxylases of *Pseudomonas aeruginosa* (PvdA) and of *Aspergilus fumigatus* (SidA), as well as lysine hydroxylase from *Escherichia coli* (IucD) are the most widely studied NMOs. PvdA shares 40% identity and 73% similarity with SidA and 25% identity and 59% similarity with IucD. The structure of PvdA described in chapter 6 is the first structure of an N-hydroxylating monooxygenase. Prior to the PvdA structure, the hydrophobic-residue rich putative FAD binding motif (a, in yellow) commonly found in FAD dependent monooxygenases [52] was hypothesized to be conserved in all three homologs. The putative NADPH binding motif (b, in red) was also hypothesized to be conserved among NMOs, including arginine 239 in PvdA, proposed to confer NADPH vs NADH selectivity in this class of enzymes[52]. Prior to structure of PvdA, the ornithine binding motif was proposed to be a “FATGY” motif (c, blue) conserved among the three homologs[52]. This motif will be discussed in chapter 6.

7.5 References

1. Palfey, B.A. and C.A. McDonald, *Control of catalysis in flavin-dependent monooxygenases.* Archives of Biochemistry and Biophysics, 2010. **493**(1): p. 26-36.

2. Fraaije, M.W., et al., *Identification of a Baeyer-Villiger monooxygenase sequence motif.* FEBS Lett, 2002. **518**(1-3): p. 43-7.

3. van Berkel, W.J.H., N.M. Kamerbeek, and M.W. Fraaije, *Flavoprotein monooxygenases, a diverse class of oxidative biocatalysts.* Journal of Biotechnology, 2006. **124**(4): p. 670-689.

4. Meneely, K.M. and A.L. Lamb, *Biochemical characterization of a flavin adenine dinucleotide-dependent monooxygenase, ornithine hydroxylase from Pseudomonas aeruginosa, suggests a novel reaction mechanism.* Biochemistry, 2007. **46**(42): p. 11930-7.

5. Meneely, K.M., et al., *Kinetic mechanism of ornithine hydroxylase (PvdA) from Pseudomonas aeruginosa: substrate triggering of O2 addition but not flavin reduction.* Biochemistry, 2009. **48**(20): p. 4371-6.

6. Meneely, K.M. and A.L. Lamb, *Biochemical characterization of a flavin adenine dinculeotide-dependent monooxygenase, ornithine hydroxylase from Pseudomonas aeruginosa, suggests a novel reaction mechanism.* Biochemistry, 2007. **46**(42): p. 11930-11937.

7. Ziegler, D.M., *An overview of the mechanism, substrate specificities, and structure of FMOs.* Drug Metabolism Reviews, 2002. **34**(3): p. 503-511.

8. Schlaich, N.L., *Flavin-containing monooxygenases in plants: looking beyond detox.* Trends Plant Sci, 2007. **12**(9): p. 412-8.

9. Choi, H.S., et al., *A novel flavin-containing monooxygenase from Methylophaga sp strain SK1 and its indigo synthesis in Escherichia coli.* Biochem Biophys Res Commun, 2003. **306**(4): p. 930-6.

10. Suh, J.K., et al., *Yeast flavin-containing monooxygenase generates oxidizing equivalents that control protein folding in the endoplasmic reticulum.* Proceedings of the National Academy of Sciences of the United States of America, 1999. **96**(6): p. 2687-2691.

11. Burnett, V.L., M.P. Lawton, and R.M. Philpot, *Cloning and sequencing of flavin-containing monooxygenases FMO3 and FMO4 from rabbit and characterization of FMO3.* Journal of Biological Chemistry, 1994. **269**(19): p. 14314-22.

12. Celius, T., et al., *Flavin-containing monooxygenase-3: induction by 3-methylcholanthrene and complex regulation by xenobiotic chemicals in hepatoma cells and mouse liver.* Toxicol Appl Pharmacol, 2010. **247**(1): p. 60-9.

13. Gagliardi, S., et al., *Flavin-containing monooxygenase mRNA levels are up-regulated in als brain areas in SOD1-mutant mice.* Neurotox Res, 2011. **20**(2): p. 150-8.

14. Jackh, C., et al., *Characterization of enzyme activities of Cytochrome P450 enzymes, Flavin-dependent monooxygenases, N-acetyltransferases and UDP-glucuronyltransferases in human reconstructed epidermis and full-thickness skin models.* Toxicol In Vitro, 2011. **25**(6): p. 1209-14.

15. Lawton, M.P. and R.M. Philpot, *Functional characterization of flavin-containing monooxygenase 1B1 expressed in Saccharomyces cerevisiae and Escherichia coli and analysis of proposed FAD- and membrane-binding domains.* Journal of Biological Chemistry, 1993. **268**(8): p. 5728-34.

16. Mitchell, S.C., *Flavin mono-oxygenase (FMO)--the 'other' oxidase.* Curr Drug Metab, 2008. **9**(4): p. 280-4.

17. Novick, R.M. and A.A. Elfarra, *Purification and characterization of flavin-containing monooxygenase isoform 3 from rat kidney microsomes.* Drug Metab Dispos, 2008. **36**(12): p. 2468-74.

18. Reddy, R.R., et al., *Characterization of human flavin-containing monooxygenase (FMO) 3 and FMO5 expressed as maltose-binding protein fusions.* Drug Metab Dispos, 2010. **38**(12): p. 2239-45.

19. Alfieri, A., et al., *Revealing the moonlighting role of NADP in the structure of a flavin-containing monooxygenase.* Proc Natl Acad Sci U S A, 2008. **105**(18): p. 6572-7.

20. Olucha, J., et al., *Two structures of an N-hydroxylating flavoprotein monooxygenase: ornithine hydroxylase from Pseudomonas aeruginosa.* Journal of Biological Chemistry, 2011. **286**(36): p. 31789-98.

21. Zhao, Y.D., et al., *A role for flavin monooxygenase-like enzymes in auxin biosynthesis.* Science, 2001. **291**(5502): p. 306-309.

22. Suh, J.K., et al., *Molecular cloning and kinetic characterization of a flavin-containing monooxygenase from Saccharomyces cerevisiae.* Archives of Biochemistry and Biophysics, 1996. **336**(2): p. 268-274.

23. Massey, V., *Activation of Molecular-Oxygen by Flavins and Flavoproteins.* Journal of Biological Chemistry, 1994. **269**(36): p. 22459-22462.

24. Gatti, D.L., et al., *The Mobile Flavin of 4-OH Benzoate Hydroxylase.* Science, 1994. **266**(5182): p. 110-114.

25. Pazmino, D.E.T., et al., *Kinetic mechanism of phenylacetone monooxygenase from Thermobifida fusca.* Biochemistry, 2008. **47**(13): p. 4082-4093.

26. Bocola, M., et al., *Converting phenylacetone monooxygenase into phenylcyclohexanone monooxygenase by rational design: Towards practical Baeyer-Villiger monooxygenases.* Advanced Synthesis & Catalysis, 2005. **347**(7-8): p. 979-986.

27. Malito, E., et al., *Crystal structure of a Baeyer-Villiger monooxygenase.* Proceedings of the National Academy of Sciences of the United States of America, 2004. **101**(36): p. 13157-13162.

28. Malito, E., et al., *Structures of Michaelis and product complexes of plant cytokinin dehydrogenase: Implications for flavoenzyme catalysis.* Journal of Molecular Biology, 2004. **341**(5): p. 1237-1249.

29. Yu, J., et al., *Genes encoding cytochrome P450 and monooxygenase enzymes define one end of the aflatoxin pathway gene cluster in Aspergillus parasiticus.* Applied Microbiology and Biotechnology, 2000. **53**(5): p. 583-590.

30. Kamerbeek, N.M., et al., *Baeyer-Villiger monooxygenases, an emerging family of flavin-dependent biocatalysts.* Advanced Synthesis & Catalysis, 2003. **345**(6-7): p. 667-678.

31. Mihovilovic, M.D., B. Muller, and P. Stanetty, *Monooxygenase-mediated Baeyer-Villiger oxidations.* European Journal of Organic Chemistry, 2002(22): p. 3711-3730.

32. Taschner, M.J., D.J. Black, and Q.Z. Chen, *The Enzymatic Baeyer-Villiger Oxidation - A Study of 4-Substituted Cyclohexanones.* Tetrahedron-Asymmetry, 1993. **4**(6): p. 1387-1390.

33. Pazmino, D.E.T., et al., *Exploring the biocatalytic potential of the novel thermostable Baeyer-Villiger monooxygenase: Phenylacetone monooxygenase.* Journal of Biotechnology, 2005. **118**: p. S129-S129.

34. Chen, Y.C.J., O.P. Peoples, and C.T. Walsh, *Acinetobacter Cyclohexanone Monooxygenase - Gene Cloning and Sequence Determination.* Journal of Bacteriology, 1988. **170**(2): p. 781-789.

35. Carrea, G., et al., *Effects of Substrate Structure on the Enantioselectivity and Stereochemical Course of Sulfoxidation Catalyzed by Cyclohexanone Monooxygenase.* Tetrahedron-Asymmetry, 1992. **3**(8): p. 1063-1068.

36. Sheng, D.W., D.P. Ballou, and V. Massey, *Mechanistic studies of cyclohexanone monooxygenase: Chemical properties of intermediates involved in catalysis.* Biochemistry, 2001. **40**(37): p. 11156-11167.

37. Kayser, M.M., et al., *Baker's yeast-catalyzed synthesis of optically pure 4-tert-butyl-3-hydroxy beta-lactam cis-(3R,4S) and trans-(3R,4R) diastereomers.* Canadian Journal of Chemistry-Revue Canadienne De Chimie, 2002. **80**(7): p. 796-800.

38. Mihovilovic, M.D., et al., *Microbial Baeyer-Villiger oxidation of bicyclo 4.3.0 ketones by two recombinant E-coli strains. A novel access to indole alkaloids.* Synlett, 2002(5): p. 700-702.

39. Kertesz, M.A., K. Schmidt-Larbig, and T. Wuest, *A novel reduced flavin mononucleotide-dependent methanesulfonate sulfonatase encoded by the sulfur-regulated msu operon of Pseudomonas aeruginosa.* Journal of Bacteriology, 1999. **181**(5): p. 1464-1473.

40. Meneely, K.M., et al., *Kinetic Mechanism of Ornithine Hydroxylase (PvdA) from Pseudomonas aeruginosa: Substrate Triggering of O(2) Addition but Not Flavin Reduction.* Biochemistry, 2009. **48**(20): p. 4371-4376.

41. Chocklett, S.W. and P. Sobrado, *Aspergillus fumigatus SidA is a highly specific ornithine hydroxylase with bound flavin cofactor.* Biochemistry, 2010. **49**(31): p. 6777-83.

42. Heelis, P.F., *The Photophysical and Photochemical Properties of Flavins (Isoallozazines).* Chemical Society Reviews, 1982. **11**(1): p. 15-39.

43. Hall, L.H., B.J. Orchard, and S.K. Tripathy, *The Structure and Properties of Flavins - Molecular-Orbital Study Based on Totally Optimized Geometries .1. Molecular-Geometry Investigations.* International Journal of Quantum Chemistry, 1987. **31**(2): p. 195-216.

44. Sinnott, M., *Comprehensive biological catalysis : a mechanistic reference*, 1998, Academic Press.

45. Ghisla, S. and V. Massey, *Mechanisms of Flavoprotein-Catalyzed Reactions.* European Journal of Biochemistry, 1989. **181**(1): p. 1-17.

46. Entsch, B. and W.J.H. Vanberkel, *Flavoprotein Structure and Mechanism .1. Structure and Mechanism of Para-Hydroxybenzoate Hydroxylase.* Faseb Journal, 1995. **9**(7): p. 476-483.

47. Whiteste.Rh and H. Kamin, *Uncoupling of Oxygen Activation From Hydroxylation in a Bacterial Salicylate Hydroxylase.* Biochem Biophys Res Commun, 1970. **38**(5): p. 882-&.

48. Beaty, N.B. and D.P. Ballou, *The Reductive Half-Reaction of Liver Mircrosomal FAD-Containing Monooxygenase.* Journal of Biological Chemistry, 1981. **256**(9): p. 4611-4618.

49. de Gonzalo, G., et al., *4-Hydroxyacetophenone monooxygenase from Pseudomonas fluorescens ACB as an oxidative biocatalyst in the synthesis of optically active sulfoxides.* Tetrahedron-Asymmetry, 2006. **17**(1): p. 130-135.

50. Kamerbeek, N.M., et al., *4-Hydroxyacetophenone monooxygenase from Pseudomonas fluorescens ACB - A novel flavoprotein catalyzing Baeyer-Villiger oxidation of aromatic compounds.* European Journal of Biochemistry, 2001. **268**(9): p. 2547-2557.

51. Olucha, J. and A.L. Lamb, *Mechanistic and structural studies of the N-hydroxylating flavoprotein monooxygenases.* Bioorg Chem, 2011. **39**(5-6): p. 171-7.

52. Stehr, M., et al., *A hydrophobic sequence motif common to N-hydroxylating enzymes.* Trends in Biochemical Sciences, 1998. **23**(2): p. 56-57.

Chapter 8: Structures of *Pseudomonas aeruginosa* PvdA

The work discussed in this chapter has been published as a research article:

Olucha J, Meneely KM, Chilton AS, Lamb AL, Two structures of an N-hydroxylating flavoprotein monooxygenase: ornithine hydroxylase from Pseudomonas aeruginosa. Journal of Biological Chemistry, 2011. 286(36): p. 31789-98.

and an invited review:

Olucha, J. and A.L. Lamb, Mechanistic and structural studies of the N-hydroxylating flavoprotein monooxygenases. Bioorg Chem, 2011. 39(5-6): p. 171-7.

8.1 Introduction

For successful infection, gram negative bacteria have evolved mechanisms to acquire nutrients essential for survival in low nutrient environments [1, 2]. One of these mechanisms is the production and secretion of siderophores, small molecules with high affinity for iron that allow the bacteria to sequester ferric iron from infected tissues [3, 4]. Siderophores are not only important for iron acquisition; these small molecules have also been shown to play an important role in quorum sensing [5, 6]. In Pseudomonas and Yersinia species it has been shown that siderophores are essential components for virulence [5-7]. For these reasons siderophore biosynthetic pathways are being considered as potential drug targets.

As outlined in the previous chapter, *Pseudomonas aeruginosa* produces two siderophores, pyochelin and pyoverdin via two distinct biosynthetic pathways. Pyoverdin

is a large peptide-based siderophore with two iron chelating *N5-formyl-hydroxy*-ornithine hydroxamate moieties at the core of the molecule **(see Chapter 6 figure 5)**. The ornithine hydroxamates are synthesized via a two-step process; PvdA hydroxylates the side chain amine of the L-ornithine, and a transformylase, PvdF, formylates the hydroxyornithine. The formyl-hydroxyornithine is incorporated onto the siderophore by non-ribosomal peptide synthases [5, 8, 9].

PvdA belongs to the class B family of flavoprotein monooxygenases and therefore should meet the following criteria [10]: **1.)** it uses FAD as a redox cofactor, **2.)** NADPH but not NADH serves as electron donor, **3.)** $NADP^+$ remains bound in the active site until all products are released, **4.)** it is encoded by a single gene and **5.)** based on sequence homology, PvdA has well defined α/β-nuclotide binding FAD and NAPH binding domains [11, 12]. PvdA meets most of these requirements with some qualifications: albeit using FAD exclusively as flavin redox center (as opposed to FMN), PvdA does not bind FAD stably in solution, prior to the work described in this chapter there was no structural information and it was uncertain whether $NADP^+$ remained bound through the oxidative half reaction[13-17].

As described in the previous chapter, Class B flavoproteins are divided into three distinct subclasses: **1.)** flavin containing monooxygenases (FMOs) that hydroxylate heteroatoms through a hydroperoxyflavin intermediate, **2.)** Baeyer-Villiger monooxygenases (BVMOs), which catalyze monooxygenation via a peroxyflavin intermediate and a Crieggee adduct[15, 18-20]; and **3.)** N-hydoxylating monooxygenases (NMOs), the subclass PvdA belongs to.

The most studied of the *NMOs* are PvdA (ornithine hydroxylase from *Pseudomonas aeruginosa)* [21-23], SidA (the ornithine hydroxylase from *Aspergillus fumigatus*) [11] and the lysine hydroxylase from *Escherichia coli* (IucD) [24]. Although all three enzymes have been characterized biochemically in detail, the structure of PvdA described in this chapter is the first structure of an NMO enzyme *and* the first structure of a class B enzyme with redox center (FAD), electron donor ($NADP^+$) and product (hydroxyornithine) bound in the active site together. Overall sequence identity between the three enzymes is 15% and similarity is 46%. The two ornithine hydroxylases (SidA and PvdA) share 40% sequence identity and 73% sequence similarity, whereas IucD and PvdA share 25% sequence identity and 59% similarity [12, 25]. Detailed biochemical work on each of these three enzymes reveals differences between the catalytic mechanisms of PvdA and the other two NMOs. PvdA carries out catalysis via a unique FAD redox cycle, unlike that of either SidA or IucD. Unlike SidA, IucD and flavin containing monooxygenases (FMOs), a peroxyflavin intermediate is observed during the catalytic cycle (like Baeyer-Villiger monooxygenases), and like Class A monooxygenases, the peroxyflavin intermediate forms most efficiently in the presence of substrate. Unlike Baeyer-Villiger monooxygenases, however, the reactive intermediate is the hydroperoxyflavin intermediate, not the peroxyflavin [14, 17, 22, 26]. Like other members of this family however, the electron donating NADPH remains bound (as NADP+) until the product is released [14, 17, 21-23]. Moreover, in spite of the conserved sequence identity, out of the three enzymes, only SidA is able to bind FAD tightly; neither IucD or PvdA bind the cofactor stably in solution [11, 12, 24].

In this chapter I present the crystallographic structures with the oxidized and reduced forms of the flavin, at different points of the FAD redox cycle, and show structural evidence that PvdA is structurally a member of the N-hydroxylating monooxygenase subclass and of the Class B FDMOs. Finally, we show small active site changes in the oxidized and reduced forms of PvdA that represent different modes of binding of substrate/products during catalysis.

8.2 Materials and methods

8.2.1 Over-expression and Purification

Native PvdA. PvdA was cloned, over-expressed and purified as previously described [22].

Seleno-methionine PvdA (SeMet PvdA). The method for over-expression of PvdA SeMet was adapted from Van Duyne *et al.* 1992 [27] with several modifications. M9 Minimal media was inoculated with 10 mL of overnight culture per liter of media. The methionine biosynthesis pathway was inhibited by adding a solution containing 100 mg each of L-lysine, L-phenylalanine, and L-threonine, 50 mg each of of L-isoleucine, L-leucine, and L-valine, and 60 mg of DL-selenomethionine per liter of culture. Protein purification was induced 15 minutes after the addition of the amino acid solution with the addition of IPTG to a final concentration of 400 μM. SeMet PvdA was purified using the same protocol as native PvdA with the addition of 1 mM βME to all buffers.

8.2.2 Crystallization

Native PvdA. The best crystals of native PvdA were obtained through the hanging drop vapor diffusion method in 9.5% PEG 8000, 25% glycerol, 60 mM phosphate monobasic

(pH 5.0) some of which can be seen on **figure 8-1, a, b, and c**. PvdA did not form crystals without FAD, NADPH and L-Ornithine, so the protein solution was prepared by adding FAD and substrates to a 16 mg/ml (as measured by Bradford) solution of PvdA to a final molar ratio of 1:3:20:150 (protein:FAD:NADPH:L-Ornithine). The protein solution was allowed to incubate on ice for 30 minutes prior to setting up the experiments. After the incubation period, 3 µl drops with a 1:1 ratio of protein solution to mother liquor solution were prepared over 600 µl of mother liquor solution. Rod shaped yellow crystals grew to a size of ~200 µm x 50 µm x 50 µm in 3 days at 18 °C.

8.2.3 SeMet PvdA.

Crystals of SeMet PvdA were obtained in similar conditions to native PvdA (8% PEG 8000, 15% glycerol, 80 mM MES, pH 5.5). As with native PvdA, SeMet PvdA did not form crystals without FAD, NADPH and L-Ornithine, so protein solution was prepared with FAD and substrates with the same ratios as native PvdA. The best SeMet crystals grew to a size of ~150 µm x 40 µm x 40 µm in 5 days at 18 °C at a protein concentration of 9 mg/ml (measured by Bradford) in 2 µl drops. In order to keep a reduced environment, 10µl of 1M β-mercapto ethanol (βME) was added to each well prior to drop setup)

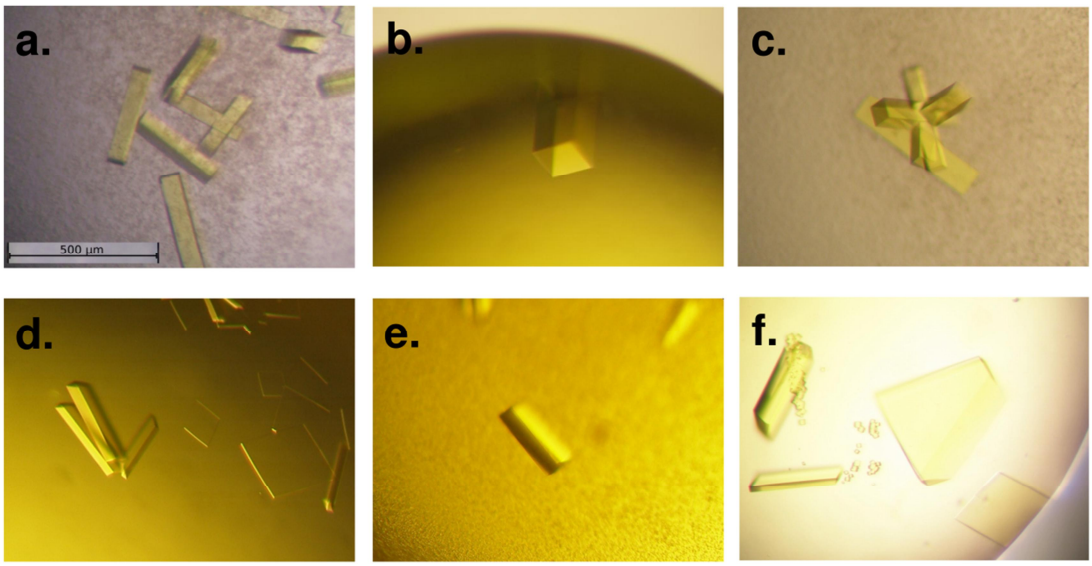

Figure 8-1: Different PvdA crystal morphologies. Different concentrations of the precipitant (PEG 8000) led to a range of rod-shaped crystals (a, b, c). Modification of the pH led to different morphologies (rod-shaped in a,b and c versus pizza boxes in d, e, and f). Rod-shaped crystals were used to solve the structure of PvdA. Pizza box shaped crystals did not result in usable data.

8.2.4 Native PvdA – reduced.

A flake of sodium hydrosulfite (sodium dithionite) was added to a native PvdA experiment **(Figure 8-2)**. The flake was allowed to dissolve and the drop and crystals were monitored for discoloration from yellow to clear for 30 minutes. Crystals were harvested after the 30 minute incubation period, cryo-protected and flash cooled.

8.2.5 Cryoprotectants.

Native PvdA crystals were harvested and transferred to a mother liquor drop with 11% PEG 8000, 60 mM KPi monobasic, and 20% glycerol. In order to prevent crystals from cracking because of diffusion of FAD and substrates/products out of the crystal, these were added to the drop to a final concentration of 21 mM FAD, 41 mM NADPH and 166 mM L-ornithine. Harvested SeMet PvdA crystals were transferred to a cryo-protectant with the same composition as the native PvdA cryo-protectant, with the addition of 2mM βME. Reduced PvdA crystals were harvested and transferred to a cryo-protectant with the same composition as native PvdA cryo-protectant, with a flake of sodium dithionite allowed to dissolve in it to maintain a reducing environment. All crystals were flash cooled to 77 K in liquid nitrogen.

8.2.6 Data Collection, processing and structure determination

8.2.6.1 SeMet PvdA.

Multiple anomalous dispersion experimental data for SeMet PvdA crystal were collected on beamline 9-2 at the Stanford Synchrotron Radiation Lightsource (SSRL). Peak (0.979112 Å), Inflection (0.979304 Å) and remote (0.918402 Å) wavelengths were

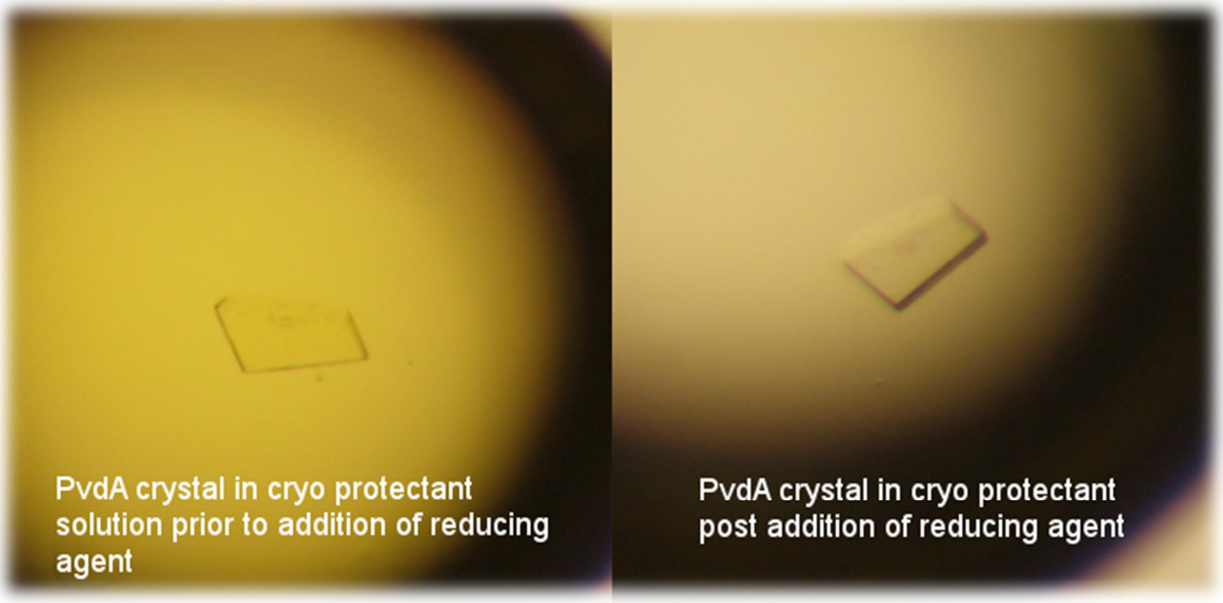

Figure 8-2: Reduction of PvdA crystals. 30 minutes after the addition of sodium dithinite to a drop of PvdA cryoprotectant containing a PvdA crystal, drop and crystal lost the yellow flavin color, characteristic of oxidized flavin, indicating the flavin is reduced.

determined by a selenium fluorescence scan (K-edge 12.6578 keV). Data were collected for 120° of the crystal in 0.5° oscillations and exposure time of 5 seconds. Detector distance was set to 360.5 mm. Data were indexed and scaled to 2.8 Å resolution using X-ray Detector Software (XDS) [28]. (**Table 8-1**). AutoSolve and AutoBuild, from the Python-based Hierarchical Environment for Integrated Crystallography (PHENIX) software suite [29] were used to determine the location of 12 Se atoms (FoM = 0.42, overall score= 63), initial phase estimates, and to build the initial model. The initial model was built with 750 residues. Further model building refinement of the structure was accomplished using Coot [30] and Refmac5 from the CCP4 software suite [31] (**Table 8-1**).

8.2.6.2 Native PvdA.

Data for native PvdA were collected on beamline 9-2 at the SSRL for 180° in 0.5° oscillations with 10 second exposures at 1 Å wavelength and a detector distance of 200 mm **(Figure 8-3)**.

Data were scaled and indexed to 1.95 Å resolution using XDS. SeMet and native crystals were isomorphous so the initial SeMet model and phase estimate was used to build the higher resolution native PvdA model using Refmac5 from the CCP4 software suite [31]. Further model building refinement of the structure was accomplished using Coot [30] and Refmac5 from the CCP4 software suite (**Table 8-1**).

8.2.6.3 Reduced Native PvdA.

Data for native PvdA were collected on beamline 9-2 at the SSRL for 120° in 0.25° oscillations with 5 second exposures at 0.97946 Å wavelength and a detector distance

Table 8-1: Data Collection and Refinement Statistics

Data Collection[1]					
	Selenomethionine			***Native***	
	Peak	*Inflection*	*Remote*	*Oxidized*	*Reduced*
Wavelength (Å)	0.9791	0.9793	0.9184	1.000	0.9795
Space Group		$I4_122$		$I4_122$	$I4_122$
Unit Cell (Å)	a = b = 130.94, c = 316.50			a = b = 130.94, c = 318.52	a=b=128.16, c=316.51
Resolution range (Å)		36.6 - 2.7		36.8 - 1.9	39.26-3.03
Completeness (%)	99.7 (98.4)	99.7 (97.6)	99.7 (98.4)	99.5 (97.5)	99.4 (96.0)
Total reflections	275715	275906	275985	741798	246515
Unique reflections	37946	37964	37949	108180	26002
I/s	17.1 (4.4)	17.1 (4.5)	19.0 (4.6)	15.3 (4.1)	25.1 (5.8)
Rsym[2] (%)	9.1 (42.1)	9.1 (42.8)	8.8 (42.9)	6.7 (41.2)	8.0 (40.7)
Multiplicity	7.3 (7.3)	7.3 (7.3)	7.3 (7.3)	6.9 (6.5)	9.5 (9.2)
Number of refined selenium sites		12			
Anomalous correlation between half sets	0.36	0.33	0.16		
Mean Figure of Merit [4]		0.42		0.97	0.91
Mid slope of anomalous probability	1.2	1.2	1.1		
Refinement					
Resolution range (Å)				36.74-1.90	39.26-3.03
Number of reflections				102726	23360
R_{factor}[6]				19.2	21.5
R_{free}				21.7	27.1
Number of protein, nonhydrogen atoms				6561	6541
Number of ligand and solvent atoms				584	220
Ramachandran Allowed (%)				100	100
R.m.s. bond length (Å)				0.0154	0.0162
R.m.s. bond angles (°)				1.56	1.89
Average B (Å^2)					
Protein				32.0	59.0
Ligands				27.4	68.0
Water				33.5	n/a

[1]All data were collected that the Stanford Synchrotron Radiation Laboratory, beamline 9-2. Values in parentheses are for the highest resolution shells: 2.84 - 2.7 Å for selenomethionine data, 2.0 - 1.9 Å for oxidized data, and 3.19-3.03 Å for reduced data.

[2]R_{sym} =∑| *I* - < I >| / ∑*I*, where *I* is the observed intensity and á*I*ñ is the statistically weighted absolute intensity of multiple measurements of symmetry related reflections.

[3]Anomalous correlation between half sets = ∑||FPH ± FP| -FH(calc) |/∑|FPH| reported for all centric reflections.

[4]Mean figure of merit = $<\alpha\sum P(a)e^{i\alpha}/\sum P(\alpha)>$, where a is the phase and P(α) is the phase probability distribution.

[5]Phasing power = <|FH|>/<||FP + FH|-|FPH||> reported for all reflections.

[6]$R = \sum|F_o - k|F_c||/\sum|F_o|$, *R* from the working set and R_{free} from the test set. 10% percent of the refelctions were reserved for the calculation of the R_{free}.

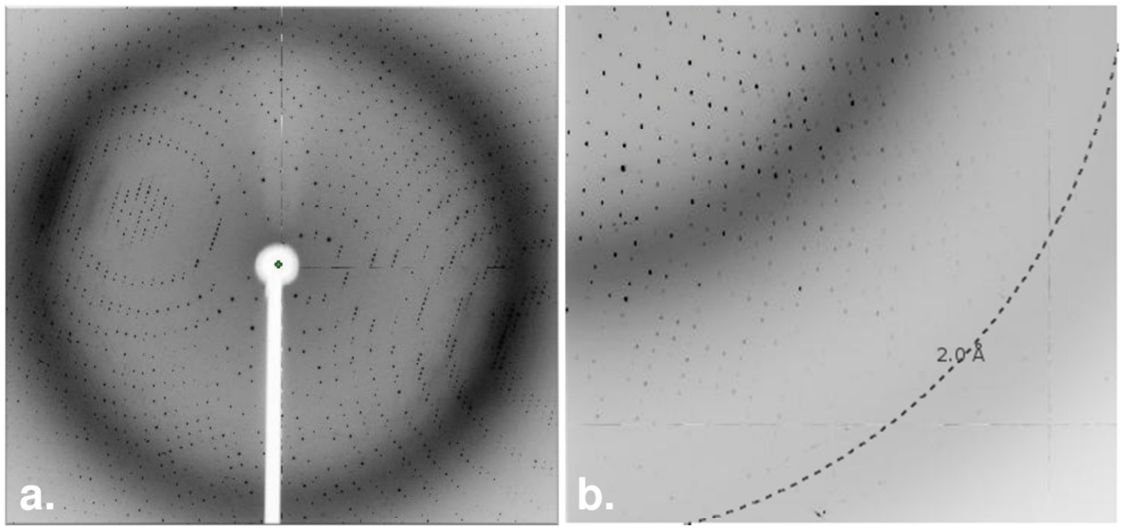

Figure 8-3: Diffraction images of datasets collected and used to determine the structure of PvdA.

of 408 mm. Data were scaled and indexed to 3.1 Å using XDS. Structure determination was performed via molecular replacement using Phaser from the CCP4 software suite with chain B of the native structure with waters, FAD and substrates omitted as model. Further model building refinement of the structure was accomplished using Coot and Refmac5 from the CCP4 software suite [31] (**Table 8-1**).

8.2.7 Crystallographic models

The final native PvdA model contains two chains per asymmetric unit **(Figure 8-4)**. Chain A is missing residues 1-9, 199-205, 360 and 428-443, while chain B is missing residues 1-9, 200-206, and 420 – 443. Missing residues are located in flexible loops and had poor electron density due to low occupancy. Both chains have FAD, $NADP^+$ and hydroxy-ornithine in the active site. The NADP+ nicotinamide moiety and ribose in chain A active site are not modeled due to poor electron density, as is the nicotinamide moiety in chain B. The model includes 376 waters and 4 phosphate molecules. Ramachandran analysis as calculated by PROCHECK [32] shows good geometry and angles, with 90.8% of residues in allowed regions and 9.2% of residues in additionally allowed regions.

The reduced native PvdA model contains two chains per asymmetric unit, but with different lattice contacts. Both chains A and B have poor or no electron density for residues 1-8, 200-207, and 428-443. In addition chain B is missing residues 359 and 360. Both chains contain FAD, hydroxy-ornithine, and NADP+ in the active site. In contrast to the non-reduced native model, the NADP+ nicotinamide moiety in both active sites had density and therefore was able to be modeled.

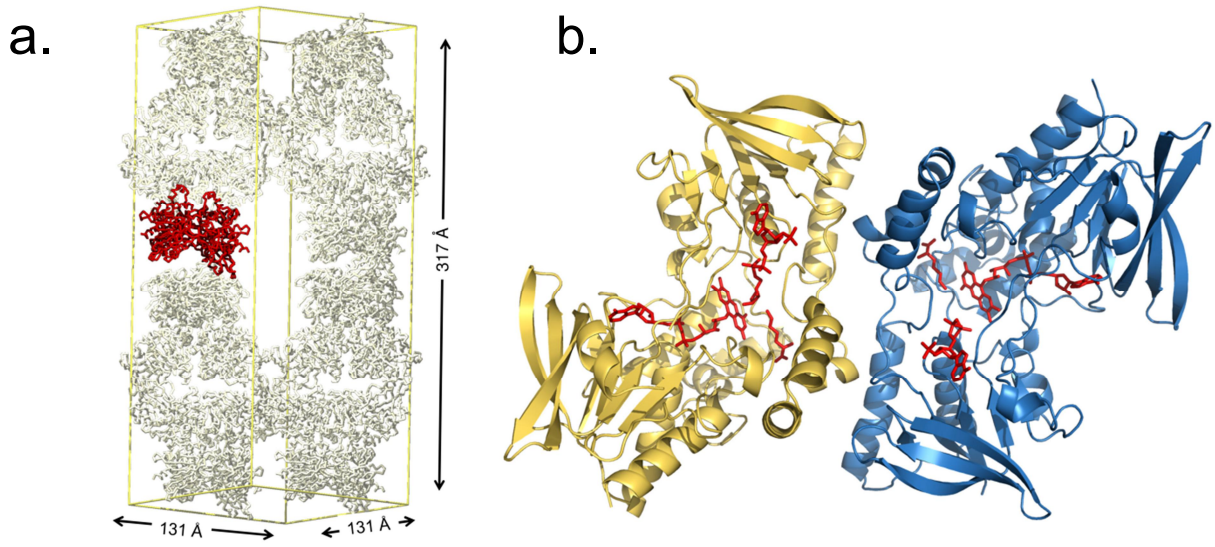

Figure 8-4: Shape of the unit cell and assymetric unit. Rod shaped crystals had a large unit cell (a) with a centered-tetragonal spacegroup ($I4_122$) and two PvdA molecules in the assymetric unit (b) forming a dimer with twofold crystallographic symmetry.

8.2.8 Structural alignments

Root mean square deviations were calculated using LSQMAN [33] of the DEJAVU program suite.

8.3 Results

8.3.1 Molecular Replacement

The first attempts at structure determination were performed using molecular replacement using Phaser from the CCP4i suite [31], and PHENIX [29]. There were no structures for the closest homologs to PvdA (SidA and IucD), therefore molecular replacement models were generated from hypothesized functional homologs with known structures: class A enzymes phenol hydroxylase (PHHY) from *Trichosporum cutaneum (PDB 1FOH), para*-hydroxybenzoate hydroxylase from *Pseudomonas fluorescens (PDB 1PBD),* and Class B enzymes bacterial flavin containing monooxygenase from *Methylophaga aminisulphidivorans (PDB 2VQ7)* and cyclohexanone monooxygenase from genus *Acinetobacter (PDB 3GWD).* These enzymes' structures were used as complete models and as chimeric combinations of domains. Log Likelihood Gains never surpassed 100 points (acceptable) but the R_{sym} never dropped below 0.5 (indicating random placement of the model versus the density map).

8.3.2 Twinning

Initial improper processing of native datasets using a space group with lower symmetry (I4 vs I422) indicated twinning of the data (two or more lattices overlapping at an angle). After further investigation it was determined that there was indeed no twinning, but rather the programs used for processing (HLK and Mosfilm) were not processing the data correctly unless specifically given the correct spacegroup.

8.3.3 Surface entropy reduction

Protein crystallization is dependent on whether it can reproducibly form intermolecular contacts that can sustain a three dimensional lattice. In some instances crystallization is prevented by an "entropic shield" composed of clusters of residues with high intrinsic conformational entropy [34]. Crystallization is very sensitive to entropy changes involving both the solvent and the protein. Incorporation of protein molecules into the lattice carries a negative entropy term, and a thermodynamic cost [34]. The surface entropy reduction approach involves the replacement of surface exposed, high entropy amino acids with residues that have small, low entropy side chains such as alanines. Using the SerP server [34], a high entropy cluster (Q120/E121/Q122) was located and confirmed to be on the surface via homology modeling using PHHY as model. Attempts to purify the entropy reduction mutant PvdA Q120A/E121A/Q122A were never successful as the protein readily precipitated out of solution.

8.3.4 Heavy atom soaking

As an alternative to molecular replacement, I began the process of soaking crystals in heavy atoms, to obtain data for multiwavelength anomalous dispersion or multiple

isomorphous replacement **(Table 8-2)**. Dissolving the heavy metal compounds and adding the solution to the crystal drops resulted in dissolution of the crystals due to high sensitivity to small changes in the ionic strength of the solution. Adding small flakes of the undissolved heavy metal compound to the drops overcame this obstacle, but I could not measure the amount of heavy metal compound added to the solution correctly. I was only able to incorporate tungsten and mercury successfully into the crystal lattice, but never in enough quantity to be useful in MAD. Other metals that incorporated successfully destroyed the architecture of the lattice, which was not evident until data was collected at the synchrotron.

8.3.5 *Phasing and Overall Structure*

An initial phase estimate was determined by multiwavelength anomalous dispersion using a selenomethionine (SeMet) substituted form of PvdA. Crystallographic statistics can be seen in **Table 8-2**. The initial SeMet model was used to phase an isomorphous 1.9 Å native dataset. The assymetric unit contains two PvdA monomers related by a non-crystallographic two-fold axis and a 950 $Å^2$ interface (PROTORP[35]). This dimer is a crystallographic artifact; dynamic light scattering and size exclusion chromatography experiments indicate that PvdA is a monomer in solution [21, 22] . Each monomer is composed of three well defined domains **(Figure 8-5)**. The FAD binding domain, is composed of 250 residues, separarated in three different segments from both N and C-termini. The NADPH binding domain, is composed of 144 residues in two segments.

Table 8-2: Heavy metal derivatization

Conditions	Cryoprotectant	Derivative	Heavy Atom
PEG 8K	20% Glycerol	KCl_6Ir	Ir
PEG 8K	20% Glycerol	KCl_6Os	Os
Pentaerythrol	20% Ethylene Glycol	$ThCl_3$	Th
PEG 8K	20% Glycerol	$LaNO_3$	La
PEG 8K	20% Glycerol	PCMB	Hg
Pentaerythrol	20% Ethylene Glycol	$KAuCl_4$	Au
Pentaerythrol	20% Ethylene Glycol	KBr_4Pt	Pt
Pentaerythrol	20% Ethylene Glycol	$CdCl_2$	Cd
Pentaerythrol	20% Ethylene Glycol	HgI_2	Hg/I
Pentaerythrol	20% Ethylene Glycol	$AuCl_3$	Au
Pentaerythrol	20% Ethylene Glycol	$KReCl_6$	Re
Pentaerythrol	20% Ethylene Glycol	$PrCl_3$	Pr
Pentaerythrol	20% Ethylene Glycol	HgO	Hg
Pentaerythrol	20% Ethylene Glycol	$DyCl_3$	Dy
Pentaerythrol	20% Ethylene Glycol	$EuCl_3$	Eu
Pentaerythrol	20% Ethylene Glycol	$Sm(NO_3)_3$	Sm
Pentaerythrol	20% Ethylene Glycol	$LuCl_3$	Lu
Pentaerythrol	20% Ethylene Glycol	$YbCl_3$	Yb
Pentaerythrol	20% Ethylene Glycol	IC3	I

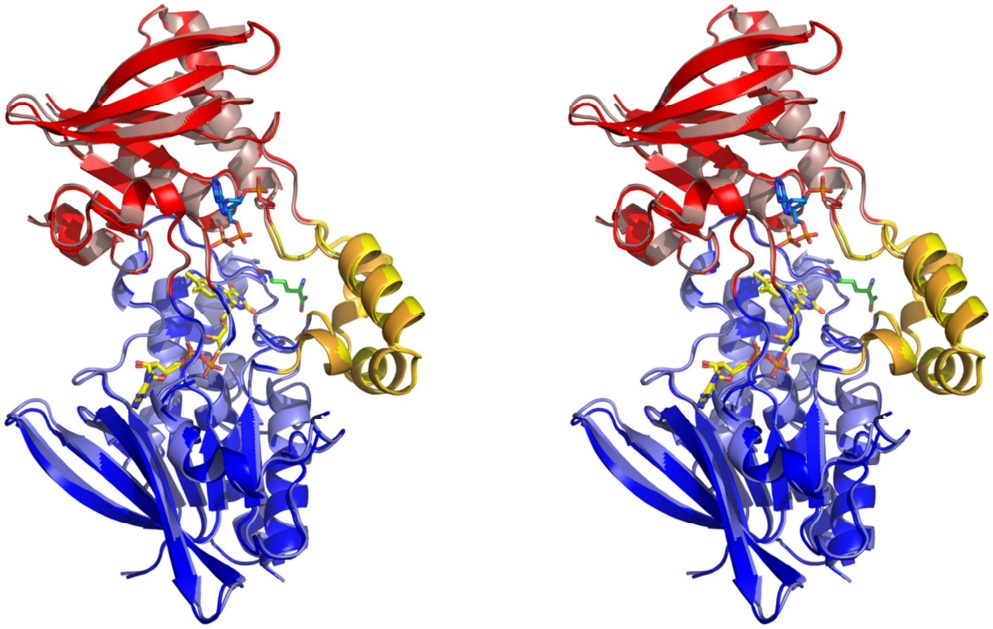

Figure 8-5: Stereo cartoon overlay of PvdA oxidized (darker colors) and reduced (lighter colors). In blue the FAD binding domain, red the NADPH binding domain, and yellow the ornithine binding domain. There are no large structural differences between oxidized and reduced structures.

Both FAD and NADPH binding domains are folded in a α/β nucleotide binding fold. The ornithine binding domain is the smallest of the three domains, composed of 45 residues in two segments; three helices inserted in a loop of the NADPH binding domain (residues 248-285) and a single helix inserted in the C-terminus segment of the FAD binding domain (residues 398-404). This can best be observed in the topology diagram (**Figure 8-6, b**), and sequence alignment between SidA, IucD, and PvdA (**Figure 8-7**)

8.3.6 FAD binding domain

The overall architecture of the FAD binding domain is a prototypical α/β-dinucleotide binding fold characteristic of the glutathione reductase family of flavoproteins [36]. In PvdA, a central five-stranded parallel β-sheet flanked to one side by five helices and to the other by a three strand antiparallel β-sheet with an N-terminal β-α-β dinucleotide binding consensus sequence. The standard GXGXXG consensus sequence is usually found in a loop between a beta stand and an alpha helix, and allows a charge-dipole interaction between the alpha helix and the phosphate groups of the dinucleotide molecule [10, 37-39]. As shown in **figure 8-8** In PvdA, the GXGXXG consensus sequence is substituted by a GXGXXN sequence (residues 17-22, with the sidechain of the Asn-22 hydrogen- bonding to the backbone of Gly-17 and Gln-395). The FAD binds to a cleft in an extended conformation, with the isoalloxazine ring directed towards the active site, but unlike most other characterized flavoprotein monooxygenases from the same class, the cleft is shallow and most of the flavin molecule is solvent exposed, possibly explaining why PvdA does not bind FAD stably [22, 26].

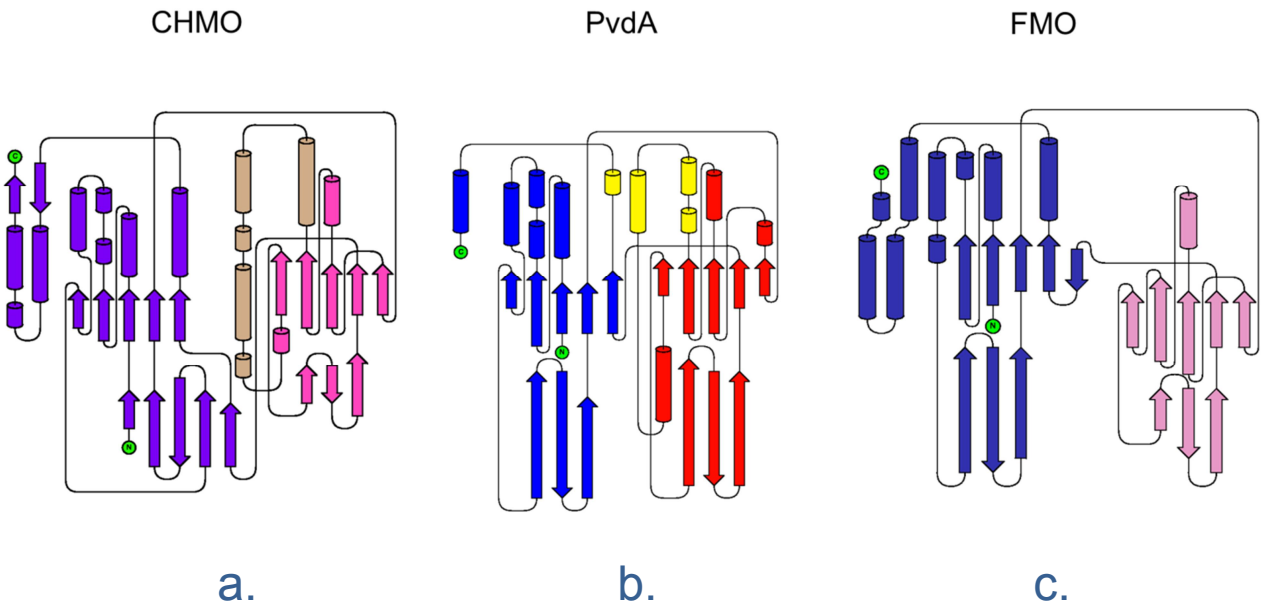

Figure 8-6: Topology diagrams of Class B enzymes. In shades blue, the FAD binding domain, red/pink the NADPH binding domains, and yellow/wheat the substrate binding domains. CHMO (a), PvdA (b), and bacterial FMO (c) all have two dinucleotide binding domains with similar topologies. However, the substrate binding domains are significantly different. FMO does not have a substrate binding domain, CHMO substrate binding domain is a 5 helix insert in the NADPH binding domain, and PvdA's ornithine binding domain is composed of a 3 helix insertion in a loop from the NADPH binding domain, and a single helix insertion from the FAD binding domain.

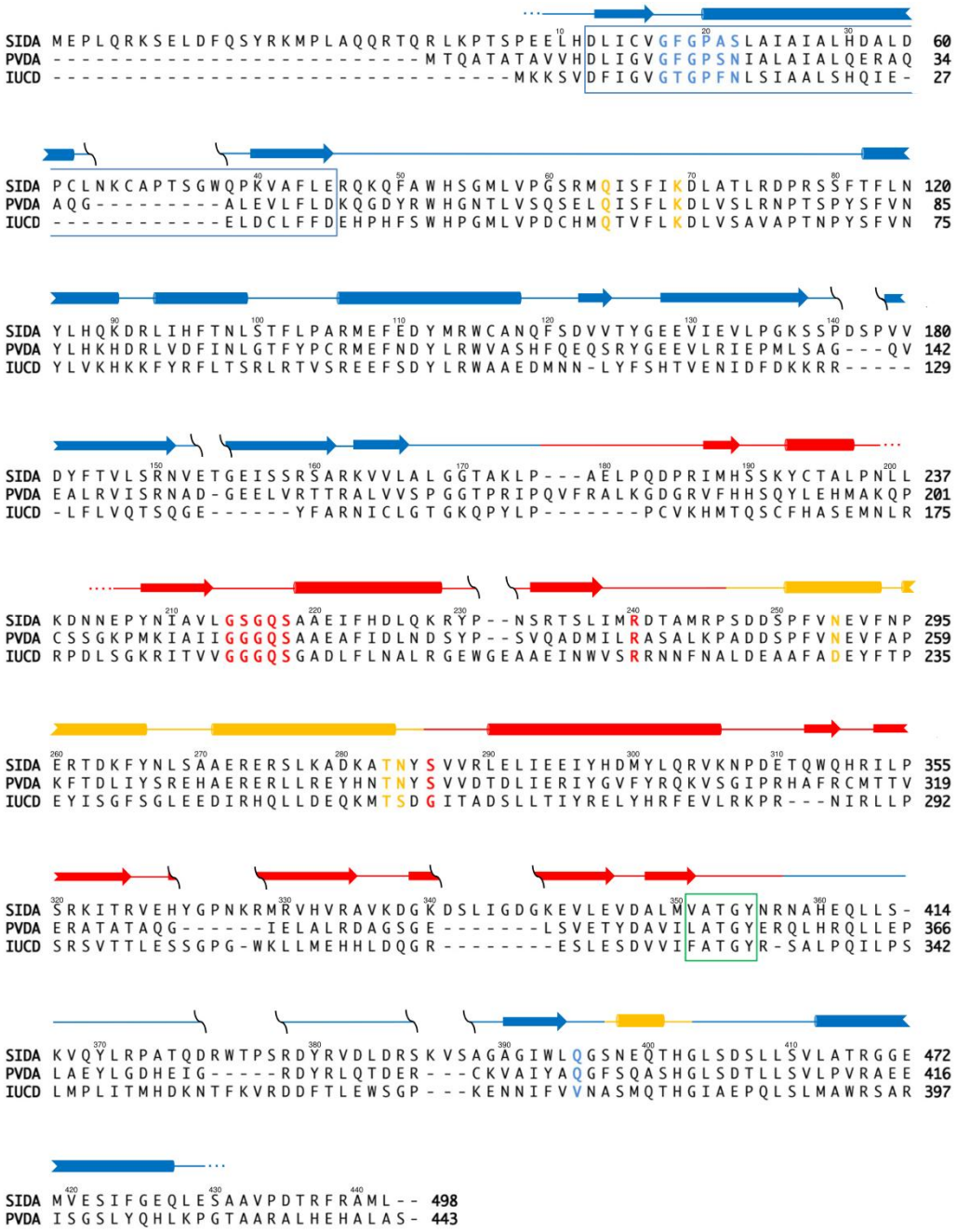

Figure 8-7: Sequence alignment of SidA, PvdA and IucD. Secondary structure over alignment based on PvdA structure (blue is FAD binding, Red is NADPH binding, and yellow is ornithine binding). Highlighted in blue are residues involved in FAD binding. The blue rectangle indicates the βαβ motif. Highlighted in red are the residues involved in NADPH binding. The green rectangle indicates a consensus sequence previously hypothesized to be involved in substrate binding[11]. This sequence in actually part of the NADPH binding cleft in PvdA. In yellow, the five residues that form a hydrogen bonding and salt bridge network that stabilizes the ornithine substrate.

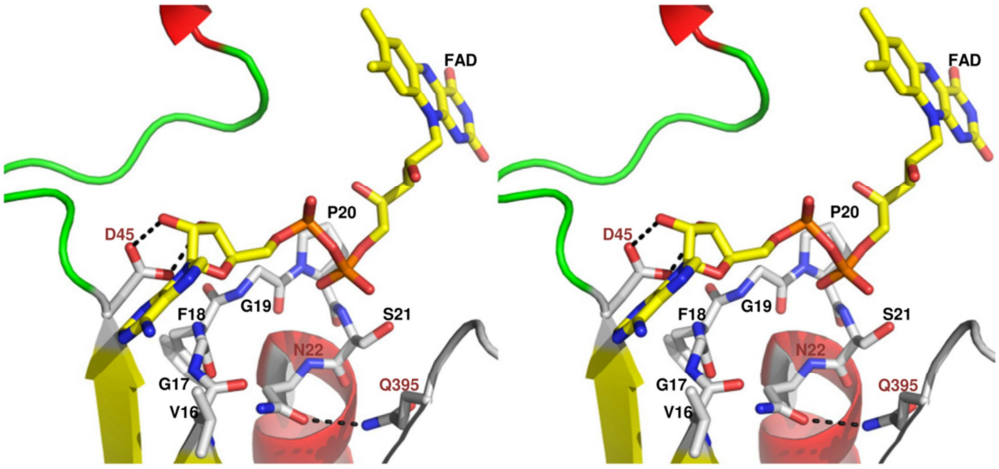

Figure 8-8: Stereo view of the FAD binding region of PvdA. The FAD binding motif in PvdA is the characteristic β-α-β with a glycine rich 6 residue loop that permits a dipole/charge interaction between the phosphate groups of the FAD and the alpha-helix. In PvdA one of the glycines is replaced by an asparagine (GXGXXN consensus sequence vs GXGXXG) that hydrogen bonds with glutamine 395. Figure adapted from Olucha and Lamb, 2009 [12]

8.3.7 NADPH binding domain

The NADPH binding domain is analogous (albeit smaller) to the FAD binding domain in overall structure. PvdA conserves the α/β architecture of nucleotide binding domains, with a central five-stranded parallel β-sheet flanked to one side by a three stranded antiparallel β-sheet and on the other by three helices. At the core of the domain, is the β-α-β motif with the glycine rich consensus sequence (residues 214-218) that allows the previously mentioned dipole-charge interaction between an α-helix and the phosphates of the NADPH. Two residues, Arg-240 and Ser-286 form hydrogen bonding interactions with the phosphate of the adenine ribose, and confer the specificity of PvdA for NADPH vs NADH [22, 26] **(Figure 8-9)**. The nicotinamide moiety of the $NADP^+$ product bound to the active site is not modeled due to the lack of density. This lack of density suggests some flexibility of the NADPH molecule in the active site required for catalysis.

8.3.8 Ornithine binding domain.

The ornithine binding domain is composed of 4 helices coming from loop insertions in the FAD and NADPH binding domains. In the model, hydroxyornithine lies in the cleft formed at the interface between the FAD and ornithine binding domains. Five residues, Gln-64 and Lys-69 from the FAD binding domain, and Asn-254, Thr-283 and Asn 284 from the ornithine binding domain, form a salt bridge and hydrogen bond network with two waters and the ornithine. The network stabilizes the ornithine in place poised for hydroxylation, 5.5 Å away from the C4a, a distance enough to fit a dioxygen molecule (~3 Å long). Asn 254 and the backbone of Thr-283 form hydrogen bonds, and Lys-69 forms a salt bridge with the backbone of the ornithine, conferring the stereoselectivity of

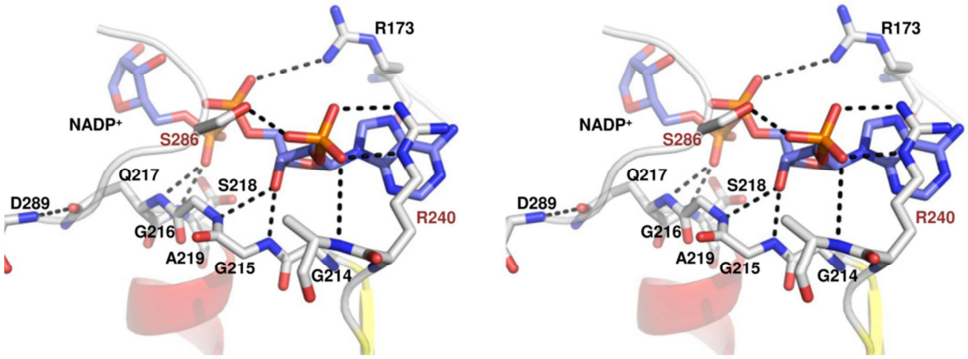

Figure 8-9: Stereo cartoon of the NADPH binding motif. Also an β-α-β motif with a glycine rich loop. NADPH vs NADH specificity is conferred by arginine 240 and serine 286, which hydrogen bond with the phosphate group of the 2' position of the adenine ribose.

PvdA for L-ornithine (vs D-ornithine). Gln-64 and Asn-284 form a hydrogen bond network with the sidechain of the ornithine, positioning the substrate in the right orientiation in the active site for hydroxylation. The electron density for the active site can be seen in **figure 8-10** and a stereo view of the active site of the oxidized structure can be seen in **figure 8-11**

8.3.9 Reduced Structure

A structural alignment of oxidized and reduced structures of PvdA using LSQMAN (r.m.s.d. of 0.4 A for all Cα) reveals no large overall structural differences between the two structures (**Figure 8-5**). The most significant differences can be observed in the active site itself. The reduced structure was determined to 3.03 Å, therefore no structured waters were observable. The most notable difference however is the density for NADP+/NADPH. There is no density for the nicotinamide moiety of the NADP+ in the oxidized structure. On the other hand, the NADPH in the reduced structure has well defined density for the nicotinamide moiety, in spite of the significantly lower resolution. The density for the hydroxyornithine is very well defined in the oxidized structure, which is not the case in the reduced structure, and the molecule had to be modeled as ornithine for lack of density for the hydroxyl group. Finally, Gln-64 and Asn-284 are slightly rotated in the reduced structure as compared to the oxidized structure. This rotation is enough for the Gln-64 to no longer hydrogen bond with the side chain of the ornithine, but the Asn-284 is still able to form a hydrogen bond with the side chain amine **(Figure 8-12)**.

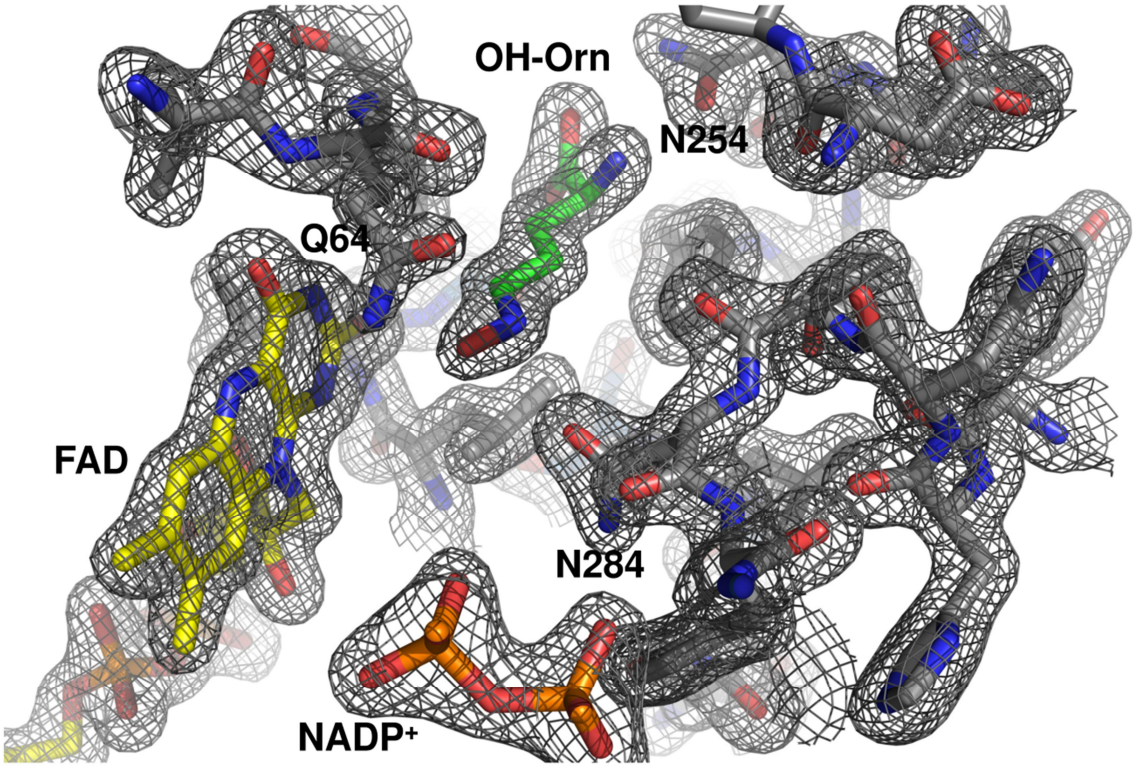

Figure 8-10: Electron density map overlayed on the model of the oxidized structure's active site (to σ=1.5). There is well defined density for the hydroxyornithine (including the hydroxyl group), but there is no density for the nicotinamide moiety of the $NADP^+$

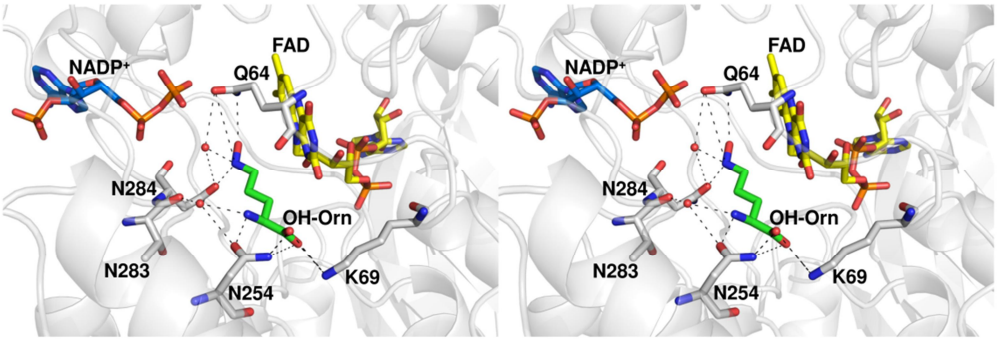

Figure 8-11: Stereo cartoon of the active site of PvdA (oxidized). Five residues (Q64, K69, N254, T283 and N284) form a hydrogen-bond and salt bridge network with two waters and the substrate/product. This network confers the PvdA active site high specificity and stereoselectivity.

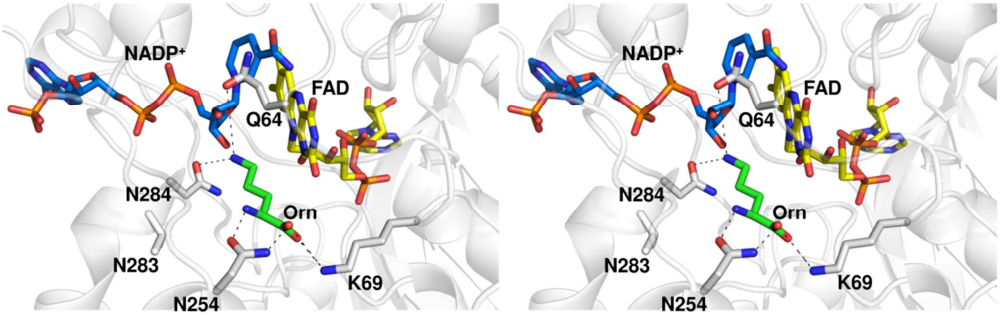

Figure 8-12: Stereo cartoon of the active site of PvdA (reduced). Ornithine, not hydroxyornithine, was modeled into the active site. The nicotinamide moiety of the NADPH had well defined density and was modeled as well. At 3.03 Å resolution, no waters could be modeled into the structure.

8.3.10 Comparison With Homologs

A structural comparison between PvdA and other Class B flavoprotein with known structures indicates that PvdA is structurally distinct from other members of the family for which structures are available. A side-by-side comparison of the topologies of the individual domains of bacterial FMO, cyclohexanone monooxygenase (BVMO) and PvdA reveals that although all three enzymes maintain Rossmann-like folds (βαβ motif with β-sheets flanked by helices), the secondary structure is distinct in all three proteins.

Structural alignment with bacterial FMO using least-squares alignment using LSQMAN indicates an r.m.s.d. of 1.8 Å over 213 aligned backbone carbons (of the possible 414 modeled in the PvdA structure). Comparison of the FAD binding domains indicates indicates higher homology (r.m.s.d. of 1.6 Å over 163 Cα). Comparison of the NADPH binding domains shows 2.0 Å for 58 Cα atoms. Bacterial FMO does not have a substrate binding domain.

A structural alignment between cyclohexanone monooxygenase (closed structure) from genus *Acinetobacter* indicates slightly better structural homology, with an r.m.s.d. of 1.8 Å over 263 aligned Cα (versus 213 of FMO). An alignment of the FAD binding domains reveals a 1.7 Å r.m.s.d. over 157 Cα and and alignment of the NADPH binding domain reveals an r.m.s.d. of 2.0 Å for 93 atoms. The substrate binding domains are both alpha-helical in nature with an r.m.s.d. of 2.2 Å over 13 Cα.

8.4 Discussion

The two structures presented in this chapter are the first determined structures of a member of the N-hydroxylating flavoprotein monooxygenases. In addition, it is the first Class B structure with the flavin, $NADP^+$ *and* substrate/product bound simultaneously in the active site. As such, these structures provide insight into the structure-function relationship in these enzymes [12, 23].

The overall architecture is mostly the same in all three subclasses. Both FAD and NADPH binding domains have Rossmann-like folds, characteristic of dinucleotide binding domains [14, 40, 41]. The topology for these domains is somewhat different for each of the enzymes, partially due to the arrangement of the domains and the insertion of the substrate binding domain (which is not present in bFMO [42-44]). In CHMO the substrate binding domain is a five helix insert in the NADPH binding domain, whereas in PvdA the substrate binding domain is smaller (four helices) and divided into two insertions: three helices in an FAD binding domain loop and one in the NADPH binding domain. It has been suggested that there are large conformational changes throughout the catalytic cycle in CHMO [45, 46]. The overall structural similarities between the oxidized and reduced structures (at different points in the catalytic cycle) would indicate that this is not the case for PvdA, but it cannot be discounted without further structures at different points in the catalytic cycle.

One of the biggest differences between PvdA and other class B flavoprotein monooxygenases is the binding of FAD. Most other known class B flavoproteins bind the FAD cofactor very tightly, to the point where many enzymes are unable to

incorporate exogenous FAD *in vitro* unless the enzyme is partially unfolded and re-folded [10, 38, 39, 44, 47-52]. This makes sense from an evolutionary standpoint because FAD is energetically expensive to make, and is the redox center without which the enzyme is inactive. This is notoriously not the case for PvdA. PvdA does not purify with FAD bound, and assays have to be performed with excess exogenous FAD in the reaction buffer [22, 26].

The two structures of PvdA also provide structural evidence for the high substrate selectivity of PvdA. The orientations of the residues in the active site provide a hydrogen bonding network that not only prevents hydroxylation of amines on shorter or longer side chains, but also promotes preferential binding to the correct stereoisomer (L vs D). Biochemical evidence suggests that L-lysine (one methylene group longer than ornithine) binding promotes NADPH oxidation, but no hydroxylysine is produced [26]: the side chain amine of the substrate has to be at a precise distance from the C4a and in the correct orientation to undergo hydroxylation.

PvdA shows high selectivity for NADPH versus NADH as electron donor. This had previously been determined biochemically and it is in accordance with other class B flavoprotein monooxygenases [22, 26]. Now we have structural evidence for this preference: Arg-240 and Ser 286 bind to the phosphate group that is different between the two molecules, thus providing tighter binding for NADPH. Furthermore, NADPH seems to enter the active site from a tunnel different from ornithine or FAD. Another noteworthy observation is the lack of electron density for the nicotinamide moiety in the oxidized structure. The lack of density most likely indicates high mobility of the $NADP^+$ in the active site once the flavin has been reduced. The flexibility of the $NADP^+$ would

enable it to move “out of the way” to make room for the oxygen, since it remains in the active site throughout the oxidative half reaction. The conformational flexibility of the $NADP^+$ might also play a role in blocking solvent accessibility into the active site, thereby protecting the flavin-oxygen intermediates from non-productive uncoupling.

PvdA shows a higher uncoupling rate (NADPH oxidation and peroxide formation without product hydroxylation) than reported in other flavoprotein monooxygenases [22, 26]. This might be at least partly due to the high solvent accessibility of the active site. The C4a has to be protected from solvent in order to accept the oxygen molecule [14, 53, 54]. It has been previously shown that $NADP^+$ remains bound in the active site of some enzymes to stabilize the highly reactive hydroperoxyflavin intermediate, but the mechanism is a matter of debate. Furthermore, crystals only grow in the presence of high concentrations of ornithine, which may suggest a conformational change upon substrate binding for crystals to form. It would be possible that FAD binding encourages a conformational change that promotes NADPH binding. Ornithine binding blocks solvent accessibility while promoting reduction of the flavin (**Figure 8-13, a**), and induces a conformational change in the active site that encourages the $NADP^+$ molecule to move away from the reactive center, and further blocking solvent from entering the active site, protecting the C4a to prevent uncoupling **(Figure 8-13, b)**. This model needs to be further investigated biochemically and structurally, through single turnover experiments looking at the flavin redox cycle in more detail and though selective mutations in the active site of PvdA.

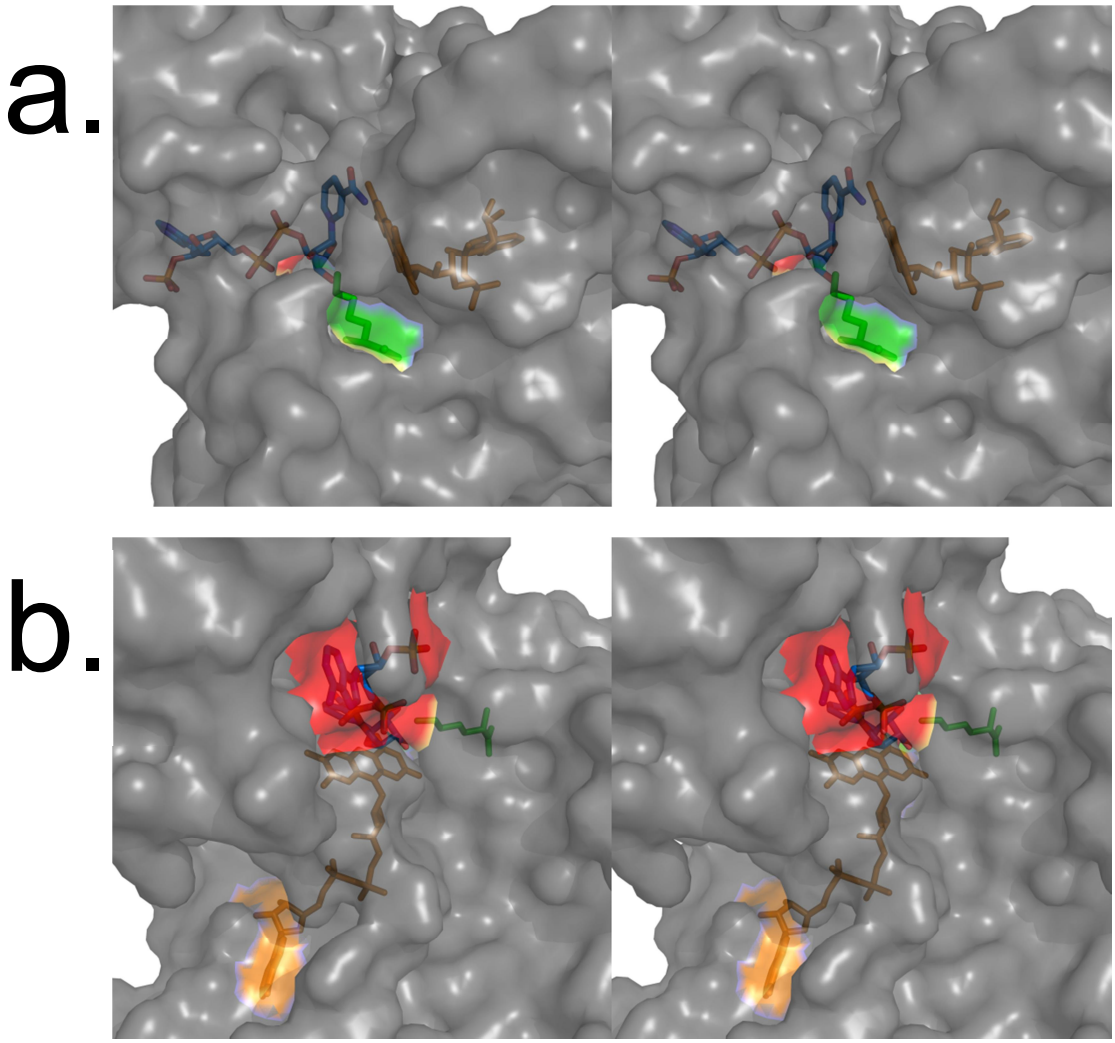

Figure 8-13: Stereo surface depiction showing ornithine solvent exposed surface (green, a) and FAD solvent exposed surface in orange and NADPH in red (b). Ornithine, FAD, and NADOH would seem to be protecting the isoalloxazine ring from solvent, blocking the tunnels of an otherwise very solvent exposed active site.

8.5 References

1. Poole, K. and G.A. McKay, *Iron acquisition and its control in Pseudomonas aeruginosa: Many roads lead to Rome.* Frontiers in Bioscience, 2003. **8**: p. D661-D686.

2. Wintergerst, E.S., S. Maggini, and D.H. Hornig, *Contribution of selected vitamins and trace elements to immune function.* Annals of Nutrition and Metabolism, 2007. **51**(4): p. 301-323.

3. Neilands, J.B., *Siderophores - Structure and Function of Microbial Iron Transport Compounds.* Journal of Biological Chemistry, 1995. **270**(45): p. 26723-26726.

4. Wandersman, C. and P. Delepelaire, *Bacterial iron sources: From siderophores to hemophores.* Annual Review of Microbiology, 2004. **58**: p. 611-647.

5. Khalifa, A.B., et al., *Virulence factors in Pseudomonas aeruginosa: mechanisms and modes of regulation.* Annales De Biologie Clinique, 2011. **69**(4): p. 393-403.

6. Musthafa, K.S., et al., *Antipathogenic potential of marine Bacillus sp SS4 on N-acyl-homoserine-lactone-mediated virulence factors production in Pseudomonas aeruginosa (PAO1).* Journal of Biosciences, 2011. **36**(1): p. 55-67.

7. Stojiljkovic, I. and K. Hantke, *Hemin Uptake System of Yesrsinia enterocolitica - Similarities With Other TonB-Dependent Systems in Gram-negative Bacteria.* Embo Journal, 1992. **11**(12): p. 4359-4367.

8. Ge, L. and S.Y.K. Seah, *Heterologous expression, purification, and characterization of an L-ornithine N-5-hydroxylase involved in pyoverdine siderophore biosynthesis in Pseudomonas aeruginosa.* Journal of Bacteriology, 2006. **188**(20): p. 7205-7210.

9. Halle, F. and J.M. Meyer, *Ferrisiderophore Reductases of Pseudomonas - Properties and Cellular Location of the Pseudomonas aeruginosa Ferripyoverdine Reductase.* European Journal of Biochemistry, 1992. **209**(2): p. 613-620.

10. van Berkel, W.J.H., N.M. Kamerbeek, and M.W. Fraaije, *Flavoprotein monooxygenases, a diverse class of oxidative biocatalysts.* Journal of Biotechnology, 2006. **124**(4): p. 670-689.

11. Chocklett, S.W. and P. Sobrado, *Aspergillus fumigants SidA Is a Highly Specific Ornithine Hydroxylase with Bound Flavin Cofactor.* Biochemistry, 2010. **49**(31): p. 6777-6783.

12. Olucha, J. and A.L. Lamb, *Mechanistic and structural studies of the N-hydroxylating flavoprotein monooxygenases.* Bioorg Chem, 2011. **39**(5-6): p. 171-7.

13. Lawton, M.P. and R.M. Philpot, *Functional characterization of flavin-containing monooxygenase 1B1 expressed in Saccharomyces cerevisiae and Escherichia coli and analysis of proposed FAD- and membrane-binding domains.* Journal of Biological Chemistry, 1993. **268**(8): p. 5728-34.

14. Entsch, B. and W.J.H. Vanberkel, *Flavoprotein Structure and Mechanism .1. Structure and Mechanism of Para-Hydroxybenzoate Hydroxylase.* Faseb Journal, 1995. **9**(7): p. 476-483.

15. Fraaije, M.W., et al., *Identification of a Baeyer-Villiger monooxygenase sequence motif.* FEBS Lett, 2002. **518**(1-3): p. 43-7.

16. Ghisla, S. and V. Massey, *Mechanisms of Flavoprotein-Catalyzed Reactions.* European Journal of Biochemistry, 1989. **181**(1): p. 1-17.

17. Massey, V., *Activation of Molecular-Oxygen by Flavins and Flavoproteins.* Journal of Biological Chemistry, 1994. **269**(36): p. 22459-22462.

18. Bocola, M., et al., *Converting phenylacetone monooxygenase into phenylcyclohexanone monooxygenase by rational design: Towards practical Baeyer-Villiger monooxygenases.* Advanced Synthesis & Catalysis, 2005. **347**(7-8): p. 979-986.

19. de Gonzalo, G., et al., *Oxidations catalyzed by phenylacetone monooxygenase from Thermobifida fusca.* Tetrahedron-Asymmetry, 2005. **16**(18): p. 3077-3083.

20. de Gonzalo, G., et al., *4-Hydroxyacetophenone monooxygenase from Pseudomonas fluorescens ACB as an oxidative biocatalyst in the synthesis of optically active sulfoxides.* Tetrahedron-Asymmetry, 2006. **17**(1): p. 130-135.

21. Meneely, K.M., et al., *Kinetic Mechanism of Ornithine Hydroxylase (PvdA) from Pseudomonas aeruginosa: Substrate Triggering of O(2) Addition but Not Flavin Reduction.* Biochemistry, 2009. **48**(20): p. 4371-4376.

22. Meneely, K.M. and A.L. Lamb, *Biochemical characterization of a flavin adenine dinucleotide-dependent monooxygenase, ornithine hydroxylase from Pseudomonas aeruginosa, suggests a novel reaction mechanism.* Biochemistry, 2007. **46**(42): p. 11930-7.

23. Olucha, J., et al., *Two structures of an N-hydroxylating flavoprotein monooxygenase: ornithine hydroxylase from Pseudomonas aeruginosa.* Journal of Biological Chemistry, 2011. **286**(36): p. 31789-98.

24. Thariath, A., et al., *Construction and Biochemical Rharacterization of Recombinant Cytoplasmic Forms of the IucD Protein (Lysine-N^6-hydroxylase) Encoded by the PCOLV-K30 Aerobactin Gene Cluster.* Journal of Bacteriology, 1993. **175**(3): p. 589-596.

25. Olucha, J., et al., *Two Structures of an N-Hydroxylating Flavoprotein Monooxygenase ORNITHINE HYDROXYLASE FROM PSEUDOMONAS AERUGINOSA.* Journal of Biological Chemistry, 2011. **286**(36): p. 31789-31798.

26. Meneely, K.M., et al., *Kinetic mechanism of ornithine hydroxylase (PvdA) from Pseudomonas aeruginosa: substrate triggering of O2 addition but not flavin reduction.* Biochemistry, 2009. **48**(20): p. 4371-6.

27. Vanduyne, G.D., et al., *Atomic Structures of the Human Immunophilin FKBP-12 Complexes with FK506 and Rapamycin.* Journal of Molecular Biology, 1993. **229**(1): p. 105-124.

28. Kabsch, W., *XDS.* Acta Crystallographica Section D-Biological Crystallography, 2010. **66**: p. 125-132.

29. Adams, P.D., et al., *PHENIX: a comprehensive Python-based system for macromolecular structure solution.* Acta Crystallographica Section D-Biological Crystallography, 2010. **66**: p. 213-221.

30. Emsley, P. and K. Cowtan, *COOT: model-building tools for molecular graphics.* Acta Crystallographica Section D-Biological Crystallography, 2004. **60**: p. 2126-2132.

31. Bailey, S., *The CCP4 Suite - Programs for Protein Crystallography.* Acta Crystallographica Section D-Biological Crystallography, 1994. **50**: p. 760-763.

32. Laskowski, R.A., et al., *Procheck - A Program to Checl The Stereochemical Quality of Protein Structures.* Journal of Applied Crystallography, 1993. **26**: p. 283-291.

33. Kleywegt, G.J., *Use of non-crystallographic symmetry in protein structure refinement.* Acta Crystallographica Section D-Biological Crystallography, 1996. **52**: p. 842-857.

34. Derewenda, Z.S., *Rational protein crystallization by mutational surface engineering.* Structure, 2004. **12**(4): p. 529-535.

35. Reynolds, C., D. Damerell, and S. Jones, *ProtorP: a protein-protein interaction analysis server.* Bioinformatics, 2009. **25**(3): p. 413-416.

36. Dym, O. and D. Eisenberg, *Sequence-structure analysis of FAD-containing proteins.* Protein Science, 2001. **10**(9): p. 1712-1728.

37. Moran, G.R., et al., *Evidence for flavin movement in the function of p-hydroxybenzoate hydroxylase from studies of the mutant Arg220Lys.* Biochemistry, 1996. **35**(28): p. 9278-9285.

38. Palfey, B.A. and C.A. McDonald, *Control of catalysis in flavin-dependent monooxygenases.* Archives of Biochemistry and Biophysics, 2010. **493**(1): p. 26-36.

39. Ziegler, D.M., *An overview of the mechanism, substrate specificities, and structure of FMOs.* Drug Metabolism Reviews, 2002. **34**(3): p. 503-511.

40. Gagliardi, S., et al., *Flavin-containing monooxygenase mRNA levels are up-regulated in als brain areas in SOD1-mutant mice.* Neurotox Res, 2011. **20**(2): p. 150-8.

41. Hall, L.H., B.J. Orchard, and S.K. Tripathy, *The Structure and Properties of Flavins - Molecular-Orbital Study Based on Totally Optimized Geometries .1. Molecular-Geometry Investigations.* International Journal of Quantum Chemistry, 1987. **31**(2): p. 195-216.

42. Celius, T., et al., *Flavin-containing monooxygenase-3: induction by 3-methylcholanthrene and complex regulation by xenobiotic chemicals in hepatoma cells and mouse liver.* Toxicol Appl Pharmacol, 2010. **247**(1): p. 60-9.

43. Choi, H.S., et al., *A novel flavin-containing monooxygenase from Methylophaga sp strain SK1 and its indigo synthesis in Escherichia coli.* Biochem Biophys Res Commun, 2003. **306**(4): p. 930-6.

44. Suh, J.K., et al., *Molecular cloning and kinetic characterization of a flavin-containing monooxygenase from Saccharomyces cerevisiae.* Archives of Biochemistry and Biophysics, 1996. **336**(2): p. 268-274.

45. Chen, Y.C.J., O.P. Peoples, and C.T. Walsh, *Acinetobacter Cyclohexanone Monooxygenase - Gene Cloning and Sequence Determination.* Journal of Bacteriology, 1988. **170**(2): p. 781-789.

46. Mirza, I.A., et al., *Crystal Structures of Cyclohexanone Monooxygenase Reveal Complex Domain Movements and a Sliding Cofactor.* Journal of the American Chemical Society, 2009. **131**(25): p. 8848-8854.

47. Pazmino, D.E.T., et al., *Kinetic mechanism of phenylacetone monooxygenase from Thermobifida fusca.* Biochemistry, 2008. **47**(13): p. 4082-4093.

48. Reddy, R.R., et al., *Characterization of human flavin-containing monooxygenase (FMO) 3 and FMO5 expressed as maltose-binding protein fusions.* Drug Metab Dispos, 2010. **38**(12): p. 2239-45.

49. Schlaich, N.L., *Flavin-containing monooxygenases in plants: looking beyond detox.* Trends Plant Sci, 2007. **12**(9): p. 412-8.

50. Sheng, D.W., D.P. Ballou, and V. Massey, *Mechanistic studies of cyclohexanone monooxygenase: Chemical properties of intermediates involved in catalysis.* Biochemistry, 2001. **40**(37): p. 11156-11167.

51. Suh, J.K., et al., *Yeast flavin-containing monooxygenase generates oxidizing equivalents that control protein folding in the endoplasmic reticulum.* Proceedings of the National Academy of Sciences of the United States of America, 1999. **96**(6): p. 2687-2691.

52. Zhao, Y.D., et al., *A role for flavin monooxygenase-like enzymes in auxin biosynthesis.* Science, 2001. **291**(5502): p. 306-309.

53. Eswaramoorthy, S., et al., *Mechanism of action of a flavin-containing monooxygenase.* Proceedings of the National Academy of Sciences of the United States of America, 2006. **103**(26): p. 9832-9837.

54. Gatti, D.L., et al., *The Mobile Flavin of 4-OH Benzoate Hydroxylase.* Science, 1994. **266**(5182): p. 110-114.

Chapter 9: Conclusions to the PvdA Research

9.1 The structures of PvdA are the first structures of an N-hydroxylating flavoprotein monooxygenase (NMOs)

Flavoproteins are ubiquitous in nature and a lot of scientific effort has been directed towards understanding these enzymes functionally and structurally [1-5]. Several of the closest functional homologs of PvdA like class A flavoprotein monooxygenases phenol-hydroxylase (PDB **1FOH**) and para-hydroxybenzoate hydroxylase (PDB **1PBD**) or class B flavoprotein monooxygenases cyclohexanone monooxygenase (PDB **3GWD**) and flavin-dependent monooxygenase (PDB **2VQ7**) have multiple published structures. However, none of the NMOs (including the most studied PvdA [6, 7], SidA [8] and lucD [9]) had published structures, resulting in a significant amount of conjecture over structural characteristics of these enzymes based on sequence alignments and homology models using other class A and class B enzymes as models [1, 10-16]. Moreover, the structures of PvdA are the first of the class B enzymes containing all three components (flavin, electron donor and substrate/product) *and* in two different positions in the catalytic cycle: the reduced structure at the beginning of the cycle (after substrate binding) and the oxidized structure at the end of the cycle (after product release). New information can be extracted from the structures that sheds new light on biochemical observations and leads the way to the formation of new hypotheses.

9.2 A network of hydrogen bonds and salt bridges stabilizes the substrate in the right orientation and confers stereospecificity

Contrary to the previously proposed hypothesis that a 'F-A-T-G-Y' motif (L-A-T-G-Y sequence in PvdA, residues 351-355) was involved in substrate binding [17], in PvdA, this sequence is actually part of the NADPH binding pocket [18]. The ornithine in PvdA is stabilized by five non-consecutive residues: Q64, K69, N254, T283 and N284: Q64 and N284 orient the N^5-amino-group of the ornithine for hydroxylation, and K69, N254, and T283 stabilize the ornithine backbone. The network of interactions stabilizes the ornithine in such a way that only the correct stereoisomer with a sidechain of the correct length will bind stably and position the amino group at the right distance from the C4a position of the flavin for hydroxylation. This explains the previously observed substrate specificity of PvdA[15, 16]. Furthermore, the majority of these residues are conserved in both SidA and IucD [11], so I hypothesize that ornithine and lysine bind in a similar manner in SidA and IucD, respectively.

9.3 The FAD binding domain was previously hypothesized to be part of a membrane binding region

Prior to the completion of the PvdA structure, it had been hypothesized that the N-terminal region of PvdA also constituted a membrane binding region overlapping with the FAD binding motif [19-21]. The structure of PvdA, however, shows that this is not

the case: the putative membrane binding region is part of the β-α-β dinucleotide binding motif [18] and cannot serve as a membrane binding region.

9.4 The shallow FAD binding cleft explains the inability of PvdA to bind FAD tightly

Most flavoproteins bind the flavin tightly[10, 13, 14, 22-28], including the ornithine hydroxylase SidA. PvdA and IucD on the other hand bind FAD weakly; where two to four *fold* more FAD than PvdA has to be added to a solution for assays and crystallization[15, 16, 29]. Comparing the solvent accessible surface structure of PvdA to the published structures flavoprotein monooxygenases shows that while in other flavoprotein monooxygenases the flavin is completely buried and solvent inaccessible [30-34], in PvdA the FAD binding cleft is shallower, leaving most of the FAD solvent exposed. It will be interesting to compare structures of IucD, and PvdA (neither of which bind the flavin tightly) to SidA, which does bind it tightly. Based on the sequence alignment in **Chapter 7, Figure 7-8**, I hypothesize that IucD, 46 amino acids shorter than PvdA, will also have a solvent exposed FAD. I also hypothesize that SidA has a buried cleft protecting the FAD.

9.5 PvdA's solvent exposed active site might account for the high rate of uncoupling observed in biochemical experiments

Biochemical characterization of PvdA indicates a high degree of uncoupling (NADPH oxidation resulting in production of peroxides instead of substrate hydroxylation)[15, 16], as compared to other flavoprotein monooxygenases. Both oxidized and reduced structures of PvdA show a solvent exposed active site. Only when NADP+ and substrate/product are bound in the right conformation in the active site are the reactive flavin/oxygen intermediates protected from the solvent. This at least partially explains why the $NADP^+$ remains in the active site throughout the oxidative half reaction (after flavin has been reduced): it protects the reactive oxygen species from solvent.

9.6 Oxidized and reduced structures suggest NADPH/+ is flexible in the active site

One observation that caught my attention was the lack of electron density for the nicotinamide moiety of the $NADP^+$ in the oxidized structure as compared to the reduced structure where the nicotinamide ring electron density is well defined. This lack of density is suggestive of a highly flexible $NADP^+$ (able to sample multiple conformations) in the active site once the flavin has been reduced. The flexibility of the $NADP^+$ could serve a dual purpose: **1.)** would enable it to move out of the way to make room for oxygen binding (since the $NADP^+$ remains in the active site throughout the oxidative half reaction) and **2.)** the conformational flexibility of the $NADP^+$ might also play a role in

blocking solvent accessibility into the active site, by allowing it to adopt conformations in which it is able to protect the flavin-reactive oxygen intermediates from solvent.

9.7 Conclusion

Determination of the PvdA structure has allowed us to place the biochemical data in a structure-function relationship context. However, further crystallographic work to identify structural determinants of flavin-intermediate stabilization is in progress. A new structure of reduced PvdA with norleucine in the active site is in progress in an attempt to capture a reactive peroxyflavin intermediate. In light of the structures mutational analyses can be performed on the active site residues to study the hydrogen bonding network, and determine what hydrogen bonds are important for catalysis. Finally, flavoproteins are believed to be poor candidates for drug design because of their ubiquity: Flavin and NAD(P)H analogs would inhibit both bacterial *and* human enzymes. However, the crystal structures of PvdA enable for the first time a detailed view of the active site and the binding mode of ornithine/hydroxyornithine. This new data opens a door to rational drug design: incorporating groups to an ornithine backbone that would increase binding affinity to the active site, or electron withdrawing/donating groups that would promote/destabilize hydroxyornithine formation.

9.8 References

1. Palfey, B.A. and C.A. McDonald, *Control of catalysis in flavin-dependent monooxygenases.* Archives of Biochemistry and Biophysics, 2010. **493**(1): p. 26-36.

2. Mihovilovic, M.D., B. Muller, and P. Stanetty, *Monooxygenase-mediated Baeyer-Villiger oxidations.* European Journal of Organic Chemistry, 2002(22): p. 3711-3730.

3. Mitchell, S.C., *Flavin mono-oxygenase (FMO)--the 'other' oxidase.* Curr Drug Metab, 2008. **9**(4): p. 280-4.

4. Reddy, R.R., et al., *Characterization of human flavin-containing monooxygenase (FMO) 3 and FMO5 expressed as maltose-binding protein fusions.* Drug Metab Dispos, 2010. **38**(12): p. 2239-45.

5. Schlaich, N.L., *Flavin-containing monooxygenases in plants: looking beyond detox.* Trends Plant Sci, 2007. **12**(9): p. 412-8.

6. Ge, L. and S.Y. Seah, *Heterologous expression, purification, and characterization of an l-ornithine N(5)-hydroxylase involved in pyoverdine siderophore biosynthesis in Pseudomonas aeruginosa.* J. Bacteriol., 2006. **188**(20): p. 7205-10.

7. Meneely, K.M. and A.L. Lamb, *Biochemical characterization of a flavin adenine dinucleotide-dependent monooxygenase, ornithine hydroxylase from Pseudomonas aeruginosa, suggests a novel reaction mechanism.* Biochemistry, 2007. **46**: p. 11930-7.

8. Chocklett, S.W. and P. Sobrado, *Aspergillus fumigatus SidA is a highly specific ornithine hydroxylase with bound flavin cofactor.* Biochemistry, 2010. **49**(31): p. 6777-83.

9. Macheroux, P., et al., *FAD and substrate analogs as probes for lysine N6-hydroxylase from Escherichia coli EN 222.* Eur J Biochem, 1993. **213**(3): p. 995-1002.

10. Chocklett, S.W. and P. Sobrado, *Aspergillus fumigants SidA Is a Highly Specific Ornithine Hydroxylase with Bound Flavin Cofactor.* Biochemistry, 2010. **49**(31): p. 6777-6783.

11. Olucha, J. and A.L. Lamb, *Mechanistic and structural studies of the N-hydroxylating flavoprotein monooxygenases.* Bioorg Chem, 2011. **39**(5-6): p. 171-7.

12. Thariath, A., et al., *Construction and Biochemical Rharacterization of Recombinant Cytoplasmic Forms of the IucD Protein (Lysine-N^6-hydroxylase) Encoded by the PCOLV-K30 Aerobactin Gene Cluster.* Journal of Bacteriology, 1993. **175**(3): p. 589-596.

13. Entsch, B. and W.J.H. Vanberkel, *Flavoprotein Structure and Mechanism .1. Structure and Mechanism of Para-Hydroxybenzoate Hydroxylase.* Faseb Journal, 1995. **9**(7): p. 476-483.

14. Fraaije, M.W., et al., *Identification of a Baeyer-Villiger monooxygenase sequence motif.* FEBS Lett, 2002. **518**(1-3): p. 43-7.

15. Meneely, K.M., et al., *Kinetic mechanism of ornithine hydroxylase (PvdA) from Pseudomonas aeruginosa: substrate triggering of O2 addition but not flavin reduction.* Biochemistry, 2009. **48**(20): p. 4371-6.

16. Meneely, K.M. and A.L. Lamb, *Biochemical characterization of a flavin adenine dinucleotide-dependent monooxygenase, ornithine hydroxylase from Pseudomonas aeruginosa, suggests a novel reaction mechanism.* Biochemistry, 2007. **46**(42): p. 11930-7.

17. Stehr, M., et al., *A hydrophobic sequence motif common to N-hydroxylating enzymes.* Trends Biochem Sci, 1998. **23**(2): p. 56-7.

18. Olucha, J., et al., *Two structures of an N-hydroxylating flavoprotein monooxgenase: the ornithine hydroxylase (PvdA) from Pseudomonas aeruginosa.* J. Biol. Chem., 2011. **submitted**.

19. Dick, S., et al., *Cofactor- and substrate-binding domains in flavin-dependent N-hydroxylating enzymes.* Trends Biochem Sci, 1998. **23**(11): p. 414-5.

20. Seth, O., et al., *A reply to Dick et al.* TIBS, 1998. **23**: p. 414-415.

21. Imperi, F., et al., *Membrane-association determinants of the omega-amino acid monooxygenase PvdA, a pyoverdine biosynthetic enzyme from Pseudomonas aeruginosa.* Microbiology, 2008. **154**(Pt 9): p. 2804-13.

22. Alfieri, A., et al., *Revealing the moonlighting role of NADP in the structure of a flavin-containing monooxygenase.* Proc Natl Acad Sci U S A, 2008. **105**(18): p. 6572-7.

23. Burnett, V.L., M.P. Lawton, and R.M. Philpot, *Cloning and sequencing of flavin-containing monooxygenases FMO3 and FMO4 from rabbit and characterization of FMO3.* Journal of Biological Chemistry, 1994. **269**(19): p. 14314-22.

24. Celius, T., et al., *Flavin-containing monooxygenase-3: induction by 3-methylcholanthrene and complex regulation by xenobiotic chemicals in hepatoma cells and mouse liver.* Toxicol Appl Pharmacol, 2010. **247**(1): p. 60-9.

25. Cho, H.J., et al., *Structural and functional analysis of bacterial flavin-containing monooxygenase reveals its ping-pong-type reaction mechanism.* Journal of Structural Biology, 2011. **175**(1): p. 39-48.

26. Choi, H.S., et al., *A novel flavin-containing monooxygenase from Methylophaga sp strain SK1 and its indigo synthesis in Escherichia coli.* Biochem Biophys Res Commun, 2003. **306**(4): p. 930-6.

27. Gatti, D.L., et al., *The Mobile Flavin of 4-OH Benzoate Hydroxylase.* Science, 1994. **266**(5182): p. 110-114.

28. Hall, L.H., B.J. Orchard, and S.K. Tripathy, *The Structure and Properties of Flavins - Molecular-Orbital Study Based on Totally Optimized Geometries .1. Molecular-Geometry Investigations.* International Journal of Quantum Chemistry, 1987. **31**(2): p. 195-216.

29. Olucha, J., et al., *Two structures of an N-hydroxylating flavoprotein monooxygenase: ornithine hydroxylase from Pseudomonas aeruginosa.* Journal of Biological Chemistry, 2011. **286**(36): p. 31789-98.

30. Alfieri, A., et al., *Revealing the moonlighting role of NADP in the structure of a flavin-containing monooxygenase.* Proc. Natl. Acad. Sci. USA, 2008. **105**(18): p. 6572-7.

31. Cho, H.J., et al., *Structural and functional analysis of bacterial flavin-containing monooxygenase reveals its ping-pong-type reaction mechanism.* J. Struct. Biol., 2011. **175**: p. 39-48.

32. Eswaramoorthy, S., et al., *Mechanism of action of a flavin-containing monooxygenase.* Proc Natl Acad Sci U S A, 2006. **103**(26): p. 9832-7.

33. Mirza, I.A., et al., *Crystal structures of cyclohexanone monooxygenase reveal complex domain movements and a sliding cofactor.* J. Amer. Chem. Soc., 2009. **131**(25): p. 8848-54.

34. Orru, R., et al., *Joint functions of protein residues and NADP(H) in oxygen activation by flavin-containing monooxygenase.* J. Biol. Chem., 2010. **285**(45): p. 35021-8.

Appendix: PvdF

PvdF catalyzes the transformylation of hydroxyornithine to generate the N5-formyl, N5-hydroxy-ornithine that is incorporated as the ferric iron binding moiety in the pyoverdin siderophore. PvdF has only been shown to be active in whole cell extract assays, using iodine oxidation reactions[1]. Biochemical characterization of the enzyme in vitro requires: **1.)** synthesizing cofactor (10-formyl-tetrahydrofolate), **2.)** synthesizing substrate (not commercially available) and **3.)** developing an assay.

A.1 Synthesis of 10-formyl-tetrahydrofolate

Sequence aligments indicate PvdF is a member of the glycinamide ribonucleotide transformylase (GART) family of transformylases [1]. This family of transformylases use 10-formyl-tetrahydrofolate as the cofactor for nucleophillic transformylation of the substrate [2]. 10-formyl-tetrahydrofolate is unstable in solution and is not commercially available. This tetrahydrofolate cofactor either has to be synthesized or biochemical assays have to be coupled with a tetrahydrofolate formylase. However, the only available assay to determine product formation was already coupled to PvdA, to produce substrate, hydroxyornithine, which also not commercially available.

As shown in **figure A-1**, 10-formyl-tetrahydrofolate can be generated from 5-formyl-tetrahydrofolate in a two-step process, according to the Himes/Rabinowitz synthesis scheme [3-5]. 5-formyl-tetrahydrofolate is dissolved in 1M βME at 2°C on ice, in order to

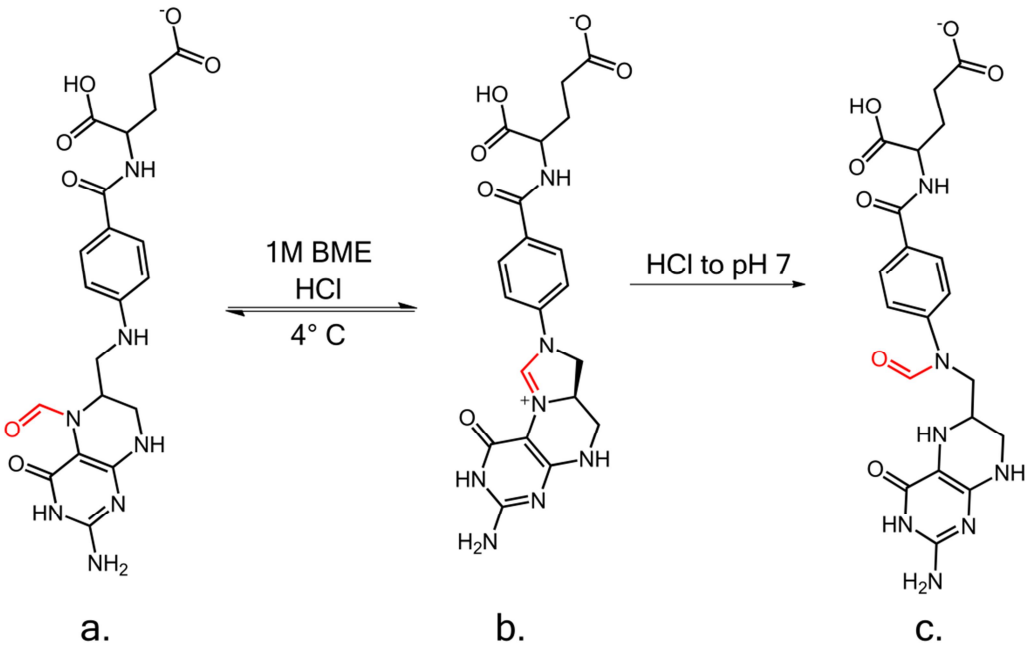

Figure A-1: Himes/Rabinowitz scheme for conversion of 5-formyl-tetrahydrofolate to 10-formyl tetrahydrofolate. 5-formyl-tetrahydrofolate (a) can be precipitated out of solution as 5,10 methenyl tetrahydrofolate (b) with the slow acidification of the solution on ice. The 5,10 methenyl compound can be stored stably at -20°C indefinitely. Generating 10-formyl-tetrahydrofolate (c) from the 5,10 methenyl tetrahydrofolate requires dissolving the 5,10 methenyl tetrahydrofolate in a solution buffered at pH above 7.

maintain a reducing environment and prevent the quick degradation of the compound at room temperature. 5-formyl-tetrahydrofolate is converted to 5,10-methenyl-tetrahydrofolate by lowering the pH of the solution with HCl, until a yellow precipitate begins to form (5,10-methenyl-tetrahydrofolate has a lower solubility in water at low pH). After a four hour incubation on ice, the precipitate is ultracentrifuged and supernatant discarded. Dry 5,10-methenyl-tetrahydrofolate is stable for long periods of time at -20°C. In order to convert the 5,10-methenyl-tetrahydrofolate into 10-formyl-tetrahydrofolate, the 5,10-methenyl-tetrahydrofolate can be resuspended in solution buffered at pH 7 or above **(Figure A-1)** [6, 7]. Due to the instability of the 10-formyl-tetrahydrofolate it has to be made fresh from a 5,10-methenyl-tetrahydrofolate stock for every experiment. As seen on **figure A-2** I could obtain all three molecules, and interconversion between the three molecules can be observed spectometrically**.**

A.2 Synthesis of hydroxy-ornithine.

In an attempt to uncouple future PvdF assays from PvdA to produce hydroxyornithine, I attempted to synthesize hydroxyl-ornithine with the help of Dr. Tom Prisinzano and his graduate student Dr. Kim Lovell. The synthesis protocol was based on that published by the Miler miller group (1999) from protected CBZ-ornithine as shown on **figure A-3**[8]. As shown on figure 3, a five step scheme would result in CBZ-hydroxyornithine as the final product with approximately 80% yield. The CBZ protective group could later be removed via hydrogenation[8]. Unfortunately, degradation of the product of step 2, resulted in small or no yields to continue with step 3. There are several factors that might have affected the degradation of the oxaziridine compound, the most likely of which is the purity of the *meta*-chloroperoxybenzoic acid (mCPBA). mCPBA is a strong

oxidant, only available for purchase at 70% purity or less, due to its propensity for violent reactions at higher purities [8]. For that reason, all of my synthesis experiments were performed with at lower purity levels than the authors of the scheme were using (they recrystallized the mCPBA to obtain higher purity). Synthesis of hydroxyornithine is still being attempted by the Prisinzano lab with mixed results.

A.3 High-Performance Liquid Chromatograph (HPLC) assay for PvdA and PvdF.

PvdA activity can be measured monitoring NADPH oxidation, but in order to observe hydroxylation of ornithine a cumbersome iodine oxidation colorimetric assay is the only available tool [1]. Assays for the measurement of PvdF transformylation are even more cumbersome, involving an iodine oxidation step similar to the PvdA assay, with an additional step where strong acid is added to the solution and then autoclaved [1, 9, 10]. The cumbersomeness of the assay resulted in inaccuracies that could be avoided with a simpler assay. Ornithine, hydroxyornithine, and formyl-hydroxyornithine have, in theory, different hydrophobic properties. This led to the hypothesis that we would be able to see small differences in HPLC traces using a C-14 reverse phase column (**Figure A-4**). However, neither ornithine, or the products hydroxyornithine or formylhydroxyornithine absorb strongly enough to be detected in a spectrophotometer. To overcome this, I derivatized the compounds after each reaction with FMOC-Cl under basic conditions, a technique most commonly used in N-terminal sequencing, and allows observation of aminoacids at 263 nm wavelengths, and due to the reactivity of the FMOC-Cl, results in 100% derivatization [11-14].

A.4 Conclusion

My contributions to this project are allowing other members of the lab to continue making progress in the biochemical and structural characterization of PvdF.

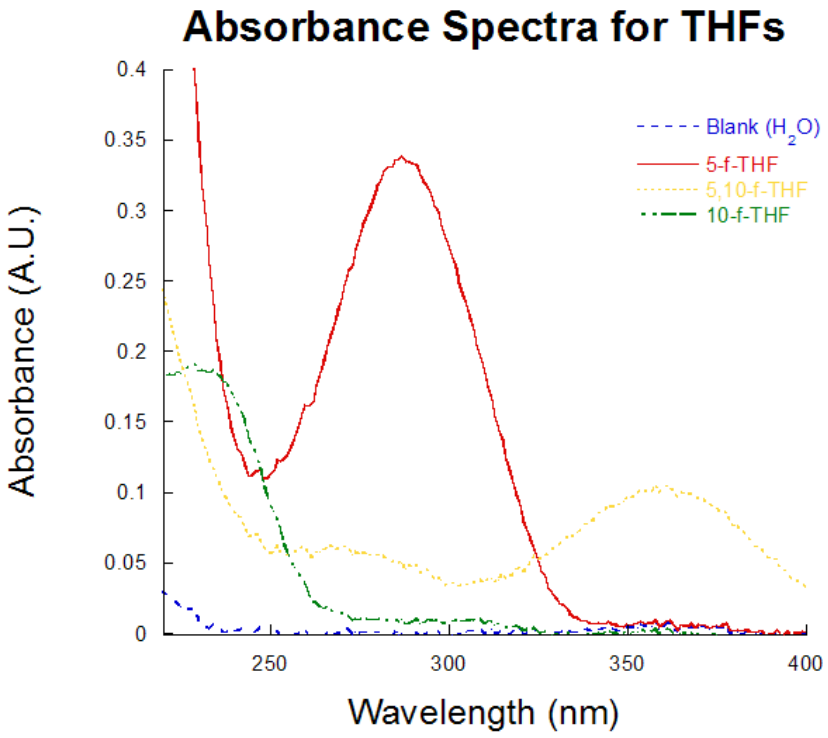

Figure A-2: Absorbance spectra of 5-formyl-tetrahydrofolate, 5,10-methenyl tetrahydrofolate, and 10-formyl-tetrahydrofolate. The three absorbance spectra (5-formyl-tetrahydrofolate in red, 10-formyl-tetrahydrofolate in green, and 5,10-methenyl tetrahydrofolate in yellow) were obtained from a single sample, showing we could generated 10-formyl-tetrahydrofolate from 5-formyl-tetrahydrofolate, and store it stably as 5,10methenyl-tetrahydrofolate. The spectra for all three molecules agree with those published in the literature [15].

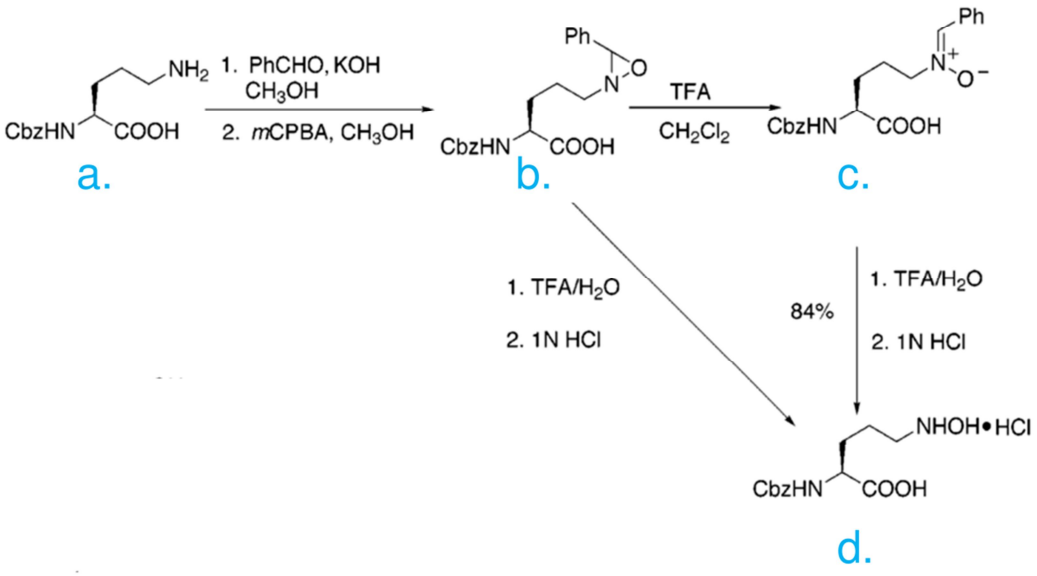

Figure A-3: Scheme for synthesis of hydroxyornithine as described by Lin and Miller (1999)[8]. CBZ protected ornithine (a) can be converted to hydroxyornithine (d) via two intermediate steps, generating first an oxaziridine (b) and nitrone (c). Unfortunately the generation of (b) proved difficult due to the instability of the compound, resulting in the inability to proceed with the synthesis further. Figure adapted form Lin *et al.* 1999

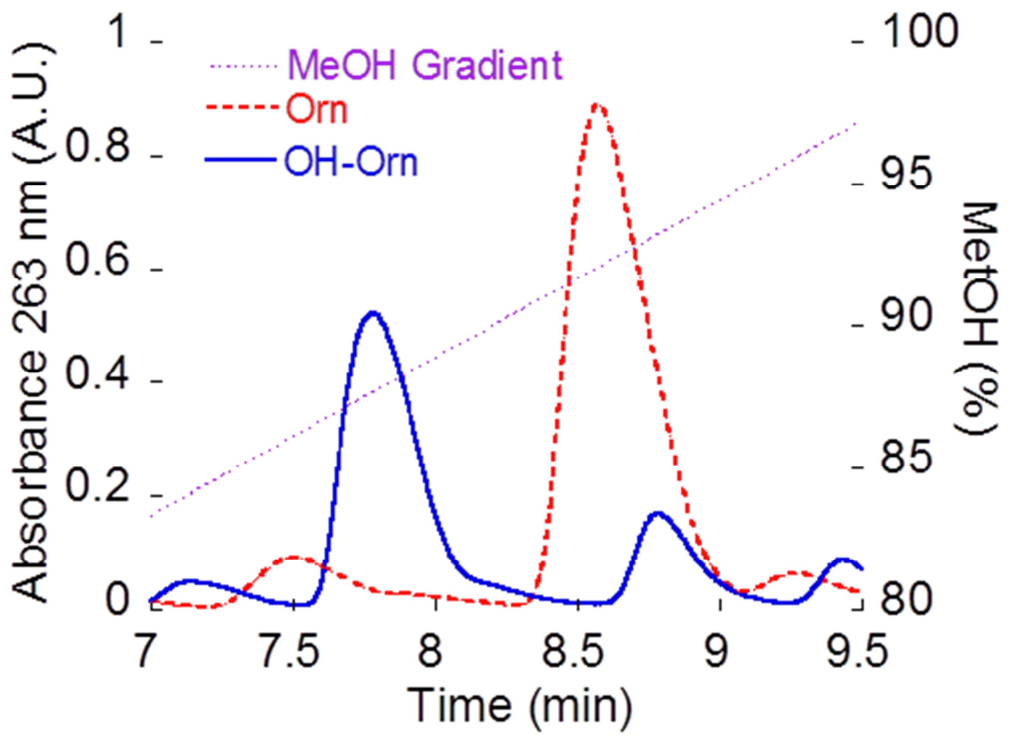

Figure A-4: HPLC traces of Ornithine and Hydroxyornithine. Ornithine (red dashed trace) and hydroxyornithine (blue trace) have enough differential hydrophobicity that they can be separated via a C-14 reverse phase column in a methanol gradient. The molecules could be visualized at 263 nm via a derivatization step with FMOC-Cl. The hydroxyornithine was generated enzymatically with PvdA.

A.6 References

1. McMorran, B.J., et al., *Involvement of a transformylase enzyme in siderophore synthesis in Pseudomonas aeruginosa.* Microbiology-Sgm, 2001. **147**: p. 1517-1524.

2. Welin, M., et al., *Structural studies of tri-functional human GART.* Nucleic Acids Research, 2010. **38**(20): p. 7308-+.

3. Rabinowitz, J.C. and W.E. Pricer, *Formation, Isolation and Properties of 5-Formiminotetrahydrofolic Acid.* Federation Proceedings, 1957. **16**(1): p. 236-236.

4. Rabinowitz, J.C. and W.E. Pricer, *Formyltetrahydrofolate Synthetase: Isolation and Crystallization of Enzyme.* Journal of Biological Chemistry, 1962. **237**(9): p. 2898-&.

5. Rabinowitz, J.C. and W.E. Pricer, *Formyltetrahydrofolate Synthetase.* Methods in Enzymology, 1963. **6**: p. 375-379.

6. Himes, R.H. and J.C. Rabinowitz, *Formyltetrahydrofolate Synthetase .2. Characteristics of Enzyme and Enzymic Reaction.* Journal of Biological Chemistry, 1962. **237**(9): p. 2903-&.

7. Rabinowitz, J.C. and R.H. Himes, *Folic Acid Coenzymes* Federation Proceedings, 1960. **19**(4): p. 963-970.

8. Lin, Y.M. and M.J. Miller, *Practical synthesis of hydroxamate-derived siderophore components by an indirect oxidation method and syntheses of a DIG-siderophore conjugate and a biotin-siderophore conjugate.* Journal of Organic Chemistry, 1999. **64**(20): p. 7451-7458.

9. Meneely, K.M., et al., *Kinetic mechanism of ornithine hydroxylase (PvdA) from Pseudomonas aeruginosa: substrate triggering of O2 addition but not flavin reduction.* Biochemistry, 2009. **48**(20): p. 4371-6.

10. Meneely, K.M. and A.L. Lamb, *Biochemical characterization of a flavin adenine dinucleotide-dependent monooxygenase, ornithine hydroxylase from Pseudomonas aeruginosa, suggests a novel reaction mechanism.* Biochemistry, 2007. **46**(42): p. 11930-7.

11. Chan, W.C., et al., *Facile Synthesis of Protected C-terminal Peptide Segments By FMOC/BU(T) Solid-Phase Procedures On N-FMOC-9-Amino-Xanthen-3-Yloxymethyl Polystyrene.* Journal of the Chemical Society-Chemical Communications, 1995(5): p. 589-592.

12. Gross, C.M., et al., *Preparation of protected peptidyl thioester inter-mediates for native chemical ligation by N-alpha-9-fluorenylmethoxycarbonyl (Fmoc) chemistry: considerations of side-chain and backbone anchoring strategies, and compatible protection for N-terminal cysteine.* Journal of Peptide Research, 2005. **65**(3): p. 395-410.

13. Ollivier, N., et al., *Fmoc solid-phase synthesis of C-terminal thioesters peptide using an intramolecular N,S-acyl shift.* Journal of Peptide Science, 2006. **12**: p. 130-130.

14. Ramli, S., I.R. Gentle, and B.P. Ross, *Efficient Manual Fmoc Solid-Phase Synthesis of the N-Terminal Segment of Surfactant Protein B (SP-B(1-25)).* Protein and Peptide Letters, 2009. **16**(7): p. 810-814.

15. Uyeda, K. and J.C. Rabinowitz, *Fluorescence Properties of Tetrahydrofolate and Related Compounds.* Analytical Biochemistry, 1963. **6**(1): p. 100-&.